Effect of Surface Treatments on Interfacial Strength and Durability of Metal-Polymer Composite Bond

by

Syeda Noor E Sumaiya

A Thesis submitted to the Faculty of Graduate Studies of

The University of Manitoba

in partial fulfilment of the requirements of the degree of

MASTER OF SCIENCE

Department of Mechanical Engineering

University of Manitoba

Winnipeg

Abstract

Effect of surface treatments on Strength and durability of aluminum 6061-Henkel Hysol EA 9891RP (room temperature curing epoxy) bond was studied using single lap shear, flatwise tensile and wedge crack test. The interfacial strength (IFSS) and % cohesive fracture varied with composite adhesive thickness and 0.03-0.04 mm that maximized the interfacial fracture was chosen to compare surface treatments. The effect of treatments on IFSS and tensile strength increased in the following order: PAA+BR127 (RT) < UT+BR127 (120oC) < Alodine < Alodine+EC3901(RT) < Alodine+BR127 (RT) < PAA < UT < UT+BR127 (RT) < Alodine+EC3901 (90oC) < PAA+EC3901(RT) < PAA+EC3901(90oC) < PAA+BR127 (120oC) < UT+EC3901(90oC) < UT+EC3901(RT) < Alodine+BR127 (120oC). The environmental durability decreased in the following order Alodine+EC3901 (90oC) < Alodine+BR127 (120oC) < PAA+BR127 (120oC) < PAA+EC3901 (90oC) < UT < UT+EC3901 (90oC) < UT+EC3901 (RT) < PAA+EC3901 (RT). PAA and Alodine, combined with BR127 (120 oC) and EC3901 (90oC) are the optimal surface treatments.

ACKNOWLEDGEMENT

I would like to express my earnest gratitude to my supervisor, Dr. Raghavan Jayaraman for his valuable guidance throughout the entire thesis work. This thesis would not have been possible without his motivation and support. I really appreciate his precious advice which is motivational for me in various academic, professional, and personal aspects.

I acknowledge the financial support from Prof. Jayaraman and Standard Aero and in-kind support from 3M. I would like to thank my co-workers for their precious support and help throughout the past few years.

And my very special and warm thanks to my husband, Monowar Hasan, my family and friends for their constant support and encouragement during my M.Sc. study.

TABLE OF CONTENTS

LIST OF TABLES

LIST OF FIGURES

Chapter 1

Introduction

Bonded joints are increasingly used in aerospace and non-aerospace applications since they result in the reduction in the weight of structures when compared to other joining methods such as fastening. In addition to aerospace, applications in automotive, marine and construction industries have been increasingly using adhesive bonding due to their multiple benefits such as reduction in cost and simplicity in fabrication. Bonding of carbon composite stiffeners to steel inside the chassis of BMW 7 series is a recent example of adhesive bonding in automotive application [1]. Adhesive bonding is also widely used in repairing structures during maintenance. Composite patches, bonded on to cracked or corroded metallic aircraft or civil structures, have shown to be a highly cost effective method for extending their service life and maintaining high structural efficiency [2].

Due to pre-dominance of aluminum (Al) in aerospace industries, bonding of Al substrates has been well researched and the bonding procedures have been established [3]. Effect of surface treatments on surface chemistry, strength of the bond at the interface between the aluminum substrate and the adhesive, and the relation between these two, are areas of past and on-going research. Surface treatments include mechanical abrasion with subsequent solvent cleaning, and chemical treatments. The former, often used in conjunction with the latter, results in clean and rough surface. The chemical treatments such as acid etching i.e. dichromate-sulphuric acid etching (FPL), chemical conversion coating i.e. Alodine coating and electro-chemical treatments i.e. anodization using phosphoric acid (PAA) or chromic acid (CAA) applied after mechanical

treatment, results in the formation of thin oxide coating on the substrate [4]. Acid etching and anodization remove the old oxide and dirt from the surface and regenerate thin and finely porous oxide layers. During formation of conversion coating by electro chemical process i.e. anodizing, the aluminum is immersed in solution of acids (usually phosphoric or chromic) while an electrostatic charge is applied.On other hand, in a chemical conversion coating process, a conversion coating is formed when the substrate surface (i.e. Al) is reacted with a suitable chemical solution; a partial or complete chemical film forms at the metal-solution interface. The thin film dries to an amorphous coating, which includes a portion of the base metal ion as one of the components of the film. The other component of this coating is chromic/phosphoric acid or fluorides [5].The metal surface is converted from its initial active condition to an inert film, which is commonly known as a chemical conversion coating. On aluminum, conversion coatings result in excellent bonding with primers or epoxy adhesives, and provide corrosion resistance. The natural oxide layer on aluminum is usually thick and has large pores. Application of conversion coating on clean abraded Al surface creates a hydrated Al oxide coating and seals the pores, which are prone to moisture or corrosion attacks [6].

However, the chromium containing treatments like dichromate sulphuric acid or chromic sulfuric acid anodization have been discouraged from use due to their hazardous nature. Hence, non-chromate surface treatments like PAA and Alodine are being used as alternative surface treatments. The thickness and the roughness of the conversion layers obtained using these treatments as well as their chemical composition has been found to influence the interfacial bond strength.

These conversion coatings are often coated with primers, before bonding, to impart environmental durability to bonded joints since oxide layers formed by conversion coatings are often attacked and degraded by moisture. Primer is a low viscous liquid substance which promotes adhesion between the substrate and the adhesive and also protects the treated surface against hygrothermal effects. The low viscosity allows it to penetrate porous and rough conversion coating surfaces, providing improved mechanical interlocking and protection of the underlying surface against moisture attack. The epoxide group in the primer also reacts with adhesive, contributing to enhance chemical bonding between the primer coated substrate and the adhesive.

Both thermoplastic and thermoset adhesives are used in bonding applications. Thermoset adhesives are most widely used in aerospace and are the focus of this research. The thermoset epoxy adhesive used in this research is reinforced with glass fibers making it a composite adhesive.

In addition to Al-Al bonded joints, Al structures are repaired using polymer composite patches resulting in Al-Composite joints. Currently, Al-Polymer composite hybrid laminated structures are used in Airbus A380. Unlike the former, no adhesive is used in the latter application and the epoxy matrix of the composite itself is used as the bonding agent. Similar type of bonding is used in the application of interest to this study.

A polymer composite rub-strip is bonded to the inside surface of the aluminum casing of an engine to prevent the rotating blades from coming in contact with the casing (shown in

Figure1.1). This rub-strip is bonded to the Al casing using an aerospace adhesive at high temperature and pressure by the manufacturer (OEM) of the engines. However, during repair and over-haul an alternate rub-strip material is applied directly onto the Al casing and cured at room temperature without using any adhesives. While the available information on surface treatments and primers is for high temperature bonding of substrates using adhesives, such information (including environmental durability) for room temperature bonding of Al substrates to composite rub-strips without using adhesives is not available.

While various bonded joints are used in design, single lap shear joints (ASTM D1002) are widely used to study the effect of substrate surface treatments on the strength of the bond between the adhesive and the substrate. Most published studies on interfacial strength of bond between the substrates and the adhesives do not report the mode of failure. If the failure is not adhesive, i.e. cohesive or mixed mode as shown in Figure 1.2 (a) and (c), the reported interfacial shear strength (IFSS) is only an apparent strength and cannot be used to compare the effect of surface treatment on bond strength. Hence, single lap shear test condition that ensures adhesive failure is required to evaluate the effect of various surface treatments. Such an optimization of single lap shear test condition that maximized adhesive failure has not been considered while evaluating the effect of surface treatments, complicating the interpretation of the results.

In order to evaluate the durability of aerospace adhesives wedge crack test (ASTM D3762) is commonly used. The wedge test simulates the combined effect of loading and hot-humid environment that a bonded joint might encounter while in service. Since the load at the wedge crack tip is tensile in nature, it is not possible to correlate the results of wedge type test (crack

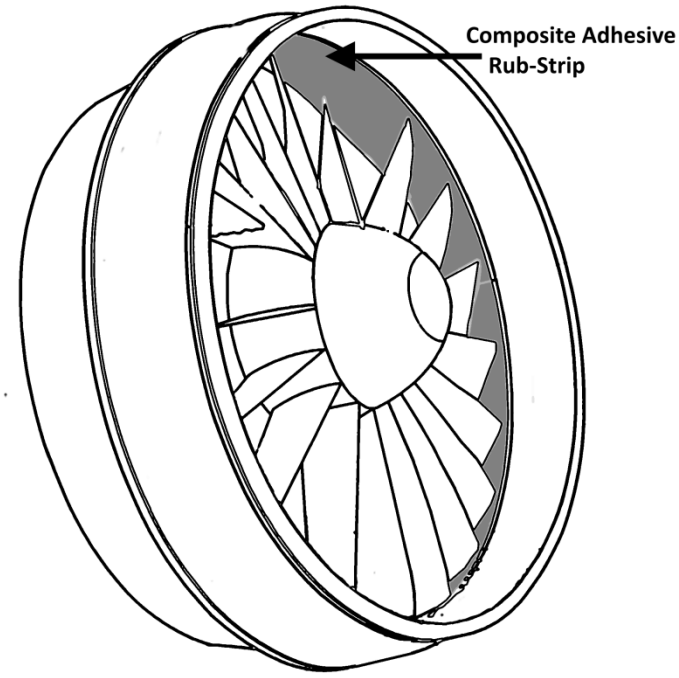

Figure 1.1 Composite rub-strip boned to Al- casing

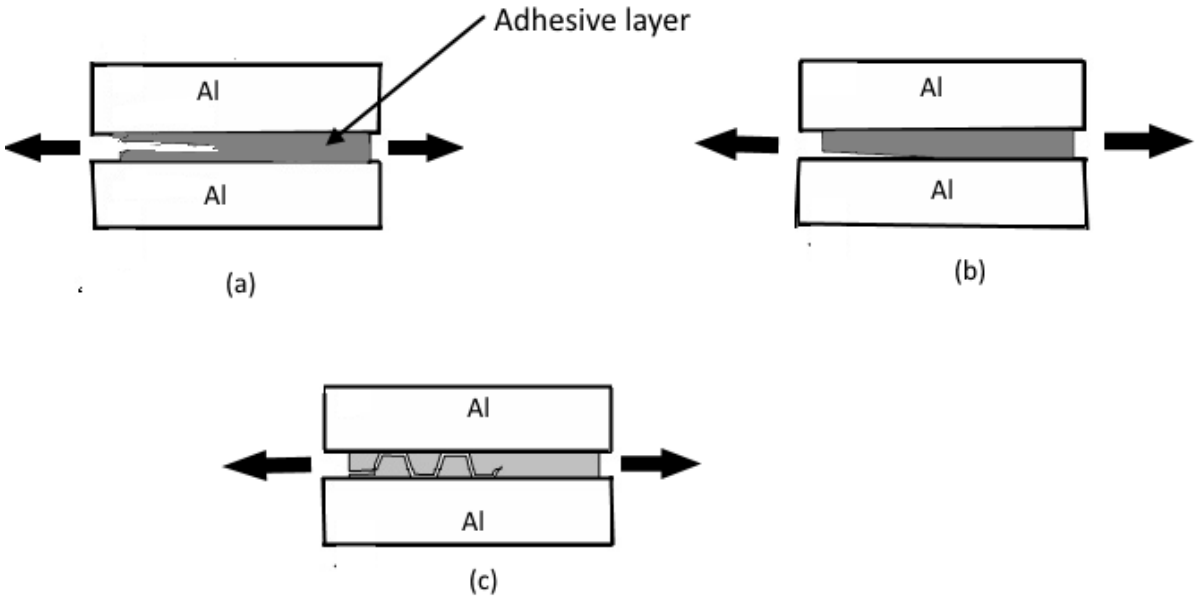

Figure 1.2: Three types of joint fracture mode (a) cohesive fracture- crack propagates into the adhesive layer, (b) interfacial fracture- crack propagates along the interface, (c) mixed mode fracture- crack path straddles between the interface and the adhesive

Length) directly to the degradation in IFSS due to environment. Hence, degradation in tensile strength of bonded joints is required in addition to degradation in IFSS to evaluate the wedge test results and the effect of surface treatments on environmental durability of bond between Al-substrate and composite rub-strip. Such correlation has not been done before.

1.1 Thesis Objectives

Hence, the objectives of this thesis are

a) Determine the optimal single lap shear test condition that maximized interfacial (i.e. adhesive) failure mode
b) Using this optimal test condition, evaluate the effect of various surface treatments on the strength of bond between an Al substrate and a room temperature curing polymer composite rub-strip, which is a thermoset epoxy adhesive reinforced with glass fibers
c) Using Wedge Crack test, evaluate the durability of bond, between the Al substrate and the composite rub-strip, under hot-humid environment
d) Study the degradation in IFSS using the SLS test and tensile strength using Flatwise Tensile test of this bond, under the same hot-humid environment used in (c) and use the results to interpret the wedge test results
e) Using results from (b)-(d), determine the optimal surface treatment for room temperature bonding of the polymer composite rub-strip to the Al substrate.

1.2 Organization of Thesis

In Chapter 2, background information is presented and published literature in this area is critically reviewed to establish the knowledge gaps in support of the thesis objectives presented

above. Experimental details are discussed in Chapter 3.Results are presented and discussed in Chapter 4.Summary of the results and conclusion based on these results are presented in Chapter 5.

Chapter Two

Literature Review

2.1 Background Information

Bonding metal to polymer composite, with or without adhesive, is demanding since they involve discontinuities in the geometry of the structure and introduce high local stress concentrations. Bonding of metals to epoxy based composite generally uses epoxy based adhesives, which is compatible with the epoxy matrix of the composite. When bonding is done without an adhesive the composite resin matrix acts as the bonding agent. However, regardless of bonding with/without an adhesive all bonded joints involve stress concentrations due to discontinuity in the substrate at the bonded location. Efforts have been made to reduce stress concentrations in the joints through various joint configurations. Commonly used joint configurations that have been analyzed in the literature are single-lap joints, double-lap joints, scarf joints, and stepped-lap joints as shown in Figure 2.1 [7]. Other configurations available are strap joints, butt joints, T-shaped joints, L-shaped joints, tubular lap joints, etc. [7]. While studying these joint configurations, the focus is usually in improving the failure load, eventually bond strength of the joints, which depends on type of loading they are subjected to, and the stress distribution within the joint. Thus, the strength of many of these joint configurations depends on the joint geometry, and the strength of the adhesion between the substrate and the adhesive. Due to multi-axial state of stress within the bonded region, the measured strength varies from one type of joint to another and does not represent the strength of the bond between the substrate and the adhesive. Hence, careful selection of test geometry is required to study the bonding between the substrate and the adhesive.

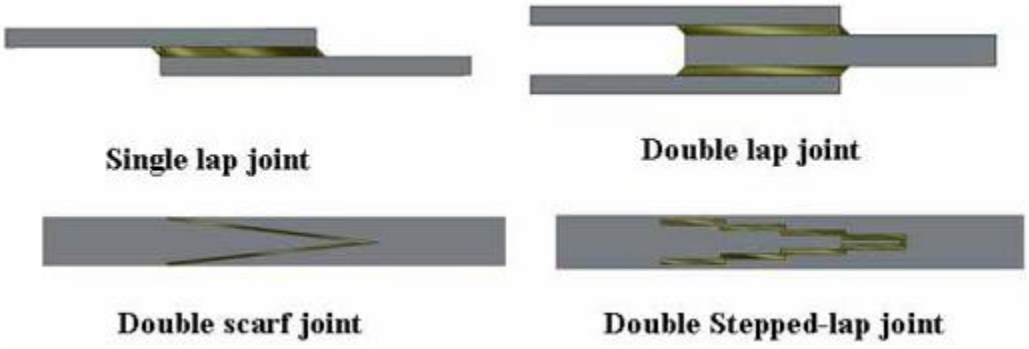

Figure 2.1: Common adhesive bonded joints [7] [received permission from Craig Myles, on behalf of SAGE Ltd. Permissions Team ,SAGE Publishing 1 Oliver's Yard, 55 City Road London, EC1Y on June 27, 2016]

2.1.1Test Methods

Test methods such as double cantilever beam (DCB) and thick adhered shear test (TAST) are used to measure the adhesive properties rather than the strength of the bond between the substrate and the adhesive [8,9,10]. While DCB is used to measure the fracture toughness and the TAST is used to measure the shear strength of the adhesive.

The test methods used to investigate the strength of the bond between a substrate and an adhesive are single lap shear (SLS), double lap shear (DLS) and peel tests (floating roller, T-peel test). While schematics of SLS and DLS tests are shown in Figure 2.1, the schematics of peel tests are shown in Figure 2.2. While peel tests measures the relative peel resistance of bonding between film and a substrate under mode I (tensile load), the SLS and DLS measure the shear strength under Mode II (shear load). However, since the stress state at the interface is never pure tensile or shear stress and hence, the strength values obtained using these tests are used for qualitative evaluation rather than in design.

For measuring shear strength the single-lap joint is the most common test geometry (ASTM D1002) used mainly due to its geometrical and manufacturing simplicity. But single lap joint under tension would rotate due to eccentricity of the loading with respect to center-line of the bond resulting in bending of the adherend [11].This would result in axial and out-of-plane (peel) tensile stresses in addition to shear stresses, within a bond and these stresses would vary across the bond area, i.e. overlap length as shown in Figure 2.3. Hence, it is difficult to relate the measured strength to substrate-adhesive interfacial shear strength (IFSS) since the failure is often

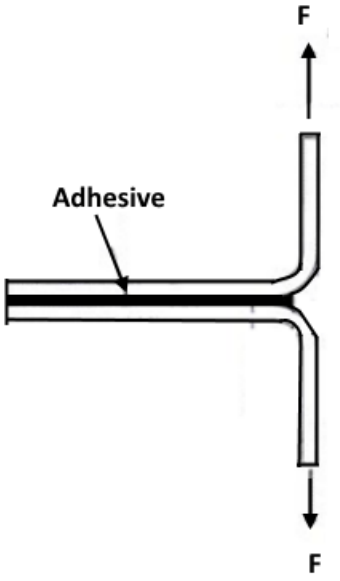

(a)

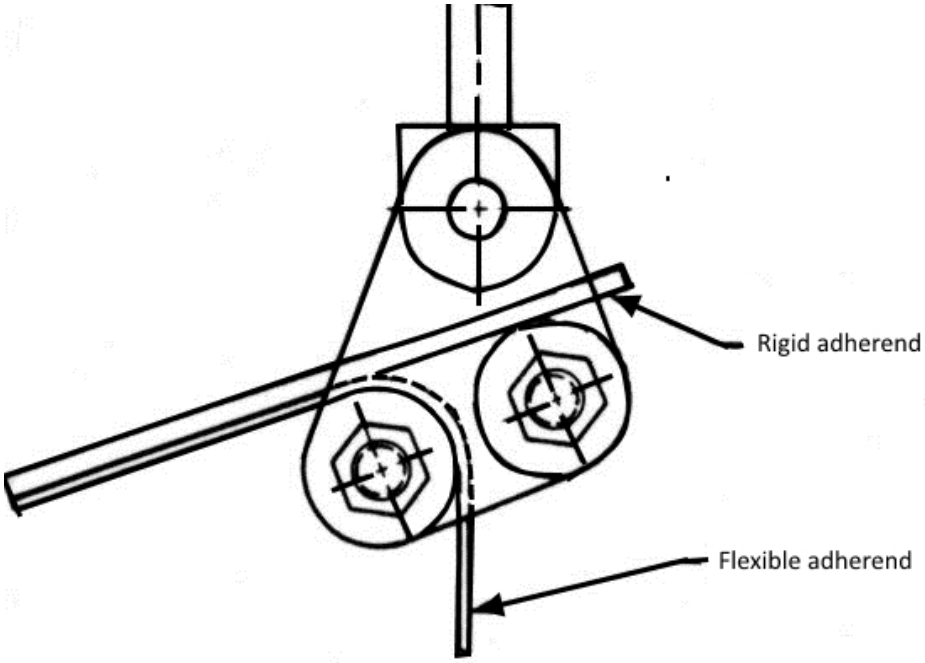

(b)

Figure 2.2 (a) Schematic of T peel test, (b) floating roller peel test

due to a multi-axial state of stress. Moreover, the above stress distribution have been found [11,12] to change with SLS geometry parameters, such as adherend thickness, overlap length and fillet length, illustrated in Figure 2.4 making the measured an extrinsic rather than an intrinsic value. Finally, if the fracture path, dictated by the multi-axial state of stress and stress distribution, is not along the interface, then the measured strength is not the true shear strength of the bond between the substrate and the adhesive.

In order to eliminate the bending of the bond and adherends due to eccentric loading, DLS geometry has been developed (ASTM D3528).It has been found to result in strength values twice that for SLS geometry [13]. However, some disadvantages of DLS geometry are (a) manufacturing difficulty (b) difficulty in removing the squeezed out adhesive to obtain geometries without any fillets (used in this study), (c) stress distribution similar to SLS. Despite the issues identified, SLS geometry was used in this study.

While the focus of the published literature is on IFSS, tensile strength of the bond between the substrate and the adhesive has not been reported. Peel tests are suitable for exploring the bond between thin films on flexible or rigid substrates; it could not be used to measure the tensile strength of bond between the substrate and the adhesive. Hence, Flatwise Tensile (FWT) test, used to study the bond between honeycomb and skins, was used in this study. In the FWTtest, two adherend blocks are vertically bonded and (shown in Figure 2.5) loaded in tension. Load is applied until failure of the bond occurs. Thus the tensile strength of the bond is measured from the failure strength diving by the bonded area. The results from Flatwise tensile tests in this study were used to evaluate the results from SLS test and durability test discussed below.

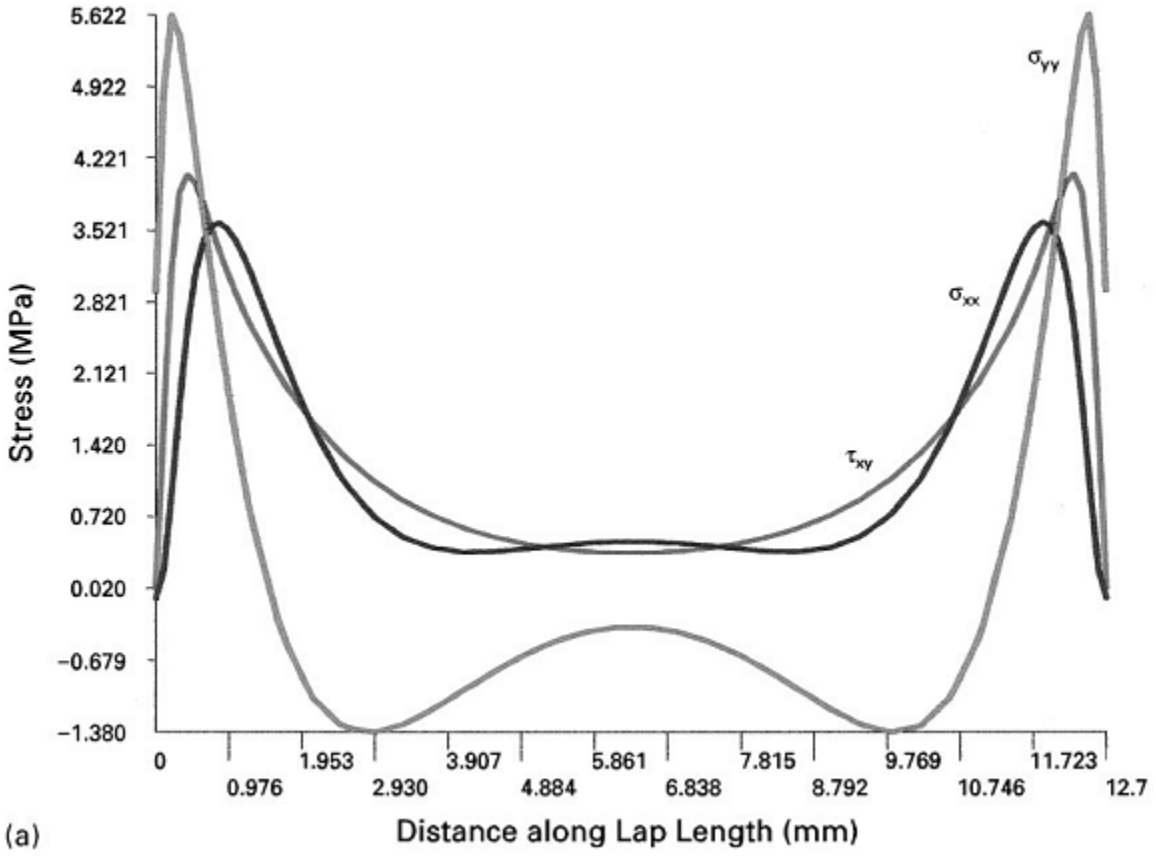

Figure 2.3: Variation of shear (τ_{xy}), peel (σ_{yy}), and axial (σ_{xx}) stress along the overlap length of a single-lap joint at the center of the adhesive thickness [12] [permission has taken from Elsevier to use contents for thesis; license number: 3890540153030]

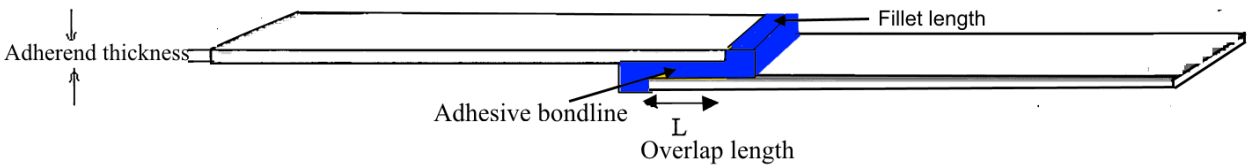

Figure 2.4: SLS coupon with all influencing geometrical parameters to bond strength

The durability of the adhesives is studied using Wedge Crack (WC) test (ASTM D3762) and this was used in this study to study the durability of the bond. In WC test a wedge is inserted forcefully to introduce a starter crack in sample as shown in Figure 2.6. To study the durability of the bond, the crack should propagate along the adhesive-Al interface. When the WC sample is placed inside an environmental chamber, the adhesive-Al interface is exposed to temperature and moisture, which stimulates the crack propagation. The crack propagation is being constantly monitored as a function of time to see periodic degradation of the Al-adhesive interface.

2.1.2 Surface Treatments

The surface treatments can be classified into two major groups.

1. Mechanical Treatment
2. Chemical Treatments
    (a) Acid etching
    (b) Conversion coating using chemical or Electrochemical method
    (c) Primers

The treatments are categorized and listed in Table 2.1 according to their type.

Mechanical treatment, such as grinding using abrasive papers / cloth and grit blasting, are used to remove any oxide scales and contaminants. This is followed by degreasing using solvents before bonding. If used alone, the roughness generated during this treatment determines the level of mechanical interlocking between the substrate surface and the adhesive, and thus the bond strength.

Often, the mechanical treatment is followed by chemical treatment either to improve the roughness and mechanical interlocking or to create reactive surface chemical groups that can react with chemical groups in the adhesive resulting in a chemical bonding.

During acid etching , etching by chromic-sulphuric acid (CAE), dichromate-sulphuric acid (FPL) and sulfo-ferric acid, the surface of the substrate is brought in contact with an acid for a very short duration during which a thin layer of surface material is dissolved and removed. This results in a rough surface that can enhance the mechanical interlocking.

Predominantly, conversion coatings are used over acid etching. These are oxide layers formed through chemical or electrochemical conversion of the surface of the substrate through latter's reaction with a chemical or mixture of chemicals. Reaction duration is longer than that used in etching. The electrochemical conversion is also known as anodization. The chemicals used in chemical and electro chemical treatments used in the past and currently in use are tabulated in Table 2.1. The morphology of the oxide layer and its stability vary with the type of chemical used.

These oxide conversion layers are susceptible to attack by moisture in the service environment resulting in poor environmental durability of the bond between the substrate and the adhesive. Hence, primers are applied over conversion coatings to prevent this and enhance the environmental durability of bonded joints. Most of the previous studies focused on using solvent based primers (i.e. Cytec's BR127), few have reported use of water based inorganic primers (i.e.

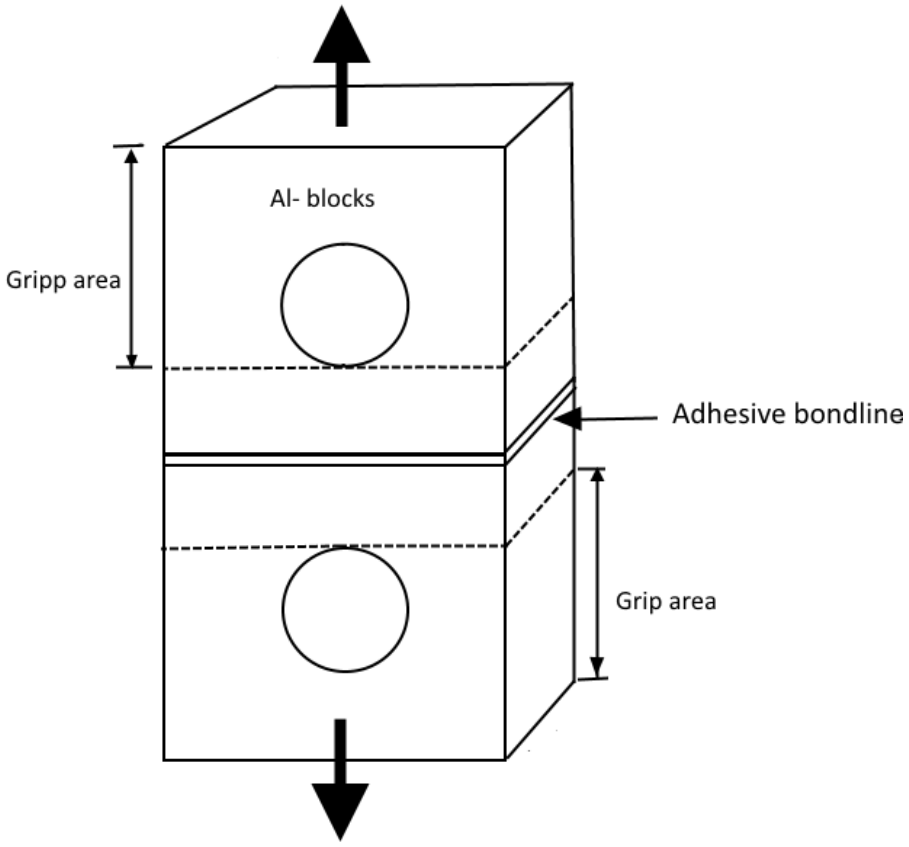

Figure 2.5: Flatwise tensile test coupon

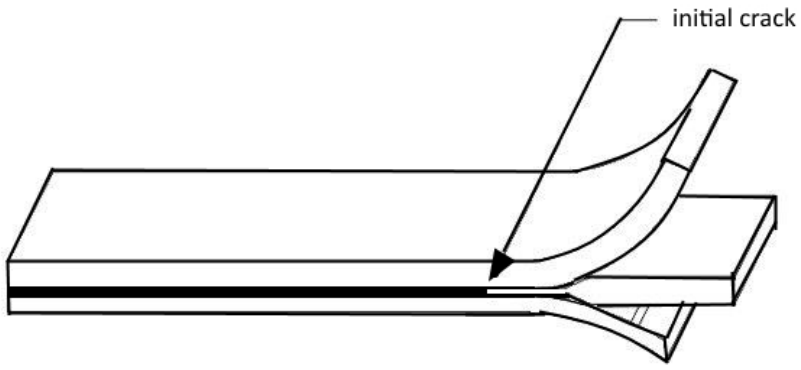

Figure 2.6: Wedge crack test coupon

Table 2.1: Summary of surface treatments for Aluminum alloys, used by previous researchers

Treatments	Type	Reference
Grit blasting by Alumina, Scotch Brite (SB), Abrasion by SiC paper, sand blasting	Mechanical	[14,15,16,17,18]
Phosphoric Acid Anodizing (PAA), Chromic Acid Anodizing (CAA), Sulfo-ferric Acid Anodizing, Boric–sulphuric acid anodizing (BSA), Phosphoric-sulphuric acid anodizing (PSA),	Electrochemical	[19,20,21,15,22]
Solvent base/water base primers, conversion coating i.e. Alodine, Pasa Jell, treatments by Solgel, Silane	Chemical	[16,22,23,10,24,17]

EA 9257, EC3960 [17,22]. Not much information is available on their chemical composition and how this water based primers react with the epoxy of the adhesive. Usually water based primers are less viscous than the solvent based ones. In addition to conversion coating, the primers also affect the strength of the bond between the substrate and the adhesive [16].

2.2 Literature Review

Published literature that have used SLS geometry are reviewed here. To start with effect of SLS test coupon's geometric parameters on measured IFSS is presented. Subsequently, published studies on effect of surface treatment on IFSS are reviewed. This is followed by a review of published studies on durability of bonded joints. This review is focused on bonding of Al substrate.

2.2.1 Effect of SLS Test Coupon Geometry

The various SLS geometry parameters identified in Figure 2.4 and previous section are adherend thickness, adhesive thickness, overlap length, and fillet length. A number of papers were reviewed in this study related to effect of overlap length and adherend thickness, since these were not the focus of our study.

2.2.1.1 Effect of Adherend Thickness

Da Silva [11] had experimentally shown that the failure load (joint strength) linearly increases as the adherend thickness increase. They explained this by plasticity of the adherend (steel) they used. As the adherend thickness increases, the area of resistance of the steel increases and the adherend becomes stronger. Thus the adhesive can develop its full shear strength capacity. This,

of course, is especially valid for the low strength steel because the high strength steel does not easily deform plastically for any thickness [11].

2.2.1.2 Effect of Overlap Length

The overlap length can influence the joint strength (failure load) if yielding occurs in the adherend [25]. Consequent yielding in a metal adherend can cause relative displacements at the aherend-adhesive interface, and if the adhesive is brittle this would cause premature adhesive failure. But ductile adhesive yielding of adherend increases the failure load since the adhesive can utilize its full strength capacity with the adherend yielding [24]. Based on global yielding of the adhesive and on the plastic deformation of the adherend a methodology to predict the failure load of single lap joints has been proposed by Adams and Devies [26] which suggests that the overlap length should be less than a critical value to avoid yielding of the adherend.

2.2.1.3 Effect of Adhesive Thickness

A number of researchers including Da Silva *et al.*[25] have found the bond strength to increase with decrease in the adhesive thickness [4,25,27]. It should be noted that the ASTM D1002 does not suggest any bondline thickness for SLS coupons. There are several proposed arguments in the literature to explain the effect of bondline thickness. Adams and Peppiatt [28] attribute this effect to increased probability of occurrence of defects, such as voids and microcracks, in thicker adhesives. Crocombe [30] shows that single-lap joints with thicker bondline have a lower strength considering the plasticity of the adhesive. He shows that a thicker bond has a more uniform stress distribution than a thin bondline, in which distribution of stress is more concentrated at the ends of the overlap. Although, a thin bondline will reach the yielding stress at a lower load than a thick bondline, when yielding occurs in a thicker joint, there is a less energy

reserve to sustain further loading.Thus, yielding spreads more quickly in a thicker bond joint, which leads to a lower failure strength of the bond joint. Gleich*et al.* [27] and da Silva *et al.* [25] have stated that interface stresses are higher for thicker bondlines. They use a finite element analysis to show that the interface stresses (peel and shear) increase as the bondline gets thicker. They explained that with an increasing bonline thickness the possibility of failure occurring close to the adhesive-adherend interface increases. Thus the higher interface stresses can influence the bond strength. Grant *et al.*[ref] attributed that a decrease in joint strength occurs due to an increase in bending moment due to increase in bond line thickness. For lap joints under tension, there is a longitudinal stress from the direct load together with an additional bending stress due to the load offset. As the applied tensile load increases the bending moment at the edge of the overlap also increases, which in turn increases the stress at the edge of the adhesive. When the stress reaches the strength of the adhesive, the joint fails. This effect of bending stress increases with the thicker adhesive bondline resulting failure of the bond joint at much lower stress levels, i.e. bond strength reduces [31].

2.2.1.4 Effect of Fillet

The available literature on fillet of single lap shear configuration mostly focuses on its effect stress distribution rather than focusing on their effects on interfacial shear strength (IFSS) of bonded joint. Muhamet [32]has studied the effect of spew fillets on failure load of SLS test coupons and have concluded that the spew fillet in SLJs subjected to tensile loading increased the load-carrying capacity of the joint significantly.

The stress distribution in SLS is not uniform. Shear and peel stresses concentrate at the overlap edgescausing a very small amount of load transfer to the centre of overlap [27,29]. The application of fillets at the overlap edges is attributed to overcome the stress concentration problem. Fillets allow the redistribution of stresses in the edge regions and, as a result, they increase the strength of bonded units. Tsai [ref] attributed this redistribution to the ability of the spew fillet to carry some shear stresses and thus plays a part in transferring some longitudinal load from one adherend to other [32,30]. Fillets usually extend over the adherend width, minimizing peak peel and shear stresses at the overlap edges [29]. The single lap shear specimen geometry by ASTM D 1002 recommends use of 3 mm fillet and tabs at the end of adherends to avoid stress concentration and bending issues.

2.2.2 Effect of Surface Treatments on IFSS

Numerous studies have been done on the effect of surface treatments on IFSS since 1980s and most of them are reviewed in a review paper by Park [23]. These studies have used a variety of adhesives, which are high temperature curing adhesive. The details from these studies are summarized Table 2.2. It is observed that the mechanical abrasion treatments are often used with primer and conversion coatings. It is also noticeable from the table that the bondline thickness and mode of fracture is not always reported. And if reported, the fracture mode is not cohesive rather than interfacial making the reported IFSS to be an apparent IFSS, which makes it difficult to compare the IFSS as a function of various surface treatments.

Table 2.2: Effect of various surface treatments on IFSS

Treatment	**Adhesive**	**Cure T, time**	**Bondline Thickness**	**IFSS (MPa)**	**Fracture mode**	**Reference**
Grit Blasting	3M's AF163	135 ^{o}C, 1 hour		40	Cohesive	[16]
Gritblast+primers (EC3924, EA9263, Melt Bond 6723)	AF163	135 ^{o}C, 1 hour		37-46	Cohesive	[16]
Alodine	820688	RT, 7days		7.79		[24]
Alodine (powder)	Betamate XD4600	180^{o}C, 30 mins	0.20	12.5		[10]
Grit Blast+Alodine	AF-163	135^{o}C, 1 hour		35	interfacial	[16]
PAA	EA 9628	120^{o}C 1 hr	0.20	39		[15]
SB +PAA	EA 9628	120^{o}C 1 hr	0.20	47		[15]
PAA+BR127	Film Adhesive	120^{o}C 1 hr		38.75~42	75-100% cohesive	[22]
PAA+EA9257(water based)	Film Adhesive	120^{o}C 1 hr		36~47	75-100% cohesive	[22]

2.2.3 Effect of Environment on IFSS

SLS test coupons have also been used to evaluate the degradation in IFSS under hot and humid environment [4,24,33] and results of such studies are summarized in Table 2.3. The IFSS values in this table correspond to values after exposure to the environment for a certain duration. Many studies do not report either the fracture mode or the adhesive thickness and hence, the IFSS in those cases are apparent IFSS. In cases where cohesive failure is observed, the degradation corresponds to degradation of the adhesive not the interface. These data indicate that moisture degrades the IFSS substantially and in many cases results in almost total loss of strength. Based on these results, it can be concluded that one surface treatment (Mechanical or Alodine or PAA) alone does not offer much protection against moisture. Among these three, mechanical treatment resulted in the maximum loss in IFSS. A combination of these (for example, Mechanical with Aldoine or Mechanical with PAA) together with a primer offers the best protection against moisture.

2.2.4 Effect of Surface Treatments on Durability of Bonded Joints

As mentioned in 2.1.1, WC tests have been used in the past to evaluate the environmental durability of adhesives and bonded joints [21,22]. Crack propagation, in WC test coupons exposed to the hot-humid environment, is monitored as a function of exposure time until crack stops propagating. The increase in crack length for various surface treatments is then compared to evaluate the effectiveness of various treatments. The results from past studies are summarized in Table 2.4. It can be observed in Table 2.4 that single surface treatment (mechanical abrasion, Alodine, PAA) alone resulted in higher crack lengths similar to the result for degradation in IFSS in Table 2.3 [13,31,27]. When mechanical treatment is combined with Alodine or PAA, the crack

Table 2.3: % Reduction in IFSS due to exposure to moisture

Treatment	**Adhesive**	**Cure T, time**	**Test condition**	**% Reductionin IFSS**	**Fracture mode**	**Adhesive Thickness (mm)**	**Ref.**
Grit Blast	AF 163	135 ^{o}C 1 hr	93^{o}C/100 % RH/2 weeks	92.5			[16]
Grit Blast+primers (EC3924, EA9263, Melt Bond 6723) +	AF 163	135 ^{o}C 1 hr	93^{o}C/100 % RH/2 weeks	93.5			[16]
Grit blasting+Alodine	AF 163	135^{o}C 1 hr	93^{o}C/100 % RH/2 weeks	94	Interfacial		[16]
Alodine	820688	RT 7 day	Water immersion	60	Interfacial		[24]
Alodine	EC 2086	200^{o}C 15 min	Water immersion	67	Interfacial		[24]

Treatment	Adhesive	Cure T, time	Test condition	% Reductionin IFSS	Fracture mode	Adhesive Thickness (mm)	Ref.
PAA	EA9628	120°C 1hr	60°C/95-100% RH/30 days	51		0.20	[15]
Scotch Brite+PAA	EA9628	120°C 1hr	60°C/95-100% RH/30 days	62		0.20	[15]
PAA+BR127	Film adhesive	120°C 1hr	60°C/100 % RH/2100 hrs	8.3~52.6	75-100% cohesive		[22]
PAA+EA9257 (water based)	Film adhesive	120C 1hr	60°C/100 % RH/2100 hrs	16~63	75-100% cohesive		[22]

Table 2.4: Crack propagation lengths, during exposure to hot-humid environment, for various surface treatments

Treatments	**Adhesive**	**Cure T,Time**	**Environment**	**Crack length (mm)**	**Fracture mode**	**Thickness (mm)**	**Ref.**
Grit blast	AF 163	135°C 1 hr	60°C/ 100%RH	66			[16]
Alodine	AF 163	135°C 1 hr	60°C/ 100%RH	97			[16]
Alodine	Betamade D4600	180°C 30 min	40°C/ 100%RH	74			[10]
SB (Scotch Brite)	AF377	120°C 2hr	35°C/ 99%RH	66			[17]
SB+ALodine	AF377	120°C 2hr	35°C/99%RH	31			[17]
SB+ALodine+ EC 3960	AF377	120°C 2hr	35°C/ 99%RH	11			[17]
SB+PAA	AF377	120°C 2hr	35°C /99%RH	9			[17]
SB+PAA+ EC3960	AF377	120°C 2hr	35 C/99%RH	6			[17]
PAA	EA9628	120°C,60 min	60°C/ RH95-100%	After 72hr debonded		0.20	[15]

Treatments	Adhesive	Cure T,Time	Environment	Crack length (mm)	Fracture mode	Thickness (mm)	Ref.
				completely			
PAA+BR127	AF 163	135°C, 1hr	60°C/ RH100%	40			[23]
	FM73	135°C, 1hr	60°C/ RH100%	39			[23]
	FM 73	120°C, 1hr	60°C/ 100%RH	33	Cohesive		[22]
	FM300	120°, 1hr	60°C/ RH100%	41.5	90% cohesive		[22]
	EA9628	120°C, 1hr	60°C/ RH100%	36.5	cohesive		[22]
	FM 94	120°C, 1hr	60°C/ RH100%	38.5	cohesive		[22]
PAA+water based primer	FM 73	120°C, 1hr	60°C /100%RH	38	75-100% cohesive		[22]
	FM 300			45			
	EA 9628			38.5			
	FM 94			38			

length reduced further [27]. Both water based and solvent based primers resulted in the least crack extension and exhibited almost comparable crack length and fracture mode. Finally, since the fracture mode was not reported, it is not clear if the published results correspond to environmental durability of the adhesive or the interfacial bonding.

In WC test coupons cracks propagates under tensile stress (Mode I) state [34,35], whereas the IFSS is measured under predominantly shear stress (Mode II) state. Hence, direct correlation between the reduction in IFSS and crack propagation length is not possible. Hence, degradation in tensile strength of bonded joints is required in addition to degradation in IFSS to evaluate the wedge test results and the effect of surface treatments on environmental durability of a bond. But such correlation has not been found in the literature.

2.3 Summary of Literature Review and Knowledge gap

Based on the literature review presented in the previous sections, the following knowledge gap was found.

- Published studies have used high temperature curing adhesives and primers and hence, applicability of these research results on the effect of surface treatments on room temperature curing adhesive and primers, which are of interest to this thesis, is not known.
- No research has been done yet to evaluate the effectiveness of using high temperature primers in combination with room temperature curing adhesive

- While discussing the effect of surface treatments on IFSS, the mode of fracture is not commonly reported and used in the evaluation. If the fracture is not interfacial, the IFSS can only be termed as the "apparent" IFSS and any observed difference in IFSS cannot be interpreted as the effect of surface treatments.
- Effect of surface treatment on environmental durability of bonded joints has been studied using WC test. Whether this reflects the environmental durability of the adhesive or the interfacial bond is not very clear since fracture mode is not mentioned in these studies. While environmental degradation of IFSS has been studied, it could not be used to interpret the environmental durability results since the former is under shear stress state the latter is under tensile stress state. Environmental degradation of the tensile strength of the interfacial bonding is required and this has not been studied.

2.4 Thesis Objectives

The goal of this thesis is to determine the optimal surface treatment that would maximize the room temperature bonding between an Al substrate and a composite adhesive as well as maximize the environmental durability of this bond. Literature review presented in this chapter indicates that the published studies were on high-temperature bonding and the applicability of these results to room temperature bonding is not known. Hence, based on the knowledge gaps identified in 2.4, the objectives, presented in 1.1 are proposed to achieve the goal of this thesis. These are presented again below for convenience.

a) Determine the optimal single lap shear test condition that maximized interfacial (i.e. adhesive) failure mode

b) Using this optimal test condition, evaluate the effect of various surface treatments on the strength of bond between an Al substrate and a room temperature curing polymer composite rub-strip, which is a thermoset epoxy adhesive reinforced with glass fibers

c) Using Wedge Crack test, evaluate the durability of bond, between the Al substrate and the composite rub-strip, under hot-humid environment

d) Study the degradation in IFSS by SLS test and tensile strength using Flatwise Tensile test of this bond, under the same hot-humid environment used in (c) and use the results to interpret the wedge test results

e) Using results from (b)-(d), determine the optimal surface treatment for room temperature bonding of the polymer composite rub-strip to the Al substrate.

Chapter Three

Experimental Details

The details on materials, manufacturing, and experiments performed to fulfill the thesis objective are described in this chapter. Section 3.1 details the manufacturing procedure used to prepare test coupons. Section 3.2 describes the procedures of various tests completed as a part of this thesis.

3.1 Test Coupons

Three test coupon geometries, illustrated in Figure 3.1, were used in this study. The SLS (Single Lap Shear) test coupons were used to measure the IFSS (Interfacial Shear Strength) of the bond between the Al substrate and the composite rub-strip. FWT (Flat Wise Tensile) test coupons were used to measure the tensile strength of the bond. WC (Wedge Crack) test coupons were used to measure the crack growth in a hot-humid environment to assess the environmental durability of the bond. The materials, the surface treatments, and the manufacturing procedure used in preparing these test coupons are detailed in sections 3.1.1, 3.1.2, and 3.1.3 respectively.

3.1.1 Materials

Aluminum 6061-T6 was used as the substrate. Flat panels of thicknesses 1.6 mm and 3.2 mm were purchased from a local supplier and were used to manufacture the SLS and WC test coupons. Additionally, blocks with square cross-section (50 mm x 50 mm) were purchased and used to manufacture FWT test coupons. Glass fiber filled epoxy adhesive (Henkel Hysol EA 9891RP) was used as the composite rub-strip whose bonding with the Al substrate was investigated in this study. For primer treatment two high temperature curing primers were used,

Cytec's BR 127 and 3M's EC3901. The recommended cure temperature for BR127 is 120^{o} C and for EC3901 is 90^{o} C. In addition to primers, one conversion coating was used which is TOUCH-N-PREP ALODINE 1132 pen from Henkel.

3.1.2. Surface Treatments

The Al substrate of all test coupons was subjected to following treatments prior to bonding with the rub-strip.

1. Untreated: Aluminum panels and blocks were degreased with acetone followed by mechanical abrasion using 120grit Alumina cloth. The panels were further cleaned by wire brush and forced air to remove any loose particle. The panels were finally wiped clean with acetone and dried in air at room temperature.

2. Alodine Treatment: TOUCH-N-PREP ALODINE 1132 pen from Henkel was used to coat the surfaces of the untreated Aluminum panel and blocks with Alodine conversion coating, followed by air drying at room temperature. Four layers of coating were applied with a wire brush. Each consecutive coating was applied at 90 degree angle with respect to the previous one. Each layer was allowed to dry in air before applying the next coat. Since the chemical composition of Alodine 1132 pen is proprietary, no data is available on its composition.

3. Phosphoric Acid Anodizing (PAA): Phosphoric Acid anodizing of untreated panel and blocks was done in a solution of 9-12 wt% phosphoric acid and 88-91wt% distilled water (concentration of phosphoric acid was 85%) using 10 Volt (DC) as per ASTM D 3933 for 20-25 minutes.

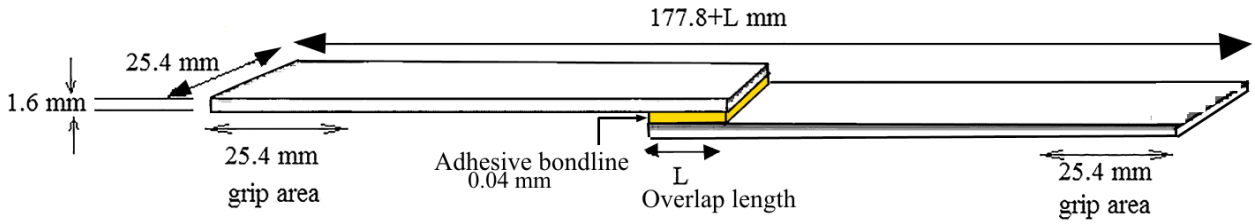
177.8+L mm
25.4 mm
1.6 mm
25.4 mm
grip area
Adhesive bondline
0.04 mm
L
Overlap length
25.4 mm
grip area

(a)

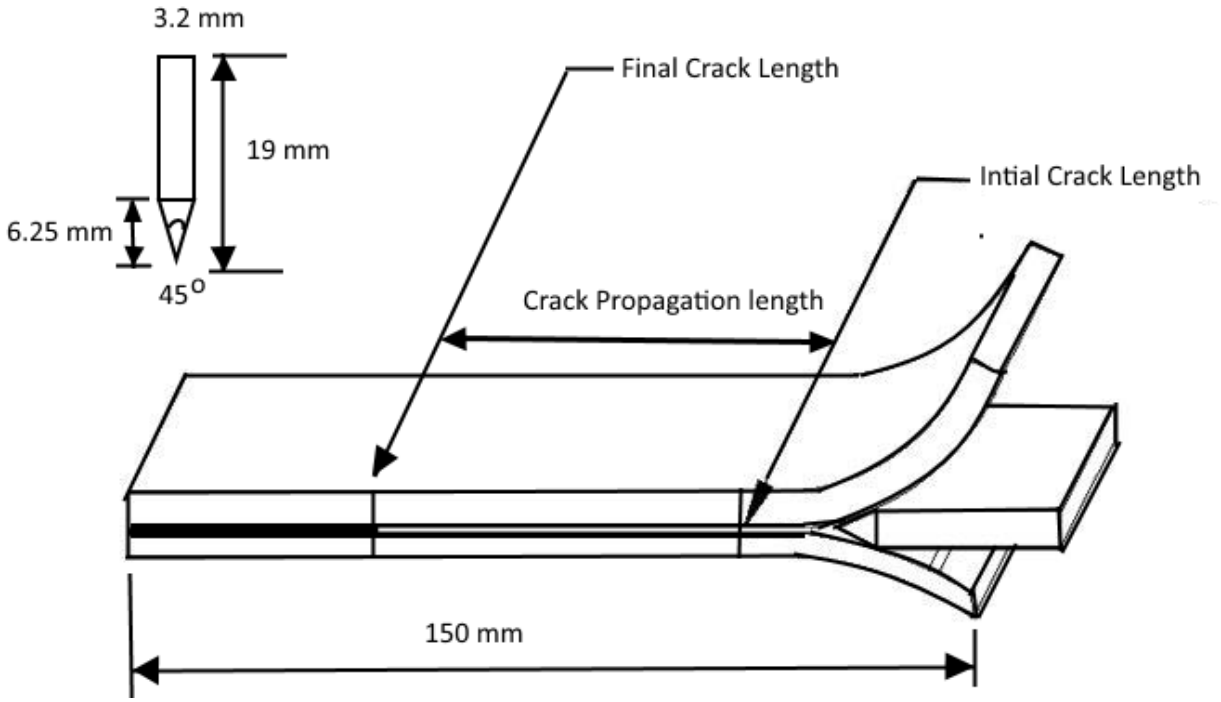
3.2 mm
19 mm
6.25 mm
45°
Final Crack Length
Intial Crack Length
Crack Propagation length
150 mm

(b)

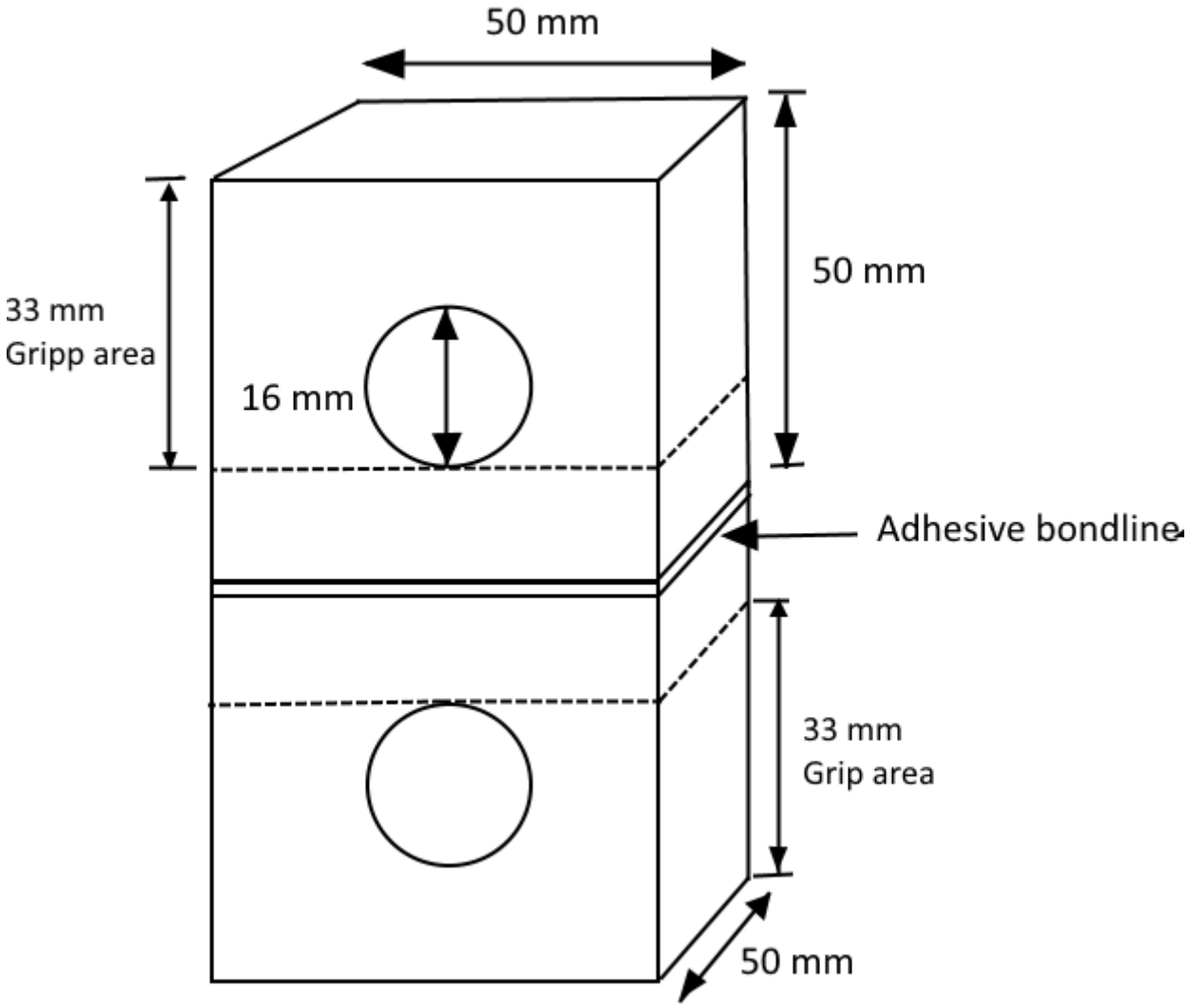

(c)

Figure 3.1: Schematic of (a) single lap shear test coupon, (b) wedge crack test coupon, (c) flat wise tension test coupons

It was a single-rack process where pH of the solution was maintained at 4.2. The pH of the solution was monitored every 4 weeks using pH meter from Hanna Instrument, Canada. If the pH diverged from 4.2, that solution was discarded and a new solution was prepared. The inside of a plastic tank was wrapped with aluminum foil and this wrapped tank was filled with PAA solution and the aluminum foil acted as the cathode as shown in Figure 3.2. The Al blocks or panels were immersed in solution hanging from a glass rod with the help of Al-wire. The Al-panels acted as anode in this process. The anode (Al-panel) was connected to the positive terminal of a DC power supply 382202, from EXTECH, using alligator clips and Al wires. The negative terminal of the power supply was connected to the Al foil (cathode) using another alligator clip and Al wires. After completion of anodizing, panels were rinsed in water and carefully watched for any water breaking on the treated surface. If the water uniformly wetted the Al surface without any breakage, the panels were allowed to be dried at 60^{o}C in an oven immediately. Any treated panel that did not pass the water break test were anodized again in PAA solution. The dried panels were used immediately for bonding to avoid any contamination.

4. Primer Application: After Alodine and PAA treatments, some panels and blocks were brush coated with Cytec's BR 127 and 3M's EC3901 primers. Three coatings were applied for BR127. Each coating was allowed to completely dry in air before the application of next coating. For EC3901 four coatings were applied in same manner as BR127. The BR127 coated test coupons were dried in air in a fume hood for 30 minutes followed by an oven curing for 60 minutes at 120^{o}C using Blue M Electronics oven from General Signal Company.

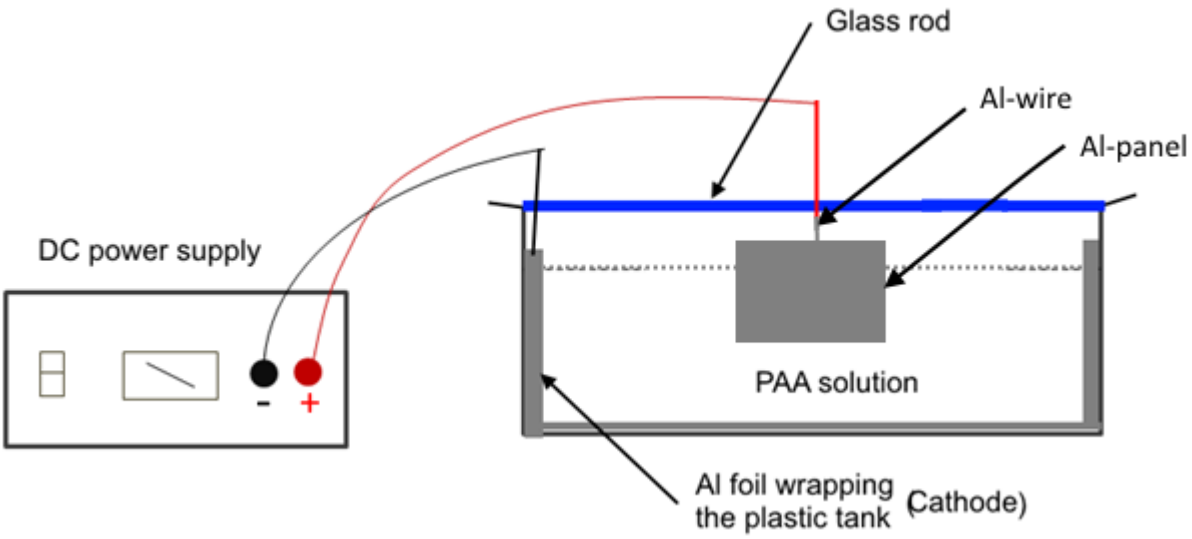

Figure 3.2 Schematic of PAA process

The EC 3901 coated test coupons were dried in air in a fume hood for 1 hour followed oven curing for 30 minutes at 90^{o}C. In order to evaluate the effect of curing at room temperature, some panels coated with both primers were air dried in fume hood (without subsequent oven curing) for 24 hours. Some untreated panels were also primed with BR127 and EC 3901 using the procedure discussed above.

3.1.3. Manufacturing

3.1.3.1 Cure Kinetics of Composite Adhesive

In order to determine the time required for complete curing of the composite rub-strip at room temperature, cure kinetics of the rub-strip was characterized using TA Instrument's Q2000 DSC (Differential Scanning calorimeter) as per ASTM D3418.The uncured composite adhesive was ramped at four ramping rates (5^{o}C, 7^{o}C, 10^{o}C and 20^{o}C per minute) from -40^{o}C to 200^{o}C and the resulting exothermic heat was recorded. A typical result for a ramp rate of 20^{o}C/min is shown in Figure 3.3. Using isothermal cure test, it was confirmed that this composite exhibited n^{th} order cure kinetics, represented by the following equation

$$\frac{d\alpha}{dt} = K(T)[1-\alpha]^n \tag{3.1}$$

where $d\alpha/dt$ = reaction rate (1/sec)

α = fractional conversion (degree of cure)

$k(T)$ = specific rate constant at temperature T

n = reaction order

Using equation 3.1, the ramp data for four different ramp rates, and the Isothermal Cure Kinetics software in the DSC, isothermal conversion curves were determined for various cure

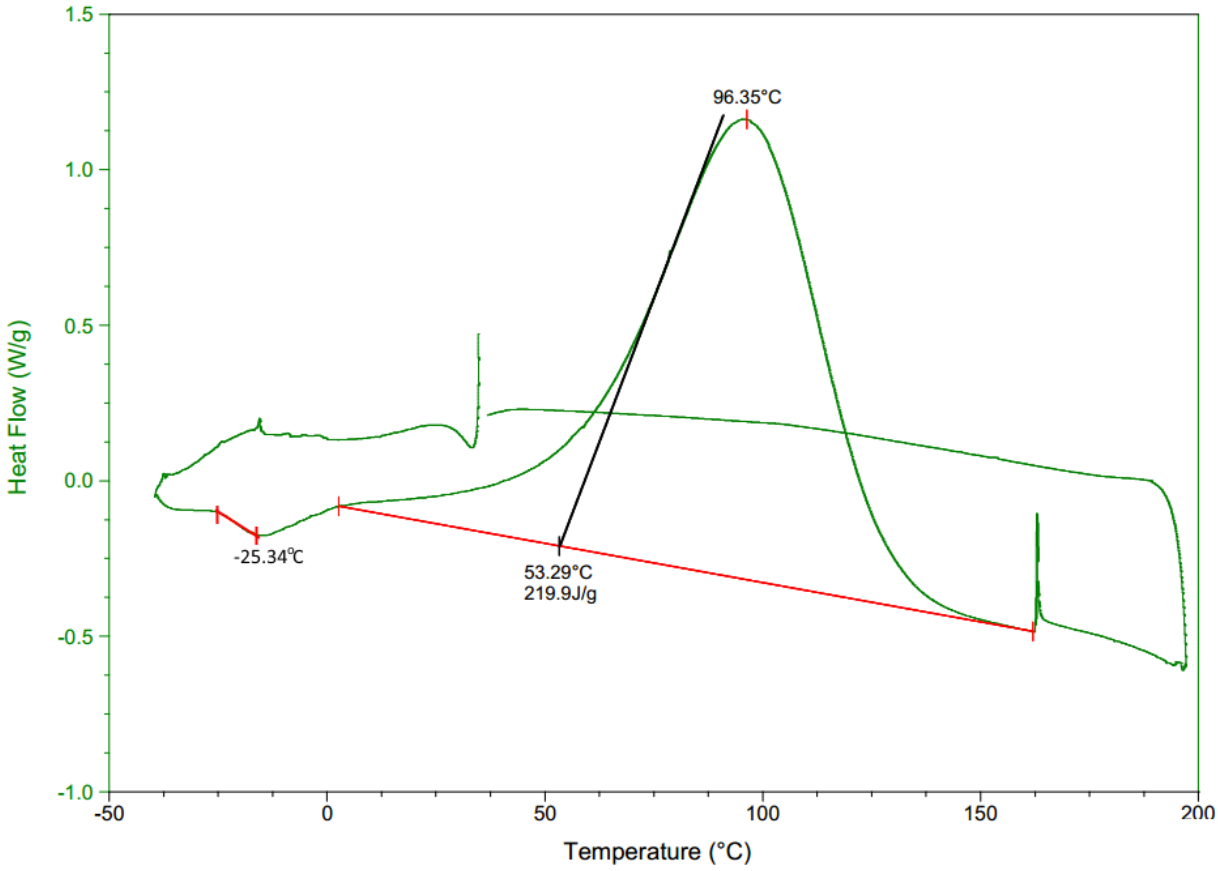

Figure 3.3: DSC plot showing exothermic heat evolution during a ramp test at the rate of 20^{o}C/min

temperatures, as shown in Figure 3.4.It can be inferred that a curing time of ~17-18 minutes is required for complete curing at room temperature.

The above prediction does not take into account the "vitrification" effect that slows/stops the curing when the T_g (Glass-to-Rubber transition temperature ~ -25^{o}C for uncured composite as shown in Figure 3.3) reaches the cure temperature. Hence, the bonded panels were cured for 24 hours to maximize the curing, before cutting and testing. A sample of the cured epoxy composite scraped out of a bonded cured panel was ramped at 10^{o}C/min in the DSC from -40^{o}C to 200^{o}C to confirm that no residual curing occurred. The plot is presented in Figure 3.5 shows absence of any exothermic peak confirming that a cure time of 24 hours is sufficient for complete curing of the epoxy composite.

In addition, the IFSS of the test coupon cured at room temperature was measured and compared with that cured at 50^{o}C, using SLS (Single Lap Shear) and DLS (Double Lap Shear) test coupons. Results shown in Figure 3.6 confirm that IFSS for curing at room temperature is same that for curing at 50^{o}C, which also indirectly confirms that a cure time of 24 hours at room temperature is sufficient to achieve complete curing.

3.1.3.2 Bonding of Test Coupons

The composite adhesive was supplied in two parts, glass fiber reinforced epoxy (Part A) and hardener (Part B). The reinforced epoxy and binder were mixed at a ratio of 2.5:1 at room temperature. The curing process was exothermic and this heat evolution was also accelerated the curing process. The viscosity of the as-received material was high at room temperature, which

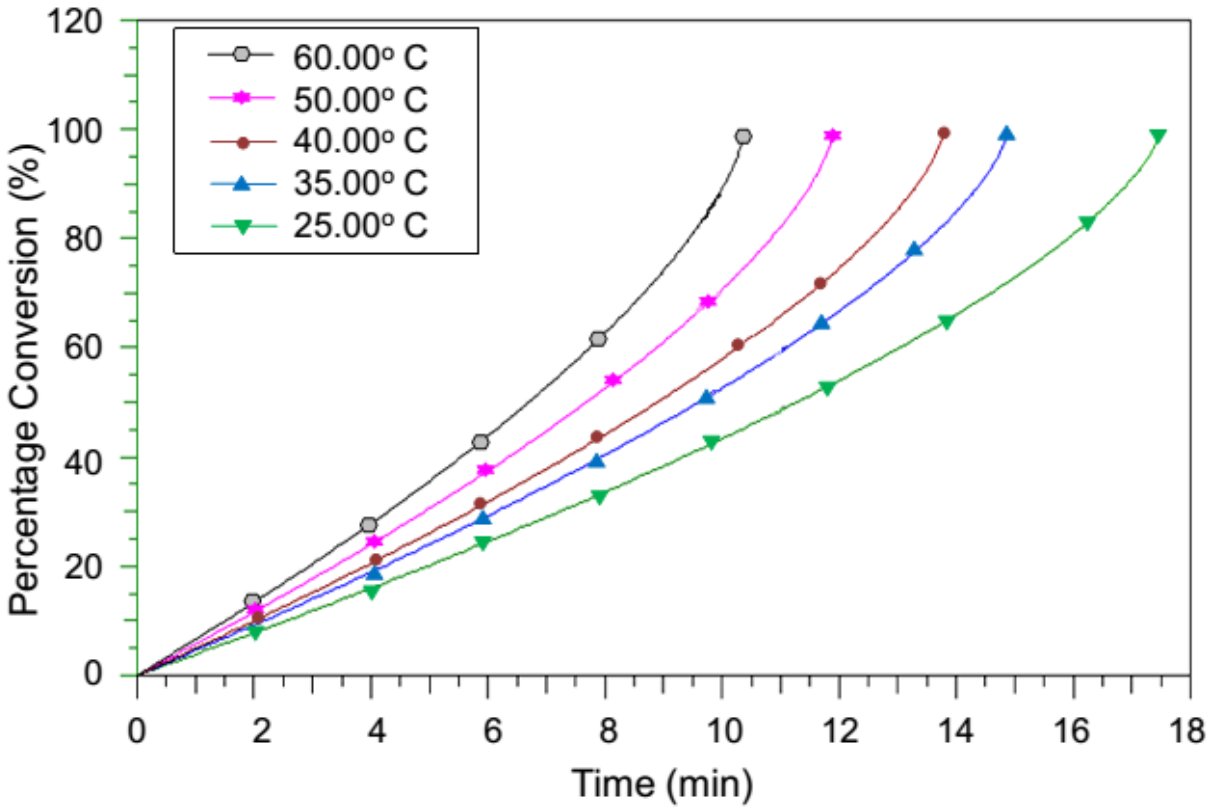

Figure 3.4: Iso-thermal conversion curves for the composite adhesive calculated at various isothermal cure temperatures

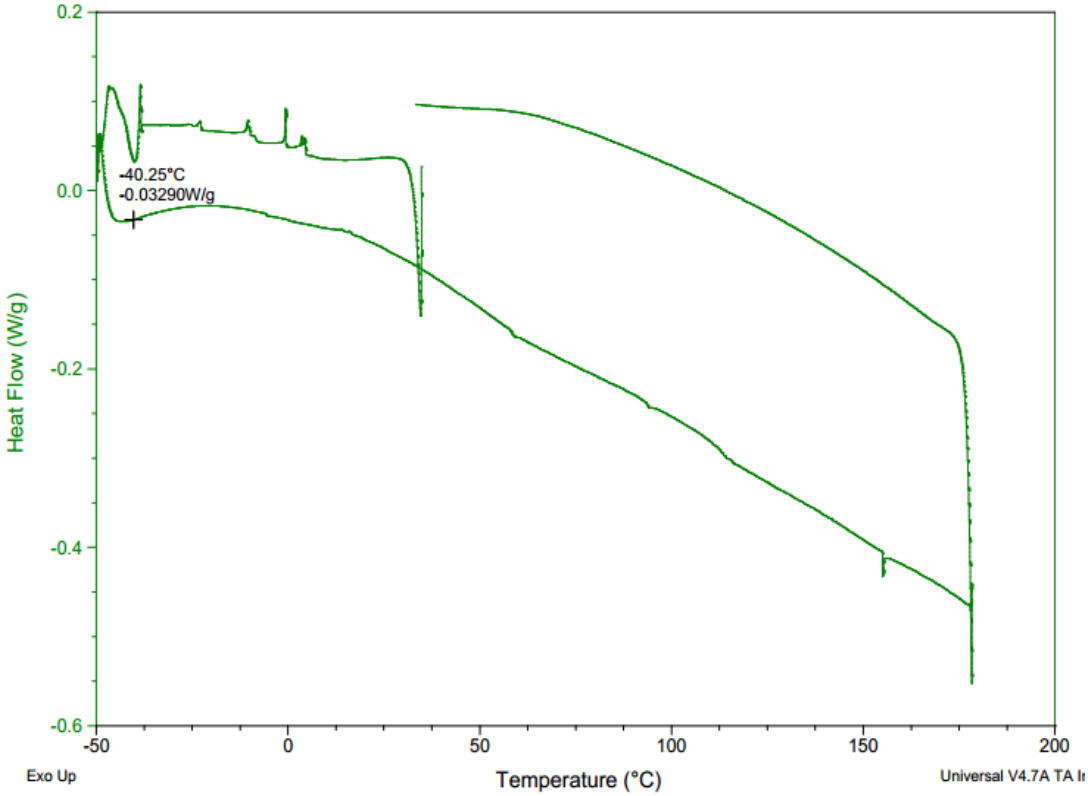

Figure 3.5: DSC plot showing heat flow during a ramp test, at the rate of 10^{o}C/min, of a cured composite sample

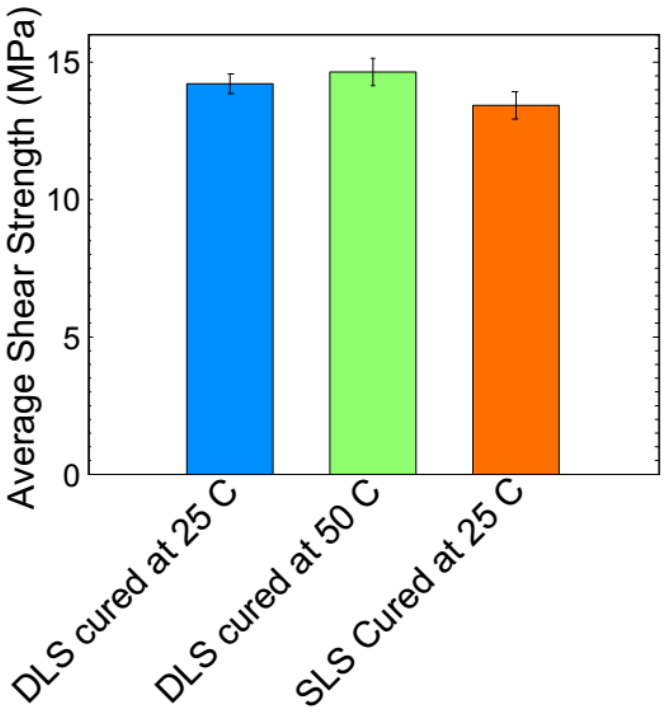

Figure 3.6: IFSS at two cure temperatures

was increased as the curing progressed. A rapid rate of curing due to exothermic heat evolved during mixing made difficult the spreading of the mixed material on the Al substrate. In order to prevent this, mixing of composite adhesive was always done over a cold plate. After mixing it was applied immediately to the surface treated panels and blocks.

3.1.3.2.1 Single Lap Shear (SLS) Test Coupons

The effect of thickness on IFSS was studied in this study using SLS test coupons and the bond-line thickness used in this study varied from 0.04mm to 0.32 mm. While test coupons with bond-line thickness over 0.15 mm were bonded using a metal mold as shown in Figure 3.7, the test coupons with thickness less than 0.15 mm were bonded using a hydraulic press.

The molds were designed to *(a)* keep the panels in place and prevent them from bending due to load applied to the mold, and *(b)* to achieve desired and uniform bond-line thickness. To prepare SLS test panels, two 4 inch x 6 inch Al panels were used. After surface preparation, the mixed composite adhesive was applied on one end of both panels as shown in Figure 3.7. First, the bottom panel(Al-1) was placed on the bottom half of the mold. The top panel (Al-2) was then placed over the two offset blocks 1 and 2as shown in Figure 3.7. These offset blocks provided the desired adhesive thickness (7 as shown in Figure 3.7) by lifting the top panel (Al-2). The top half mold was placed and locked carefully thorough the dowel pins (3-5 shown in Figure 3.7). The offset clamping block 6 was used to maintain the desired adhesive thickness by holding the bottom panel, Al-1 in place. After locking the two mold halves together, required load was

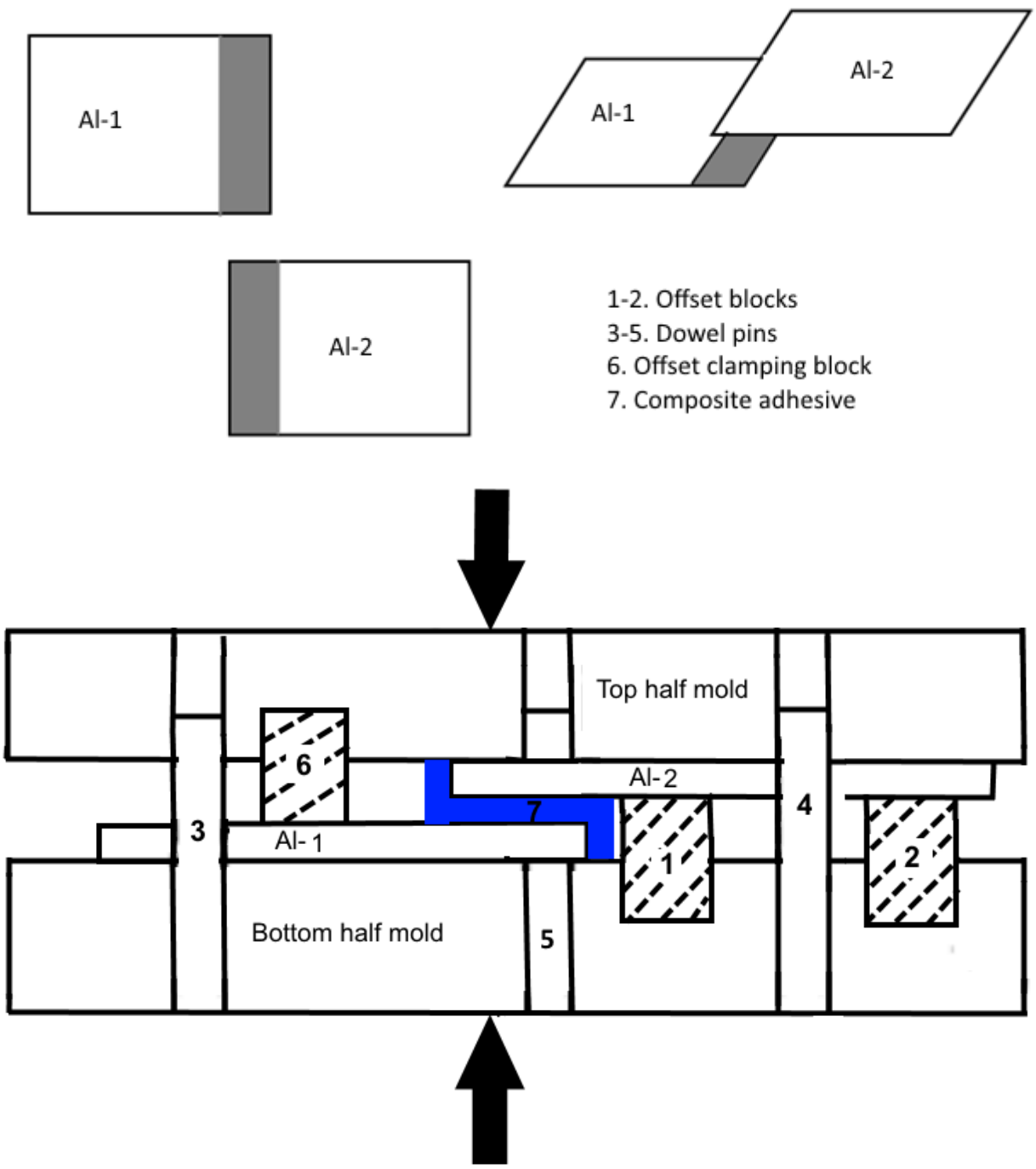

Figure 3.7: Bonding process of SLS test panel mold assembly to manufacture SLS test coupons with bond-line thickness over 0.15 mm

placed over the top half mold. Load, varying from 40 Kg to 80 Kg, was used to manufacture SLS panels with bond-line thickness from 0.15 mm to 0.32 mm. The adhesive bond-line thickness decreased as the load increased. From each surface treatment, one 4 in x 6 in SLS panel was manufactured.

A schematic of the set-up used in manufacturing test coupons with bond-line thickness less than 0.15 mm is shown in Figure 3.8. These test coupons were manufactured using a hydraulic press G50H 24 CLX from WABASH MPI, USA. Two 4 in x 6 in surface treated Al panels with a thickness of 1.62 mm were applied with composite adhesive. First an Al panel of similar dimension (4 in x 6 in and 1.62 mm thick, shown as 3 in Figure 3.8) was placed on bottom mold plate (indicated by 5 in Figure 3.8) inside the press. This was used to support the top Al- panel to prevent it from bending (shown as 1 in Figure 3.8). The bottom Al- panel (indicated as 2 in Figure 3.8) was then placed on the mold plate beside the supporting Al- panel, and then the top Al-panel was placed over them as shown in Figure 3.8. Finally the top mold plate was placed on the top of the bonding assembly. During manufacturing the adhesive was allowed to squeeze out freely. The hydraulic press platen pressure was varied in the range of 1 to 3 tons to achieve various desired bond-line thickness. Any squeezed adhesive, along the bonded edge of the panels was carefully removed to result in test coupons without any fillet.

After discarding the two coupons at either end of the panel as per ASTM 1002, the 4 in x 6 in bonded Al-panels were cut using a diamond saw to yield 4 test coupons per batch as shown in Figure 3.1 (a). The edges of these cut coupons were ground using 180 SiC papers before testing.

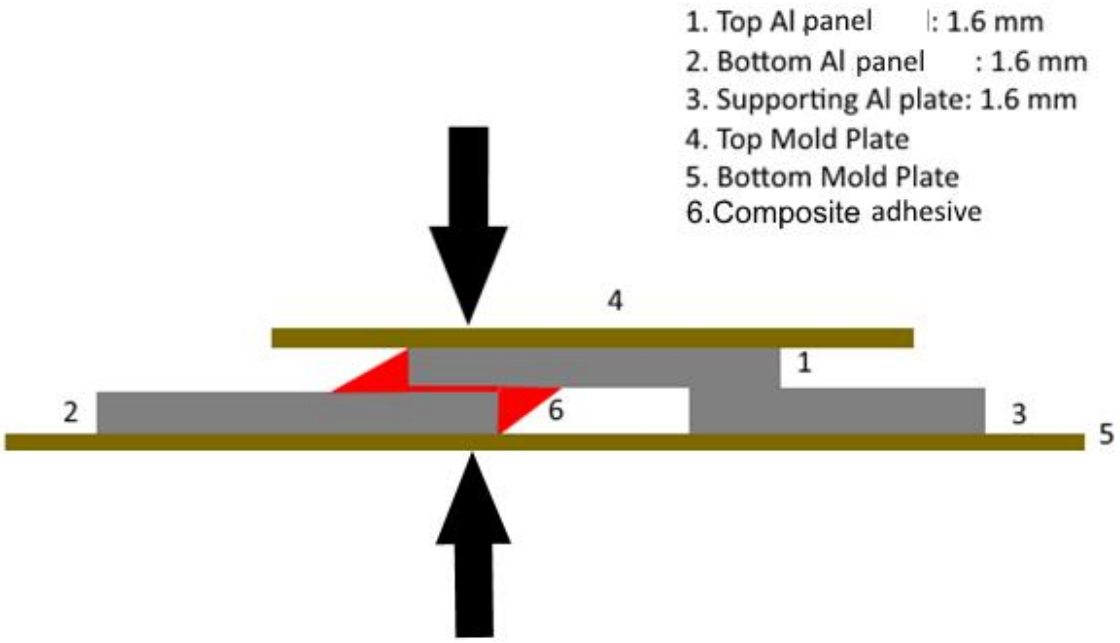

Figure 3.8: Bonding assembly for single lap shear panel manufactured in the hydraulic press

3.1.3.2.2 Flat Wise Tension (FWT) Test Coupons

FWT test coupons were manufactured and tested according to ASTM C 297. The mixed composite adhesive was applied on treated surface of Al-blocks. Bonding was done in the hydraulic press as per the schematic in Figure 3.9 (a). A sheet of silicone was spread over the assembly to ensure uniform application of pressure over the bonded region. A pressure of 3 tons was used to achieve a bond-line thickness of 0.04 mm. The composite adhesive was allowed to squeeze out freely and scraped out with a knife. In Figure 3.9 (b) a bonded and cleaned FWT test coupon is presented.

3.1.3.2.3 Wedge Crack (WC) Test Coupons

Manufacturing of WC test coupons was done according to ASTM D3762 using the hydraulic press as shown in Figure 3.10 (a). Two 6 inch x 6 inch Al panels of 3.2 mm thickness were used to manufacture each of the WC test panels. The panels were applied with adhesive and stacked as shown in Figure 3.10 (b) over a bottom mold plate. A sheet of silicone was placed over the stacked panels and a top mold plate was placed over the entire assembly. A small piece of flash breaker tape was placed between the two panels along one edge to create spacing for inserting the wedge. A bond-line thickness of ~0.04mm-0.05 mm was achieved using a pressure of 3 tons. The 6 in x 6 in bonded Al-panels were cut using a diamond saw to yield 4 test coupons per batch as shown in Figure 3.10 (b), after discarding the two coupons at either end of the panel as per ASTM D3762. The edges of these cut coupons were ground using 180 SiC papers before testing. Subsequently, 19 mm long wedges were inserted manually as shown in Figure 3.10 (b) to obtain the starter crack as well as to provide the crack opening force during durability test.

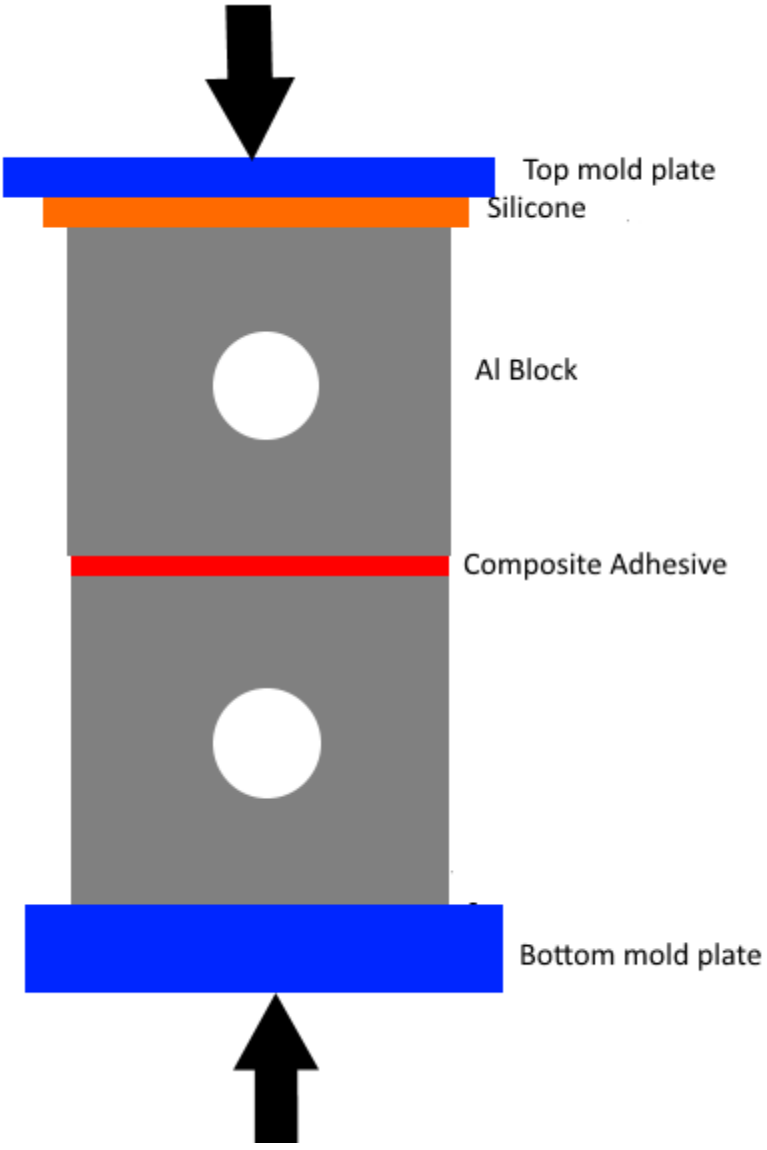
Top mold plate
Silicone
Al Block
Composite Adhesive
Bottom mold plate

(a)

(b)

Figure 3.9: (a) Bonding assembly for manufacturing FWT test coupons in the hydraulic press

(b) Bonded FWT coupon

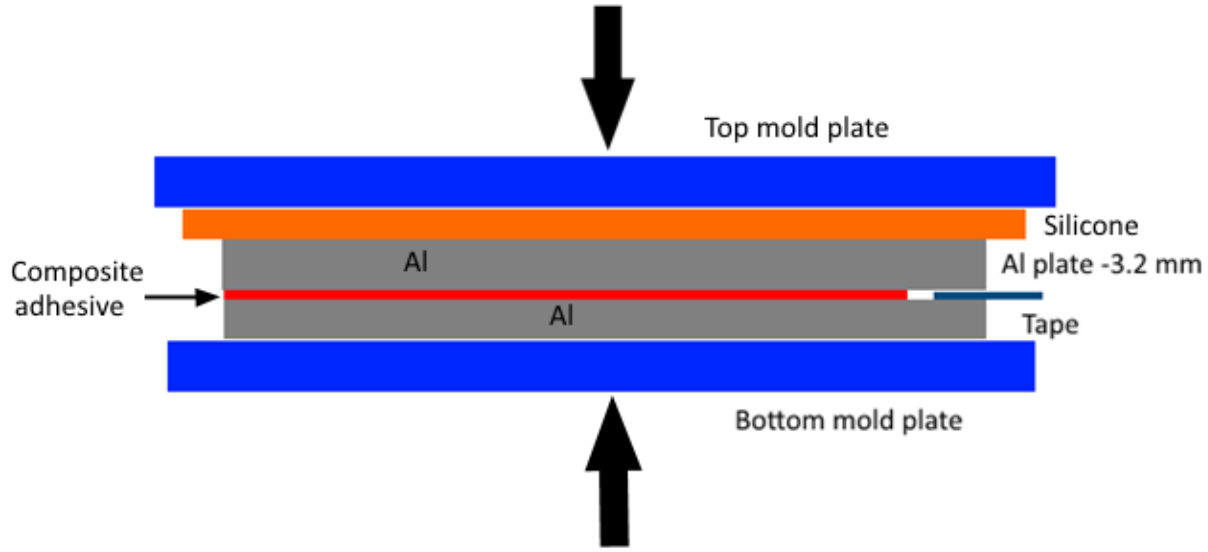

(a)

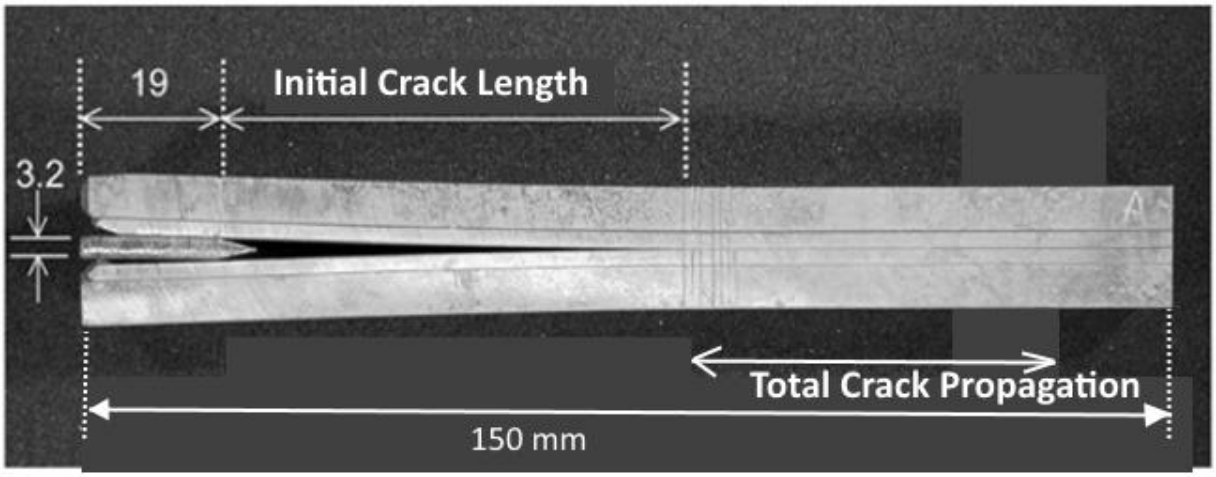

Figure 3.10: (a) Bonding assembly for WC panel(b) WC test coupon

3.2 Test Procedure

3.2.1 Environmental Conditioning

Environmental durability of the bond formed after various surface treatments was evaluated using a hot-humid environment of 95% humidity at a temperature of 40^{o}C. This environment was achieved using ZBHD-2022 environmental chamber from Associate Environmental System, USA. This environmental chamber is capable of holding % relative humidity from 10%-95% and hold or cycle temperatures from -70^{o}C to +120^{o}C. During conditioning treatment, the composite adhesive continually absorbed the moisture until a saturation amount was reached. Time to reach saturation was determined and used to select the conditioning time. The SLS and FWT test coupons conditioned to various times were subsequently tested to determine the IFSS and tensile strength of the conditioned test coupons. In addition, crack growth in the WC test coupons were monitored as a function of conditioning time.

3.2.1.1 SLS Testing

The single lap shear testing was carried out using Instron's 5550R screw driven load frame equipped with a ±25 kN load cell and the data was acquired using Instron'sBluehill software version 2.5. The two arms of the SLS test coupons are separated by the thickness of the bond-line. The regular grips and the cross-heads of the Instron are aligned and hence, the arms of the SLS test coupons would have to be bent to be clamped by the regular grips, resulting in bending of the joint. In order to avoid this, a special tension grip, as shown in Figure 3.11 was machined and used for clamping the SLS test coupons. The fixed face of the top grip was off-set from the fixed face of the bottom grip by distance equal to sum of twice the thickness of Al substrate (2*1.6 mm) and maximum bond-line thickness (0.32 mm). The movable faces of the grips were

used to clamp the two ends of the test coupon against the fixed faces as shown in Figure 3.11. When clamped, the center-line of the SLS test coupon with 0.32 mm bond-line thickness was aligned with the center-line of the top and bottom cross-heads of the load frame as shown in Figure 3.11. In order to accommodate test coupons with bond-line thickness less than 0.32 mm, steel shims with varying thickness were used. In Figure 3.12 special test grips with SLS test coupon is presented.

In order to confirm the effectiveness of this new grip, SLS test coupons were tested using regular grips of Instron and the special grip. The IFSS using regular grips was 9.68 MPa while that using special grips was 13.62 MPa. Since bending reduces IFSS, higher value obtained using the special grips confirms reduction in bending when special grips were used. Although any mis-alignment during gripping using regular grips was eliminated, the load path was yet off-set by a distance equal to bond-line thickness since the two Al substrates were off-set from the center-line by a distance equal to half of the bond-line thickness. Hence, the bending effect due to this would influence the IFSS. In order to evaluate this effect, IFSS measured using SLS testing was compared with that using DLS (double lap shear) testing. The off-set is non-existent in the latter, and hence, the IFSS from DLS testing represents a value without the effect of bending. A set of DLS test coupons were prepared with the same adhesive thickness and tested according to ASTM D3528 as shown in Figure 3.13.

The IFSS for DLS test coupon was 14.22 ± 0.68 MPa while that from SLS test coupons was 13.62 ± 0.44 MPa, for a bond-line thickness of 0.25 mm. Although these values are close, the difference between the two values is believed to be due to the effect of bond-line thickness. This

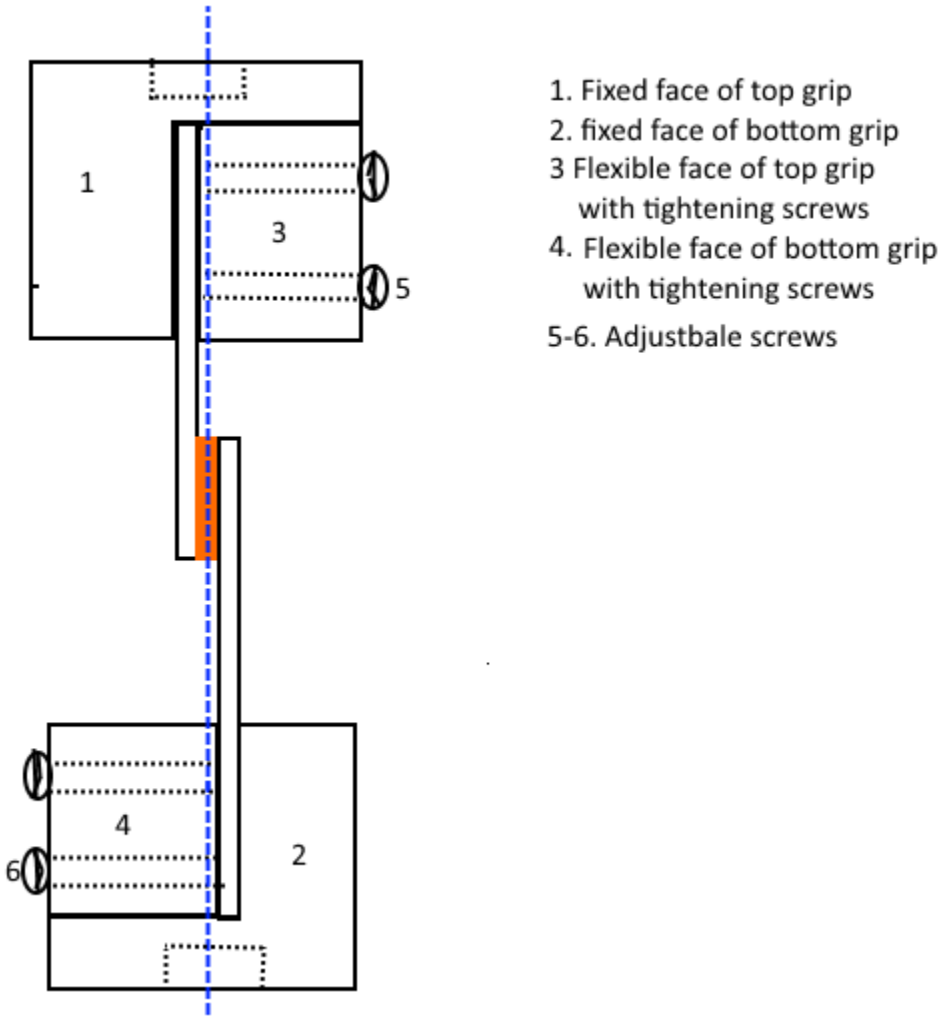

Figure 3.11: Schematic of test assembly of SLS test coupons with specially machined grips

Figure 3.12: Test assembly of SLS test coupon

effect of thickness on the IFSS measured using SLS testing is discussed further in the next chapter to delineate the effect of bond-line thickness.

SLS testing was performed according to ASTM D1002 at across head displacement rate of 0.05 inch/min. A typical load versus displacement plot is shown in Figure 3.14. The maximum load corresponds to the failure of the bond and was used along with the following equation to determine the IFSS.

$$\text{IFSS} = \frac{FailureLoad}{BondedArea} \tag{3.2}$$

The SLS testing was repeated using test coupons subjected to various surface treatments and environmental conditioning durations tabulated in Table 3.1. For each surface treatment or environmental conditioning duration, four test coupons were tested and the average value is reported.

3.2.1.2 FWT Testing

The FWT testing was carried out using Instron 8562 servo hydraulic load frame equipped with a ±250 kN load cell and flatwise tensile sandwich panel test fixture from Wyoming Test Fixture, USA. The test set-up is shown in Figure 3.15. The data was acquired using Wave Matrix software from Instron. The FWT test coupons were tested at a cross head displacement rate of 0.5 mm/s as per ASTM C 297. A typical load versus displacement plot is shown in Figure 3.16 The maximum load corresponds to the failure of the bond and was used along with the following equation to determine the tensile strength.

$$\text{Tensile Strength} = \frac{FailureLoad}{BondedArea} \tag{3.3}$$

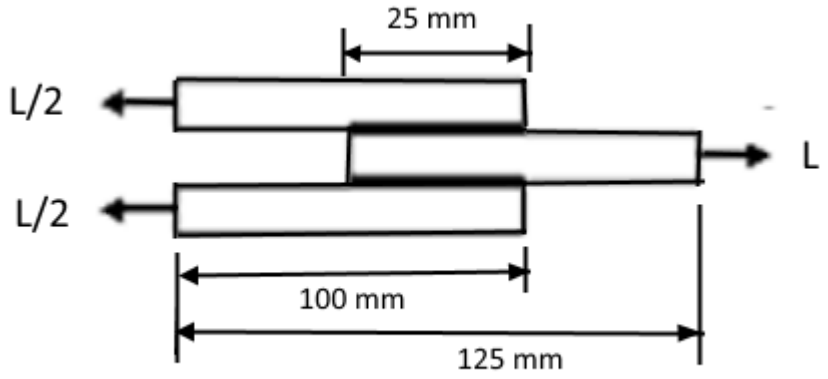

Figure 3.13: Double lap shear test coupon

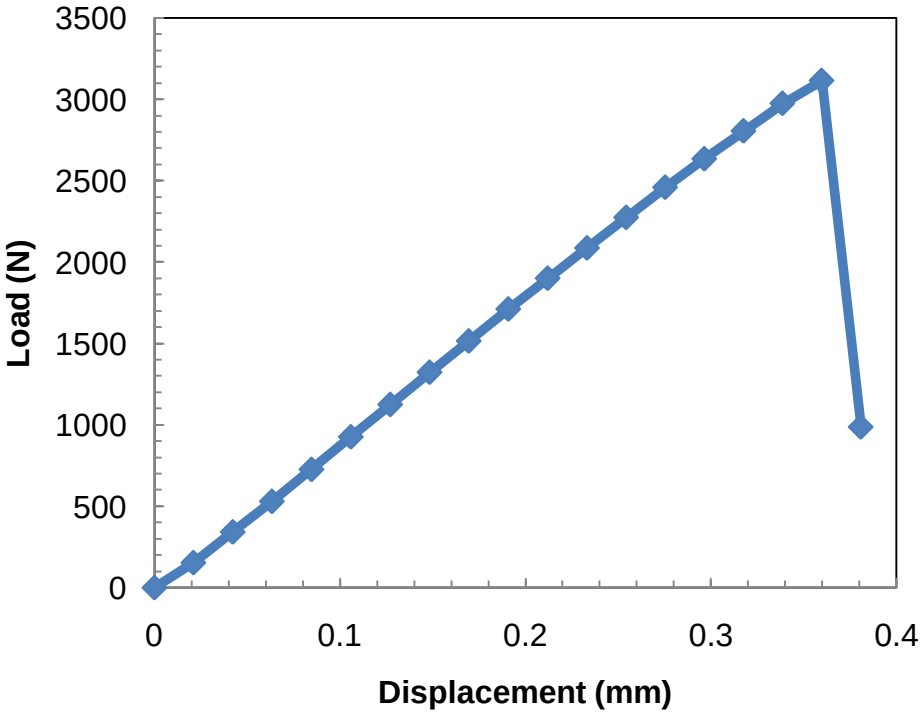

3.14: Typical load/displacement plot for SLS test coupon

The FWT testing was repeated using test coupons subjected to various surface treatments and environmental conditioning durations tabulated in Table 3.1. For each surface treatment or environmental conditioning duration, three test coupons were tested and the average value is reported.

3.2.1.3 WC Testing

The initial crack due to the opening force applied by insertion of the wedge was measured using an optical microscope (BMX4-1m LED from Olympus) and marked with a sharp stylus so that it does not fade during environmental conditioning inside the chamber as shown in Figure 3.10 (b). The crack propagation in WC test coupons was monitored at various time intervals using the optical microscope and the crack propagation length was recorded as a function of time until the crack growth stopped. Subsequently, the coupons were opened forcefully for image analysis of the surface. The WCtesting was done for various surface treatments and conditioning duration tabulated in Table 3.1. For each surface treatment and conditioning time, four test coupons were tested and the average value is reported.

3.2.2 Image Analysis of Fracture Surface

The fracture surfaces for various surface treatments revealed varying levels of mixed mode (cohesive in composite and adhesive at the interface) failure as shown in Figure 3.17.The percent cohesive and adhesive fracture areas were determined using image analysis of fractured surfaces using ImageJ software [36] and used to evaluate the IFSS values. One representative test coupon for each surface treatment was analyzed using ImageJ software to calculate the percentage of

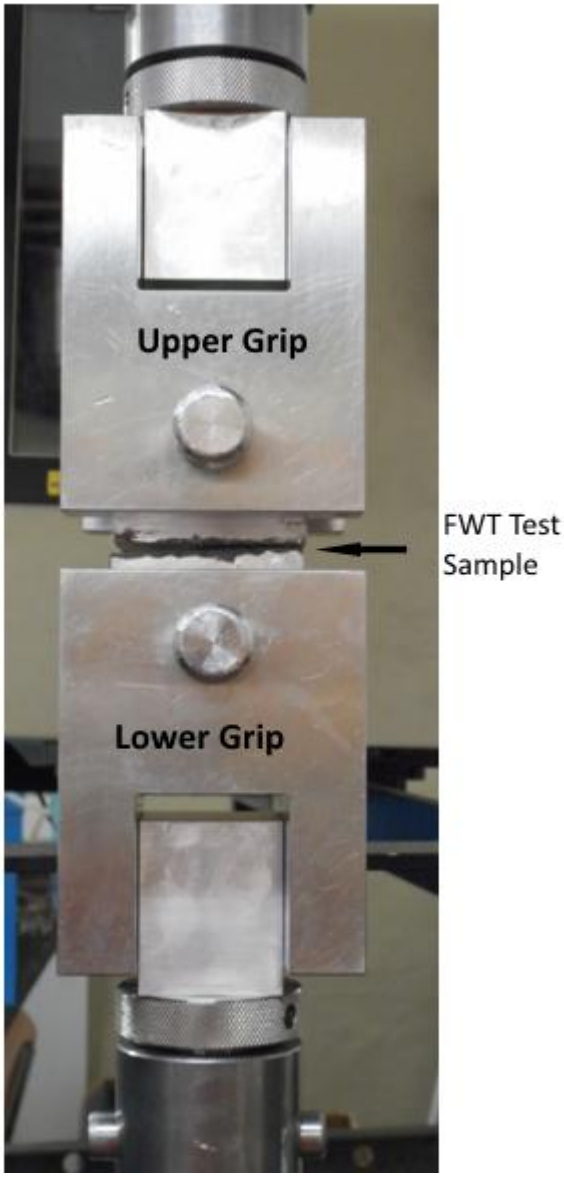

Figure 3.15: FWT test coupon gripped in Instron 8562 load frame

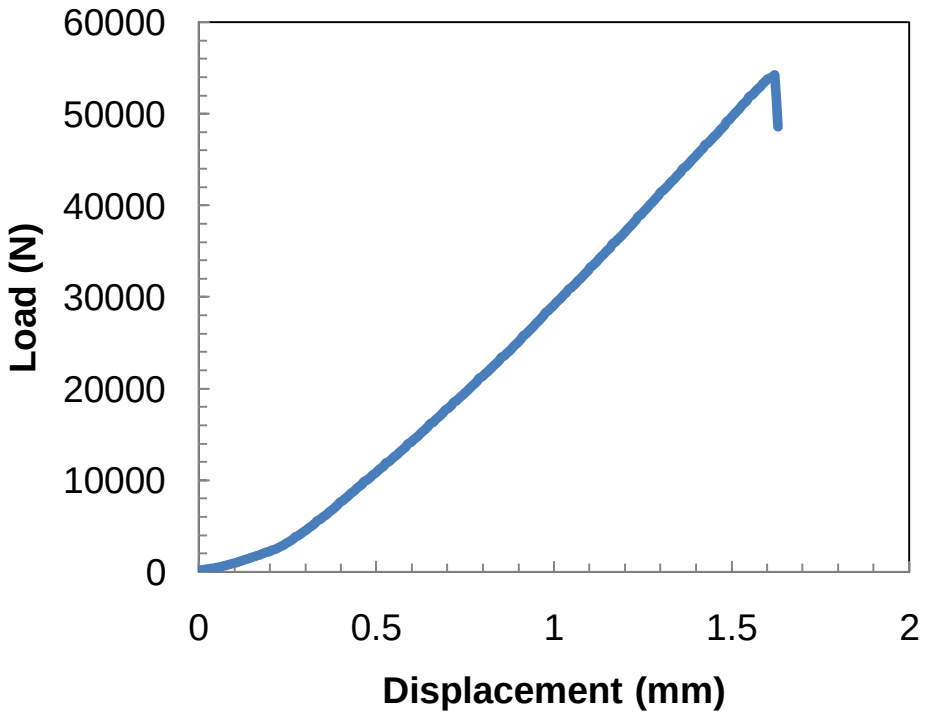

3.16: Typical load versus displacement plot for FWT test coupon

Table 3.1: List of surface treatments and test conditions used in this study

Test	**SLS**			**FWT**			**WC**	
Surface treatment	Dry test	Environmental test		Dry test	Environmental test		40^{o} C 95% RH	duration
		40^{o} C 95% RH	duration		40^{o} C 95% RH	duration		
PAA+BR127(RT)	√							
UT+BR127(120 ^{o}C)	√							
Alodine	√							
Alodine+ EC3901 (RT)	√							
Alodine+ BR127 (RT)	√							
PAA	√							
UT	√	√	0-30 days	√	√	0-30 days	√	0-20 days
UT+BR127 (RT)	√							
Alodine+EC3901 (90 ^{o}C)	√	√	0-30 days				√	0-20 days
PAA+EC3908 (RT)	√	√	0-30 days				√	0-20 days

Test	**SLS**			**FWT**			**WC**	
Surface treatment	Dry test	Environmental test		Dry test	Environmental test		40^{o} C 95% RH	duration
		40^{o} C 95% RH	duration		40^{o} C 95% RH	duration		
PAA+EC3901(90^{o})	√	√	0-30 days	√	√	0-30 days	√	0-20 days
PAA+BR127 (120 ^{o}C)	√	√	0-30 days	√	√	0-30 days	√	0-20 days
UT+EC3901 (90 ^{o}C)	√	√	0-30 days	√	√	0-30 days	√	0-20 days
UT+EC3901(RT)	√	√	0-30 days				√	0-20 days
Alodine+BR127(120 ^{o}C)	√	√	0-30 days	√	√	0-30 days	√	0-20 days

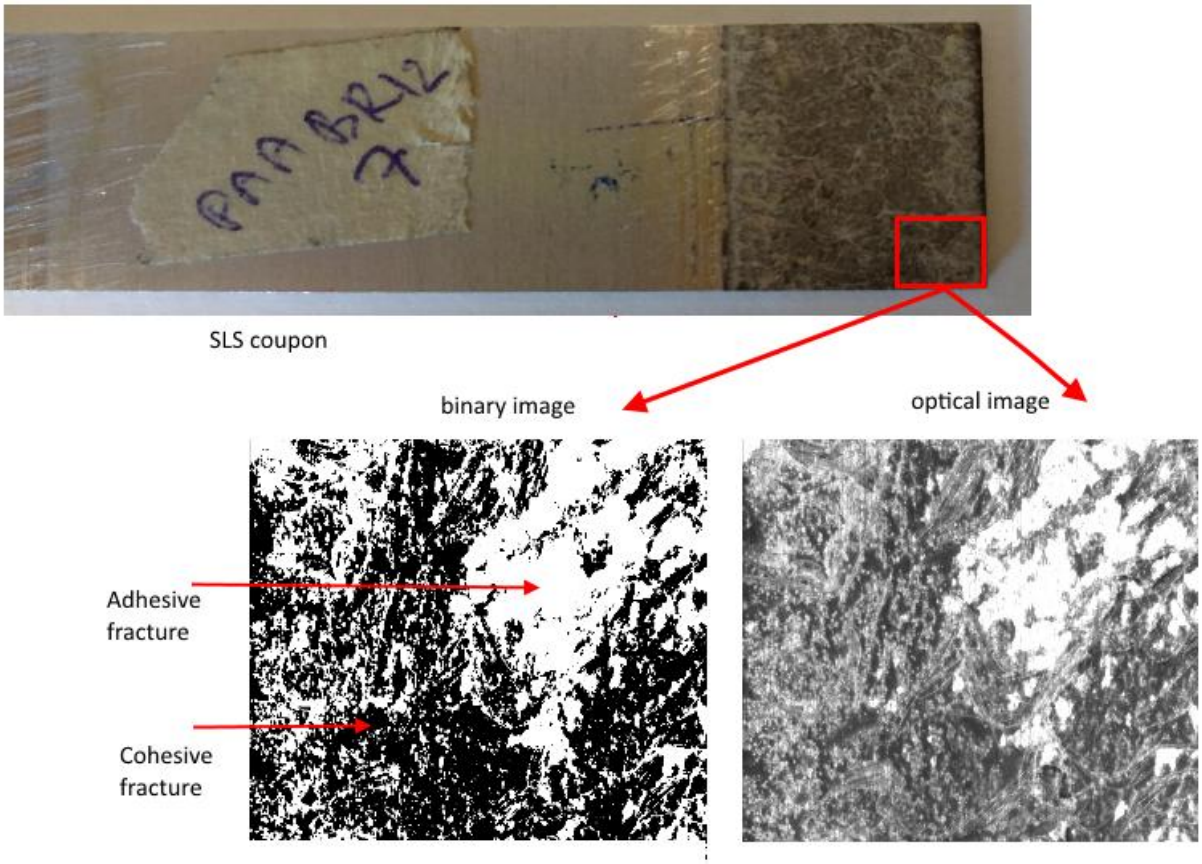

Figure 3.17 Image analysis of fractured SLS test coupons

cohesive and interfacial fracture area. Each fracture surface was divided into 12 equal areas and imaged at 5X to enable the analysis, using a stereo microscope,Clemax X204. Hence, 12 images per surface were generated. These images were converted to binary images by the ImageJ software and % cohesive and % adhesive fracture areas were calculated. The process is shown in Figure 3.17, where one of the 12 areas is presented in the frame, and the optical image captured from that area is converted to binary image. The average of the values calculated from these 12 images and reported in this study.

3.2.3 Determination of Fracture Path

In order to confirm adhesive failure in white regions (considered as adhesive failure area in the previous section), the fracture surfaces were scanned using a surface profilometer (Alpha Step 500) to identify the exact location of fracture path. The profilomerter set up is shown inFigure 3.18 (a) and (b). The stylus of profilometer moved across the surface as shown in Figure 3.19 and the surface profile data was recorded in the computer. The ASC II data from the computer was imported into MATLAB for further analysis. The vertical scan range was 2000 µm and scanning rate (stylus speed) was 200 µm/sec.

At the beginning of the scanning, stylus of the profilometer first moves down and applies a nominal force of 3.6 mg at the location of interest. It stores this point as reference. Upon giving further command to start the scan the stylus starts moving from this reference point following a straight line and measures the surface roughness with respect to that reference point. Thus, it produces a surface profile replicating the exact roughness of the scanned surface. The roughness

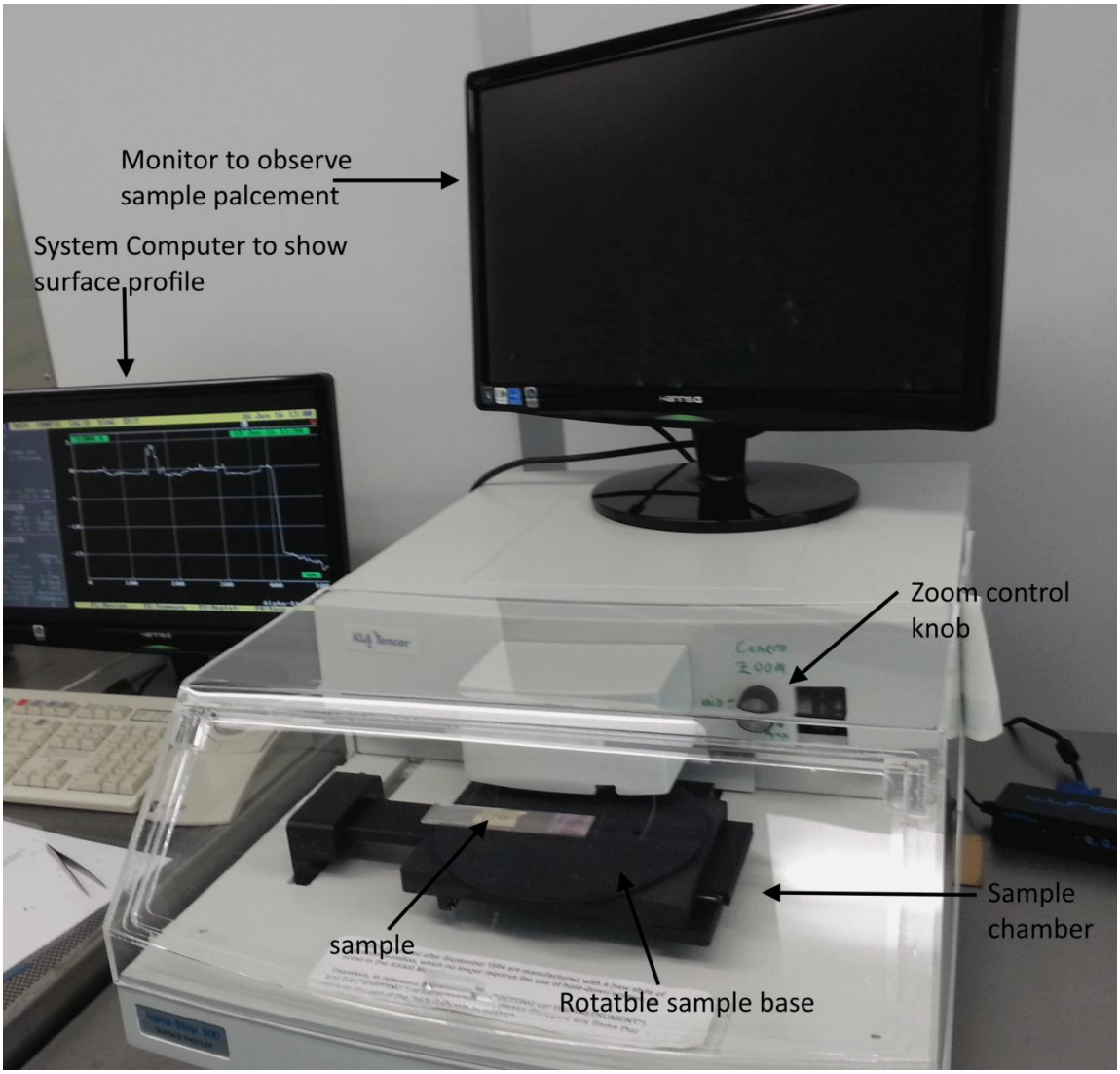

Figure 3.18: Alpha step-500 set up

was measured by using “centre line average” method, which is the arithmetic mean of the measured surface profile.

To start with the roughness of the UT test coupons was measured and the average roughness was calculated and used as a reference. During scanning of a surface treated test coupon, the scanning was started in the un-coated (untreated) region to identify the zero reference point and average roughness in UT region as shown in Figure 3.19. During scanning, the stylus traversed from the uncoated region to the coated region and thus, the roughness of the coated region corresponded to the same zero-point reference used to determine the average of the surface roughness in the uncoated region. The average of the roughness in the coated region was determined. Subtraction of the average roughness of the uncoated region from that for the coated region resulted in average coating thickness.

Subsequently, fractured surface was scanned with scanning starting in the coated region as shown in Figure 3.20. Hence, the roughness of the fractured surface was referenced to the zero position in the coated region. Using the average thickness of the coating measured as per the procedure in the previous paragraph, the zero position was moved to zero position in uncoated region and the roughness plot is redrawn. The range of roughness for uncoated and coated regions was superposed on to this revised plot as shown in Figure 3.21. The location of peaks and valleys in the roughness of the fractured surface was compared with the range of roughness for uncoated and coated regions to identify if the crack path was in the cohesive (i.e. within the composite adhesive) or in the adhesive (within the coating) as shown in Figure 3.21.

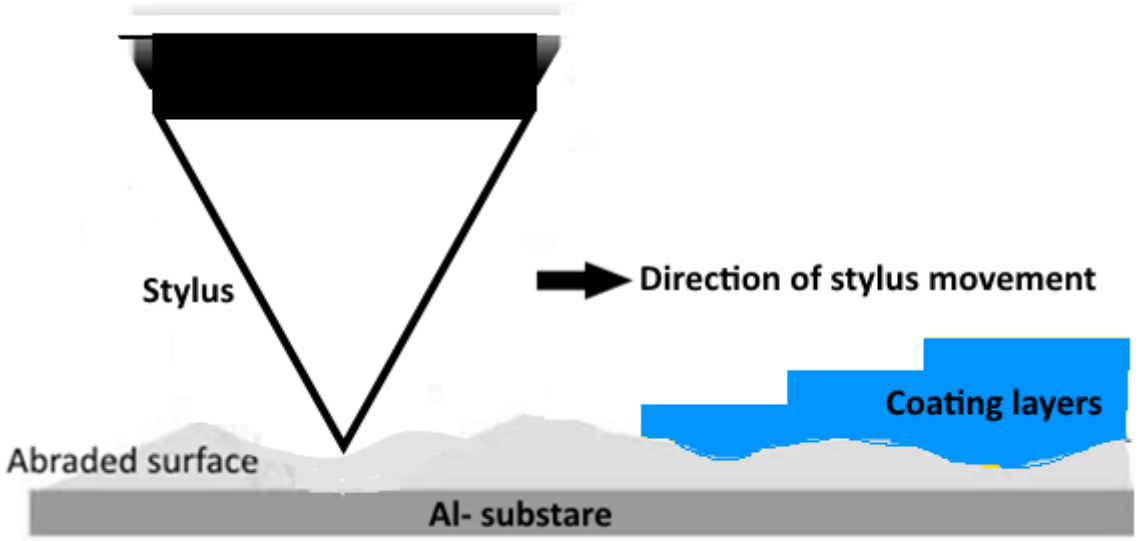

Figure 3.19: Schematic presentaion of profilometer scanning of a untreated surface to determine surface roughness (reference) and thickness of the coating

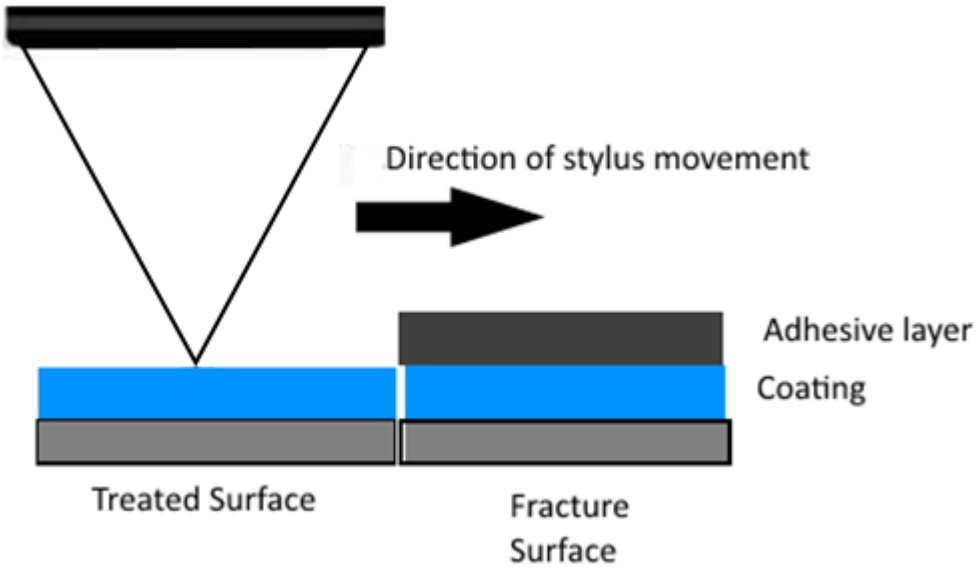

Figure 3.20: Scanning of treated panel and fracture surface

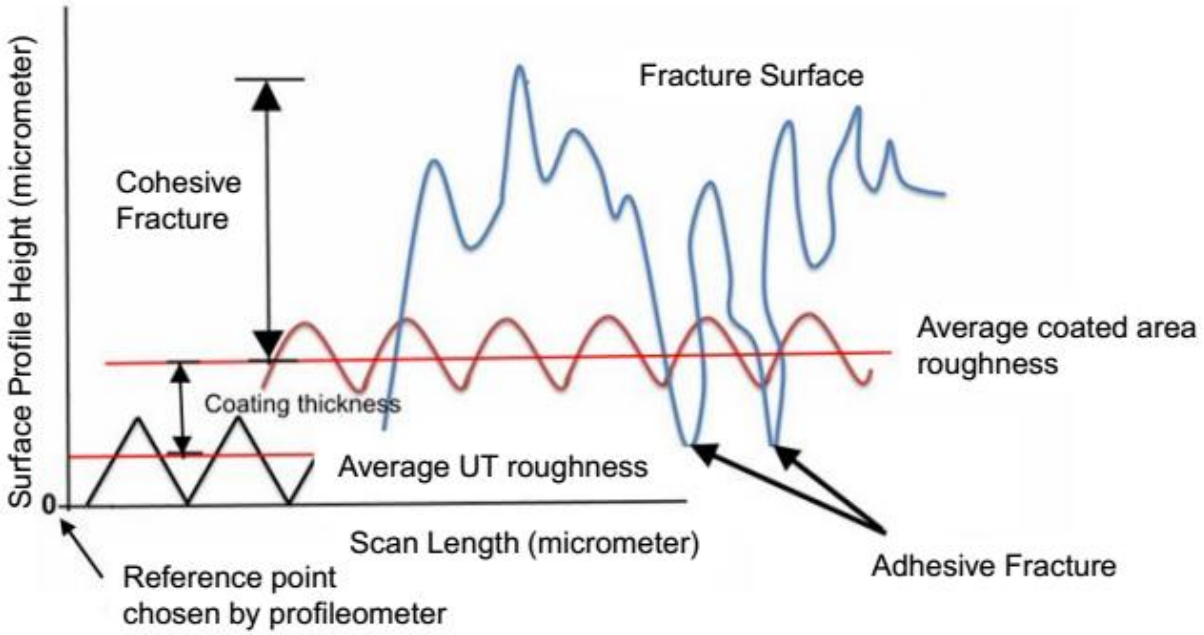

Figure 3.21: Schematic illustrating of the measurement of coating thickness and adhesive fracture path

Chapter 4

Result and Discussion

4.1 Introduction

In this chapter, the results of the experimental study on the effect of various surface treatments on the interfacial shear strength (IFSS), tensile strength, and durability of the bond between the Al substrate and the polymer composite adhesive is presented and discussed.

4.2 Optimization of SLS Test Conditions

The dimensions for minimum overlap length and fillet width recommended by ASTM D1022 are 12.5 mm and 3 mm respectively, as shown in Figure 4.1. It does not make any recommendation for adhesive thickness. IFSS for this geometry, along with the fracture mode, is tabulated in Table 4.1. Fracture initiated at the fillet by debonding of the Al substrate's edge from the fillet as shown in Figure 4.1 and subsequent crack propagation within the adhesive was mixed mode. Hence, the measured IFSS is an apparent strength. Ideally it is preferred to have debonding of the fillet from the Al substrate followed by crack propagation along the interface and the measured IFSS for this ideal fracture mode would be close to the true IFSS of the bond between the Al substrate and the composite adhesive. Hence, IFSS and fracture mode were studied as a function of the overlap length, fillet length, and adhesive thickness of the SLS test coupons to determine the optimal geometry for the SLS test coupons. The results are tabulated in Table 4.1 and discussed below.

Table 4.1 Effect of test coupon geometry on IFSS

Overlap Length (mm)	**Adhesive Thickness (mm)**	**Fillet Width (mm)**	**Fracture Load (N)**	**IFSS (MPa)**	**Fracture Mode**
12.5	0.20-0.21	2	3945±462	10.42±0.60	Type I in fillet + Mixed Mode in the bonded region
20	0.22	0	3967±781	8.89±0.31	Mixed Mode in bonded region
	0.21	2	4373±568	9.93±0.67	Type I and II in fillet and mixed mode in bonded region
25		0	5815	9.67	Mixed mode in the boned region
	0.21	1	6585±367	9.92±0.67	Type II in fillet and Mixed Mode in bonded region
	0.19-0.20	2	6140±524	8.80±0.34	Type II in fillet and mixed mode in bonded region
	0.25 - 0.26		5693±641	9.16±0.50	Type I and II in fillet and mixed mode in bonded region
	0.32		6120±539	9.73±0.34	Type I in fillet and mixed mode in bonded region
	0.21	4	5778±275	9.51±0.60	Type I in fillet and mixed mode in bonded region
	0.32		5973±212	8.76±0.79	Type I in fillet and mixed mode in bonded region

4.2.1 Effect of Overlap Length

Overlap length, that ensures joint failure without adherend failure or yielding, should be chosen. Three overlap lengths, 12.5 mm, 20 mm, and 25 mm, used in this study yielded joint failure. For a given adhesive thickness (0.20 – 0.22 mm) and fillet width (2 mm), the fracture load increased (3945 N for 12.5 mm, 4373 N for 20 mm, and 5791 N for 25 mm) and the IFSS decreased slightly (10.42 for 12.5 mm, 9.93 MPa for 20 mm, and 8.53 MPa for 25 mm) with increase in overlap length. True IFSS should be independent of the overlap length. Moreover, the fracture mode was not interfacial; the fracture initiated at the fillet at the interface through either Al edge debonding from the fillet (Type I in Figure 4.1) or Fillet debonding (Type II in Figure 4.1) followed by mixed mode failure in the bonded region. Hence, measured IFSS is an apparent value. The decrease in this apparent value with increase in overlap length is believed to be due to following reasons: (a) difference in load required to initiate different types of fracture at the fillet, (b) difference in the amount of cohesive and adhesive fracture areas within the bonded region, and (c) the shear stress distribution within the bonded region may not scale with the overlap length resulting in lower average shear stress with increase in overlap length i.e. bonded area.

The above results clearly demonstrates that the varying the overlap length would not result in adhesive failure. Hence, the effect of fillet width was studied next.

4.2.2 Effect of Fillet Width

During testing of SLS test coupons, the fracture initiates at the edges of the bond and progress towards the interior since the shear stresses are maximum near the edges. Also, due to the

bending of the joint (caused by eccentric loading), maximum peel stresses are also introduced near the edge of the bonded area. Both of these stresses determine the fracture load. Introduction of fillets alters the stress distribution near these edges [12]. Tsai and Morton [30] has observed experimentally, the reduction in shear stress and peel stress concentration near the edges as well as increase in fracture load due to fillet. However, no information on fracture mode is given. Hence, in this study the fillet width was varied in the range of 0-4 mm to study its effect in initiating adhesive fracture.

For a given overlap length (25 mm) and adhesive thickness (0.19-0.21mm) the fracture load decreased marginally with increase in fillet width (6585 N for 1 mm, 6140 for 2 mm, and 5778 N for 4 mm). The failure load for samples with no fillet was 5815N.. Hence, expected trend IFSS was not observed and this is believed to be due to (a) difference in load required to initiate different types of fracture at the fillet (Type I for 4 mm fillet versus Type II for 1 and 2 mm fillets), and (b) difference in the amount of cohesive and adhesive fracture areas within the bonded region.

However, for the adhesive thickness of 0.32 mm and overlap length of 25 mm, both the fracture load and the IFSS decreased with increase in fillet width from 2 to 4 mm. Yet, the fracture mode was not interfacial and hence, the calculated IFSS is apparent strength only. Hence, the adhesive thickness was varied over a wide range (0.03-0.32 mm) at a constant overlap length of 20 mm to study if a thickness in this range would yield interfacial fracture. The fillet width was chosen to be zero since results discussed in the previous section suggest that finite fillet width does not result in interfacial failure.

4.2.3 Effect of Bond-line Thickness

The measured IFSS for untreated specimen is plotted as a function of adhesive thickness in Figure 4.3 and tabulated in Table 4.2. The IFSS increased with increase in thickness, reached a maximum (11.35±0.51 MPa) at ~ 0.08-0.10 mm, and subsequently decreased to 8.67±0.05 MPa beyond 0.2 mm. The lowest IFSS (6.60±0.28 MPa) was obtained for a thickness of 0.03-0.04 mm. The fracture surface for all of them revealed a mixed mode failure (cohesive in composite and adhesive at the interface) as shown in Figure 4.4 and hence, the measured IFSS is an apparent IFSS. The % cohesive fracture area, determined by image analysis by ImageJ software, is also plotted in Figure 4.3 as a function of thickness. It is observed that the relative amounts cohesive area (and interfacial area) varied with adhesive thickness. Unlike the IFSS, the % cohesive area increased monotonically with increase in the adhesive thickness; it increased rapidly in the thickness range of 0.03-0.10 mm and then slowly until it reached a maximum of 89% at 0.32 mm. The minimum value (38%) of cohesive fracture area was recorded at the lowest thickness of 0.03-0.04 mm.

In order to verify that the regions identified by ImageJ software as adhesive failure regions are indeed locations where the fracture path has reached the Al substrate – composite adhesive interface, fractured surface of the test coupon was analyzed using the surface profilometer as per the procedure discussed in 3.2.3. The profilometer result for a representative UT test coupon is presented in Figure 4.5.The surface profile of the UT specimen before bonding is shown in Figure 4.5 (a). The mean line and the lines corresponding to the range of roughness data are also identified in this figure. It should be noted that the range is the total height of the roughness profile given by the sum of the amplitude from the mean line corresponding to the maximum

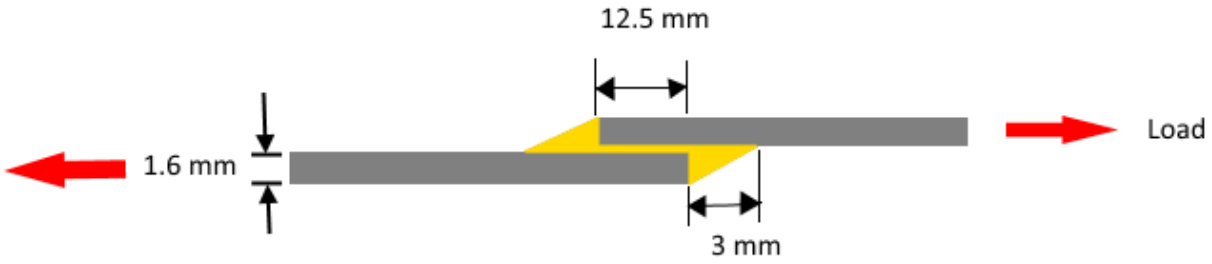

Figure 4.1: Single lap shear sample with fillets at the end of overlap

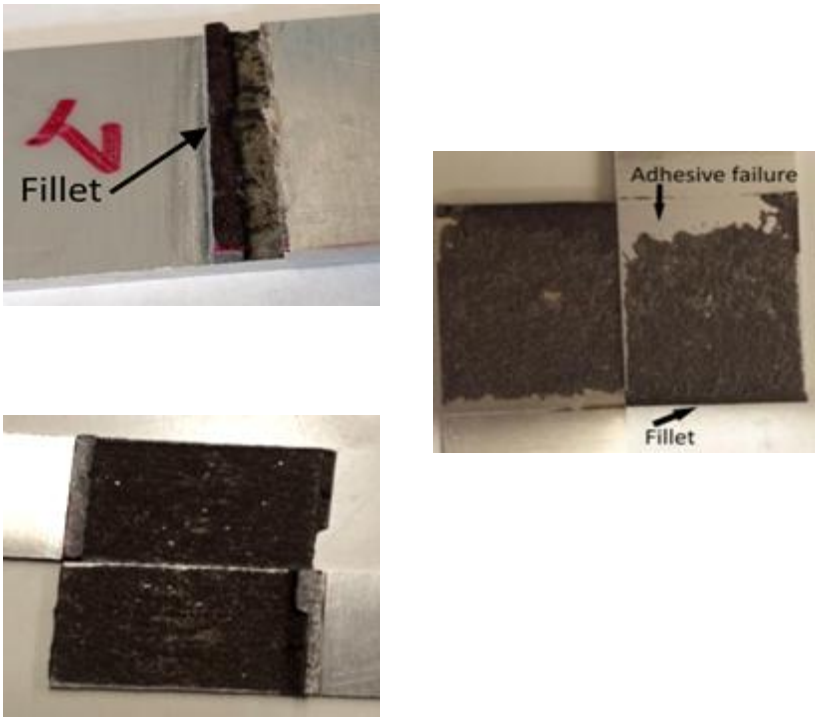

Type I b. Type II

Figure 4.2: Types of observed fracture initiation modes in the fillet of SLS test coupons

Table 4.2. IFSS and percentage of cohesive fracture for UT specimens at different adhesive thickness.

Thickness (mm)	**IFSS (MPa)**	**% Cohesive Fracture Area**
0.03-0.04	6.60±0.28	35
0.06	7.77±0.32	45
0.08-.09	11.20±0.18	58
0.10	11.35±0.51	70
0.12-0.13	10.02±0.39	81
0.16-0.18	9.27±0.39	81
0.32	8.67±0.05	89

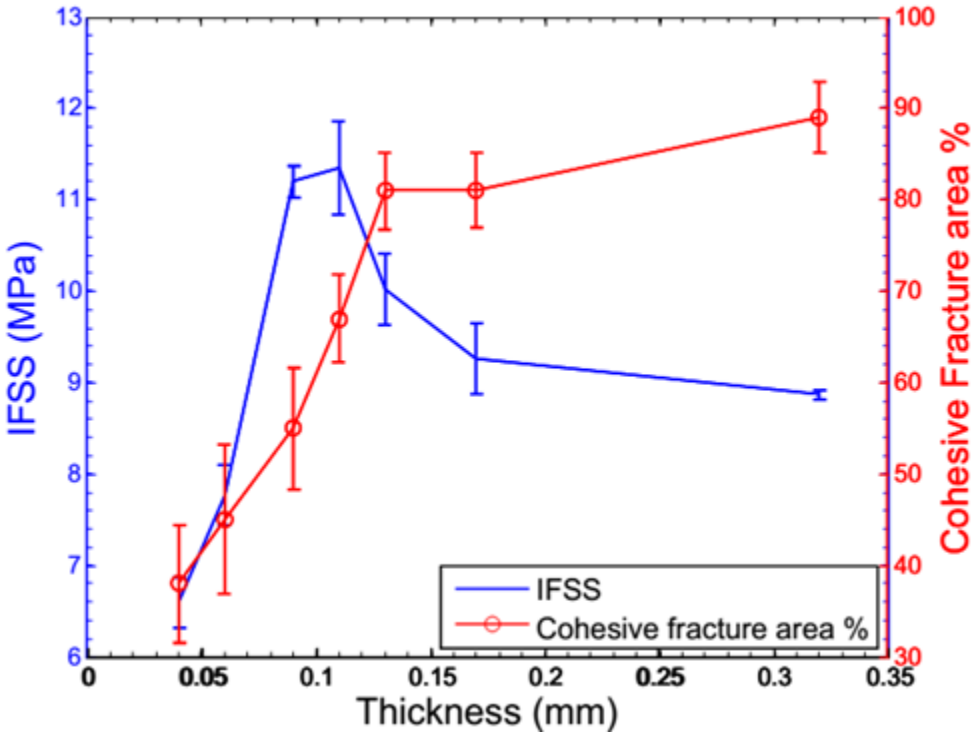

Figure 4.3: IFSS and % cohesive area as a function of thickness

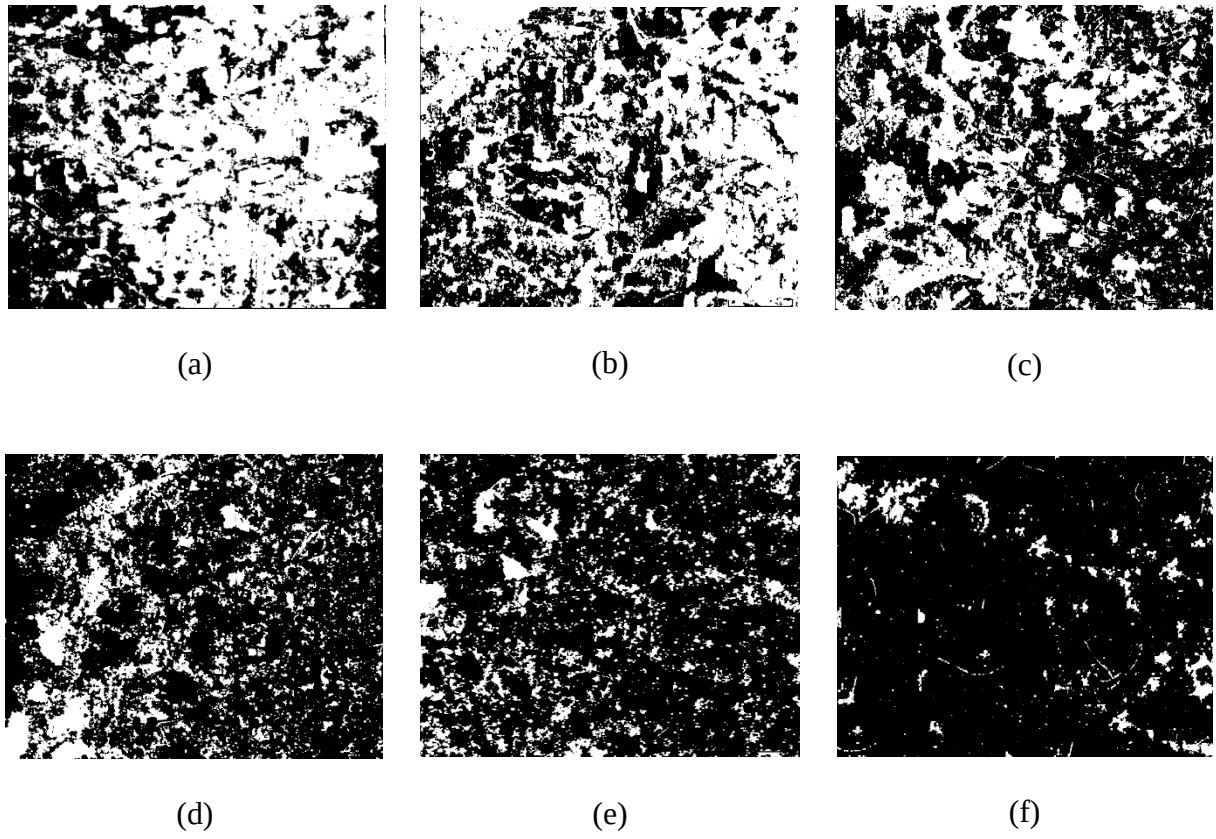

Figure 4.4: Binary images (5X) of the fracture surfaces of UT test coupons with adhesive thickness of (a) 0.04 mm, (b) 0.06 mm, (c) 0.08mm, (d) 0.10 mm, (e) 0.16 mm and (f) 0.32 mm

profile peak and minimum profile valley. In Figure 4.5(b) the surface profile of fractured UT test coupon is shown. The scan started in a region that was not bonded and continued into the fractured region and thus the profile height was referenced to the zero point in the non-bonded UT region. This allowed the superposition of the mean line and the range of the roughness profile from Figure 4.5(a) onto Figure 4.5(b).The peaks in some locations of the fractured area are in the adhesive confirming that these locations are where crack path was cohesive. In other locations of the fractured area, both the peaks and the valleys or the valleys alone are within the range of roughness corresponding to non-bonded UT region confirming that these locations are where the crack path was adhesive.

The shear strength of the brittle composite adhesive used in this study is believed to be more than the actual interfacial shear strength in UT specimens resulting in the increase of the apparent IFSS due to increase in the % cohesive fracture area when the thickness was increased from 0.03 to 0.12 mm. The reason for the increase in cohesive crack growth (and % cohesive fracture area) despite lower interfacial strength is not known at this time. Gleich*et al.* [11] have predicted numerically the peel and shear stresses at metal-adhesive interface and mid- thickness of the adhesive in SLS specimens. They have shown the maximum peel and shear stress variation as a function of thickness. Their results also show an optimal adhesive thickness for which the interfacial peel and shear stresses are minimum. Below this optimal thickness, the peel and shear stresses at the mid-thickness of the adhesive as well as at the interface are shown to decrease with increase in the adhesive thickness until the optimal thickness is reached. No reason is given by these authors for the observed trend nor is the effect of applied load on this trend shown. If confirmed, this could explain the observed trend in Figure 4.3 below ~0.12 mm, i.e the applied

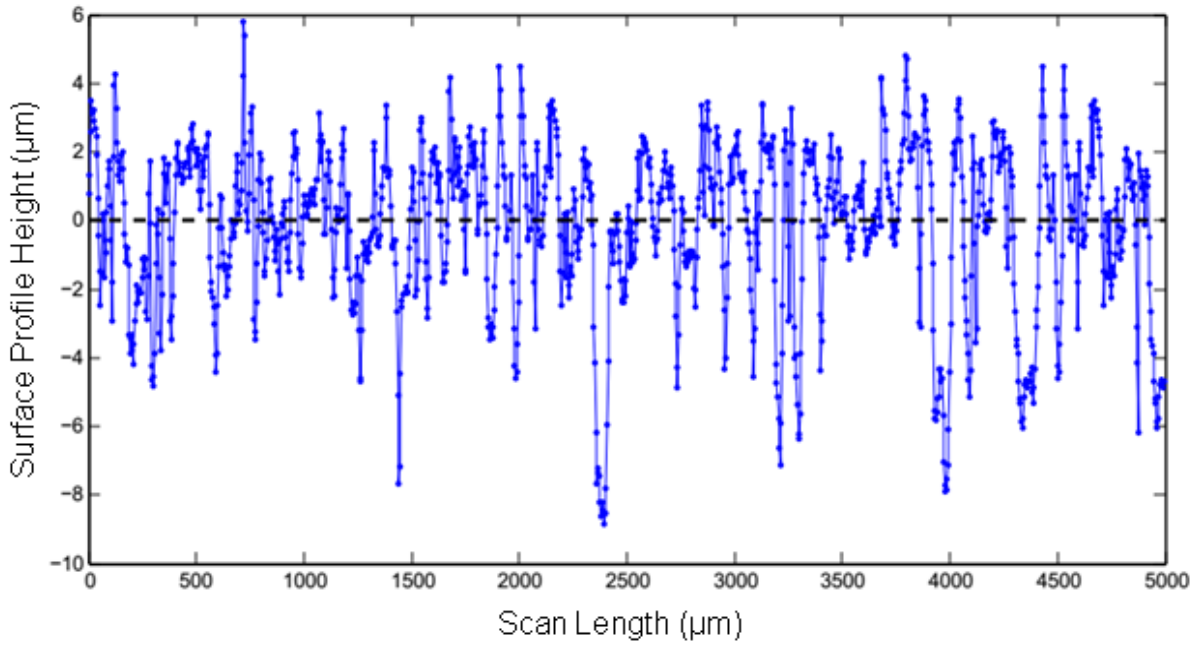

(a)

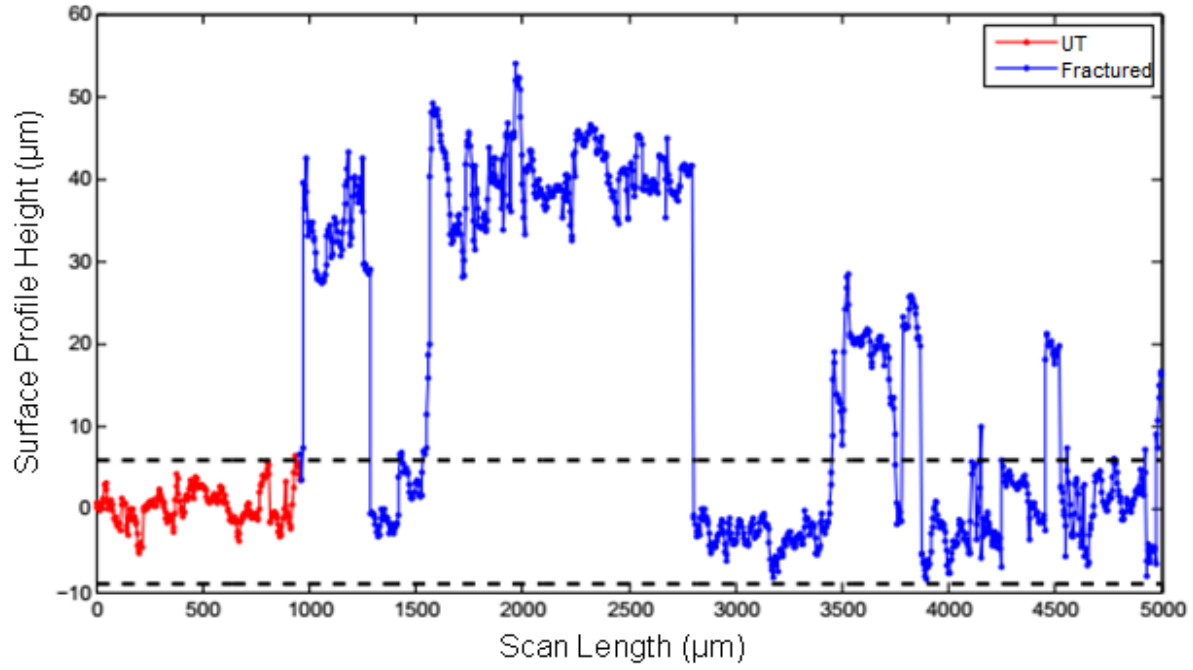

(b)

Figure 4.5 (a) Surface profile of the UT specimen before bonding, (b) surface profile of fractured UT test coupon

load required to initiate the failure will increase with adhesive thickness since the maximum shear and peel stresses at a given applied load decrease with increase in adhesive thickness. In addition, their numerical predictions appear to show that the peel and shear stresses at the mid-height of the adhesive are higher than that at the interface, below the optimal thickness. This would mean that the fracture would have initiated at the mid-thickness rather than at the interface, which could have influenced the subsequent crack propagation (cohesive versus adhesive) resulting in the observed behavior below ~0.12 mm.

Beyond 0.12 mm, the IFSS decreased with increase in thickness to 0.32 mm despite the increase in the cohesive area. Previous studies have also reported a decrease in the strength of SLS joints with increase in the adhesive thickness [1,2,11,22,4,6]These authors have reasoned this to be due to decrease in the fracture toughness of the adhesive with increase in thickness, bending of the joint during testing, and change of stress state to plane strain condition [23,5,6,8] Gleich*et al.* [11] have reasoned this to be due to increase in peel and shear stresses at the interface. However, high percent of cohesive fracture observed in these thicknesses in this study is in contradiction to the reasoning given by Gleich*et al.* [11]. In this study the IFSS decreased from 11.35±0.51 MPa to 8.67±0.05 MPa when thickness was increased from 0.12 mm to 0.32 mm. This is believed due to decrease in the fracture toughness of composite adhesives with increase in its thickness since the fracture mode is cohesive.

The load-displacement results for various adhesive thicknesses are compared in Figure 4.7 to see if bending could have played a role. Below 0.1 mm, the initial portions of the curves superpose

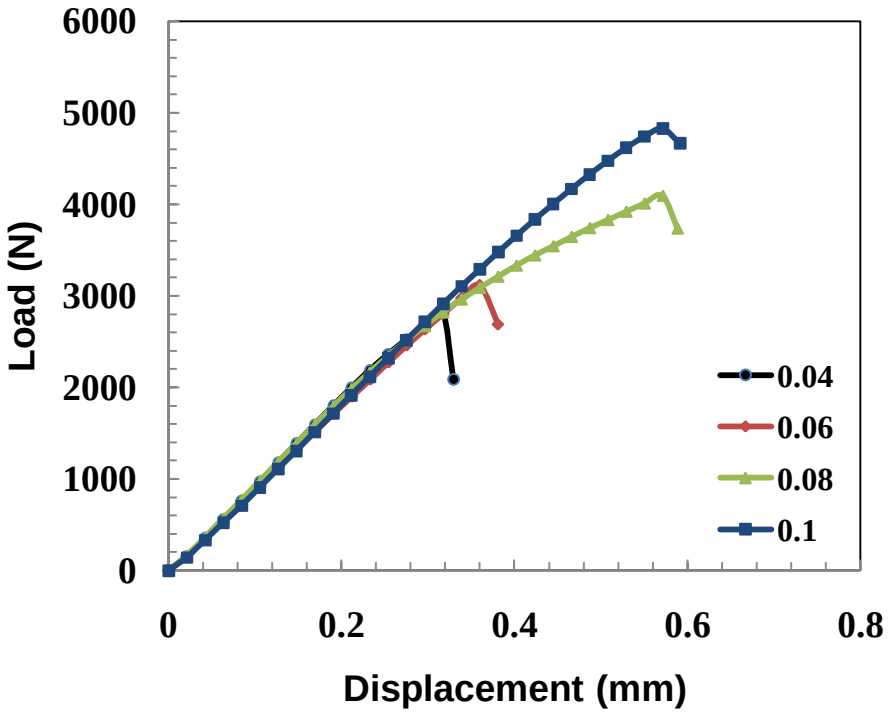
6000
5000
4000
3000
2000
1000
0
Load (N)
0
0.2
0.4
0.6
0.8
Displacement (mm)
0.04
0.06
0.08
0.1

(a)

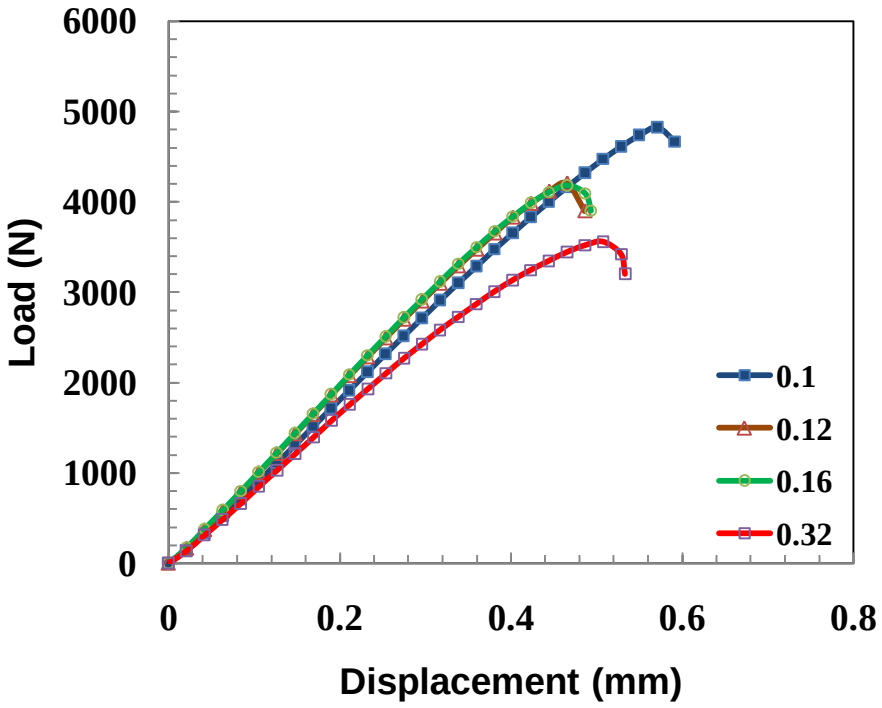

(b)

Figure 4.7: Load versus Displacement plots for UT test coupons with thickness (a) from 0.04 mm to 0.10 mm and (b) from 0.10 mm to 0.32 mm

suggesting that the stiffness of the joints are same. If there were any increase in joint bending with increase in adhesive thickness, the stiffness would have decreased with increase in adhesive thickness, which is observed only towards 0.32 mm. Hence, bending is believed to have played a minor role in the observed trend beyond 0.12 mm. The above results also demonstrate that 100% adhesive failure is not achievable in the SLS test coupons of the Al-Composite adhesive pair chosen for this study. Since the % cohesive fracture area was minimum and the % adhesive fracture area was maximum at a thickness of ~0.03-0.04 mm, the IFSS measured at this thickness was believed to be approaching the true IFSS. Hence, a bond thickness of 0.03-0.04mm was chosen to study the effect of various treatments.

4.3 Effect of Surface Treatments on IFSS

The IFSS for various surface treatments, compared in Figure 4.8 and tabulated in Table 4.3, varied in the range of 1.92 MPa to 14.32 MPa. When compared to the published IFSS results in Table 2.2 for high temperature curing adhesives, these values are significantly lower, highlighting the advantages of high temperature curing adhesives. Both the PAA and the Alodine treatments resulted in lower IFSS than the Untreated. Application of BR127 primer after these treatments prior to bonding also resulted in IFSS values lower than untreated. While the recommended curing temperature for BR 127 is 120^{o} C, it was cured at room temperature to mimic a room temperature repair process using the composite adhesive. The room temperature curing of BR127 on PAA resulted in IFSS lower than the IFSS for PAA. However, room temperature curing of BR127 on Alodine and UT resulted in higher IFSS than that for Alodine and UT, while BR127 cured at 120^{o} C on PAA and Alodine resulted in significantly higher IFSS than that for PAA, Alodine and UT, its application on UT resulted in very low IFSS. Published

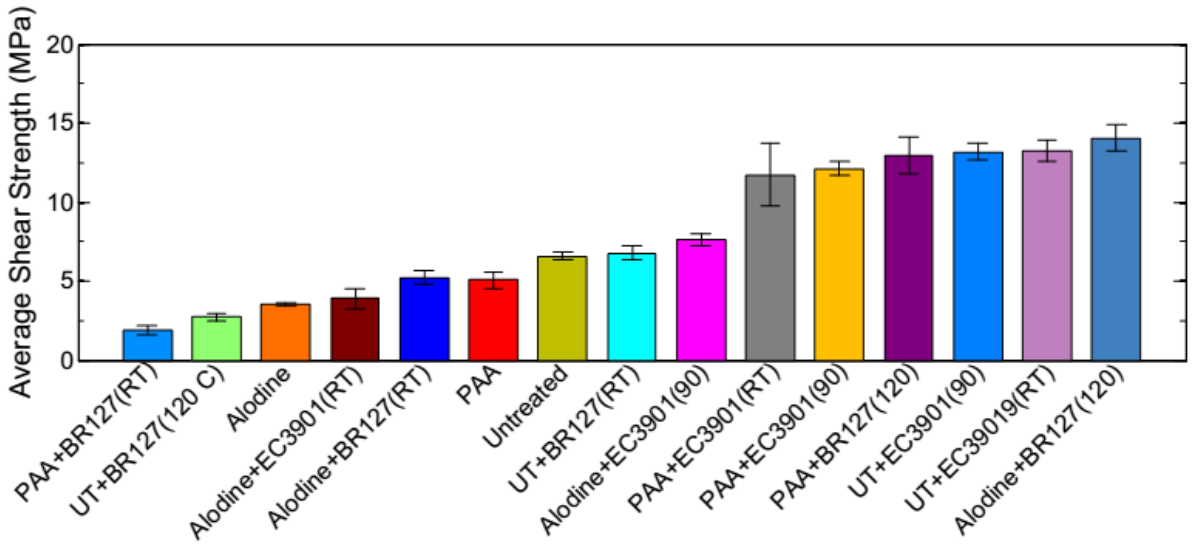

Figure 4.8: Average IFSS for all treatments

Table 4.3: IFSS and % Cohesive fracture area for different treatments

Treatments	**IFSS (MPa)**	**% Cohesive Fracture area**
PAA+BR127(RT)	1.92±0.27	19±5.02
UT+BR127 (120^{o}C)	2.72±0.26	23±5.43
Alodine	3.54±0.08	24±7.43
Alodine+EC3901(RT)	3.92±0.63	20±6.66
Alodine+BR127(RT)	5.26±0.23	31±8.57
PAA	5.05±0.52	33±9.05
UT	6.60±0.28	35±6.39
UT+BR127 (RT)	6.78±0.45	42±9.41
Alodine+EC3901(90^{o}C)	7.65±0.38	46±8.21
PAA+EC3908(RT)	11.72±1.32	73±7.67
PAA+EC3901 (90^{o}C)	12.10±0.44	79±10.43
PAA+BR127(120^{o}C)	13.08±0.21	76±11.03
UT+EC3901(90^{o}C)	13.18±0.19	81±9.11
UT+EC3901(RT)	13.28±0.50	79±9.04
Alodine+BR127(120^{o}C)	14.32±0.97	82±10.39

interfacial strength for aluminum (PAA+B127 treated) bonded with 120^{o} C curing adhesive is ~ 42 MPa with cohesive failure of the adhesive [10] Hence, it is concluded that the BR127 would not be suitable for room temperature repair process. However, it results in one of the highest IFSS values recorded in this study when combined with PAA and Alodine.

Despite the recommended cure temperature for 3M's EC3901 primer is 90^{o} C, curing it at room temperature on UT resulted in very high IFSS when compared to that for UT. The maximum interfacial strength is above 13 MPa for UT coated with EC3901primer cured at 90^{o} C and RT. These strength values are two times the value for UT.EC3901 applied on PAA and cured at 90^{o} C and RT also resulted in IFSS more than the value for UT and comparable to the values for PAA+BR127 (120^{o} C). With Alodine, EC3901 cured at 90^{o} C resulted in higher IFSS than that for UT while room temperature curing resulted in lower IFSS than UT.

The fracture surfaces for various surface treatments revealed varying levels of mixed mode (cohesive in composite and adhesive at the interface) failure as shown in Figure 4.9. Like untreated specimens with various thicknesses the treated fracture surfaces also confirm that the measured IFSS is an apparent value. The percent of cohesive fracture area for various treatments, measured using ImageJ software are tabulated in Table 4.3 and compared with the respective IFSS values. Similar to the trend observed in Figure 4.4, the IFSS increased with percent cohesive fracture area. Although the adhesive thickness of 0.03-0.04 mm resulted in the lowest percent of cohesive area of 38% (and maximum adhesive failure area 62%) in untreated specimens, additional surface treatments caused it to vary between 19 to 83%.

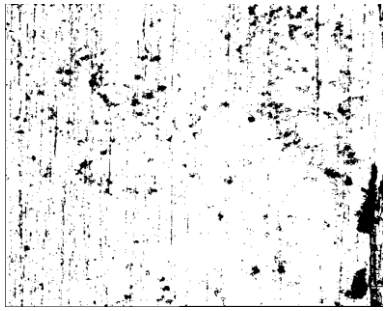

(a)

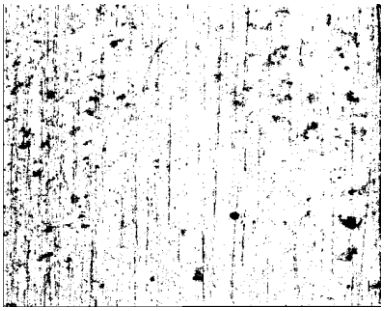

(b)

(c)

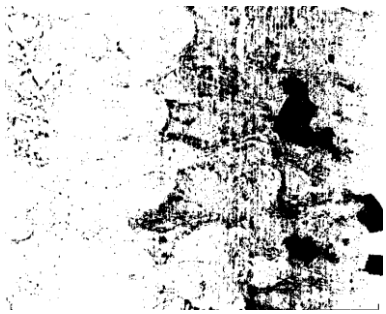

(d)

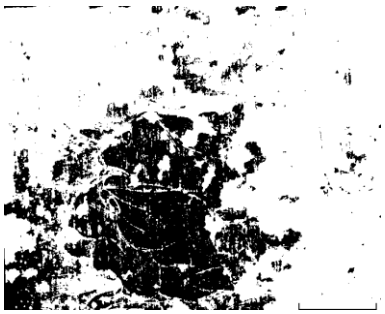

(c)

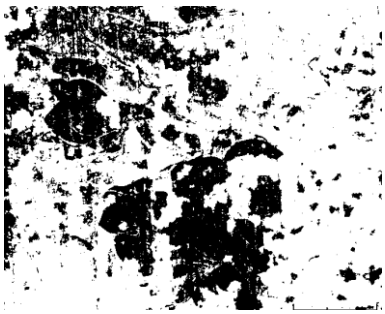

(f)

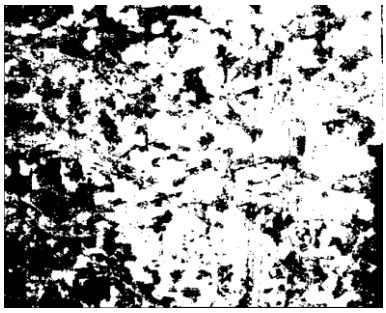

(g)

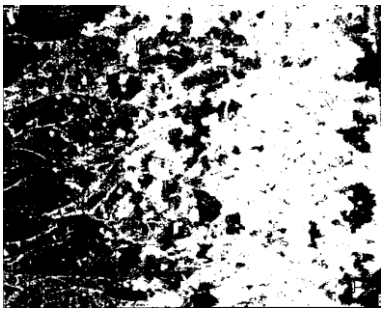

(h)

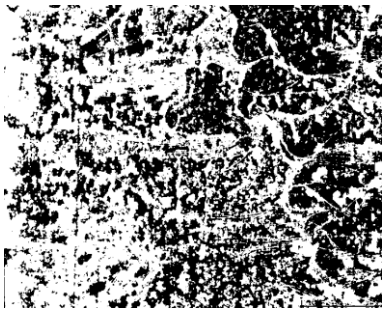

(i)

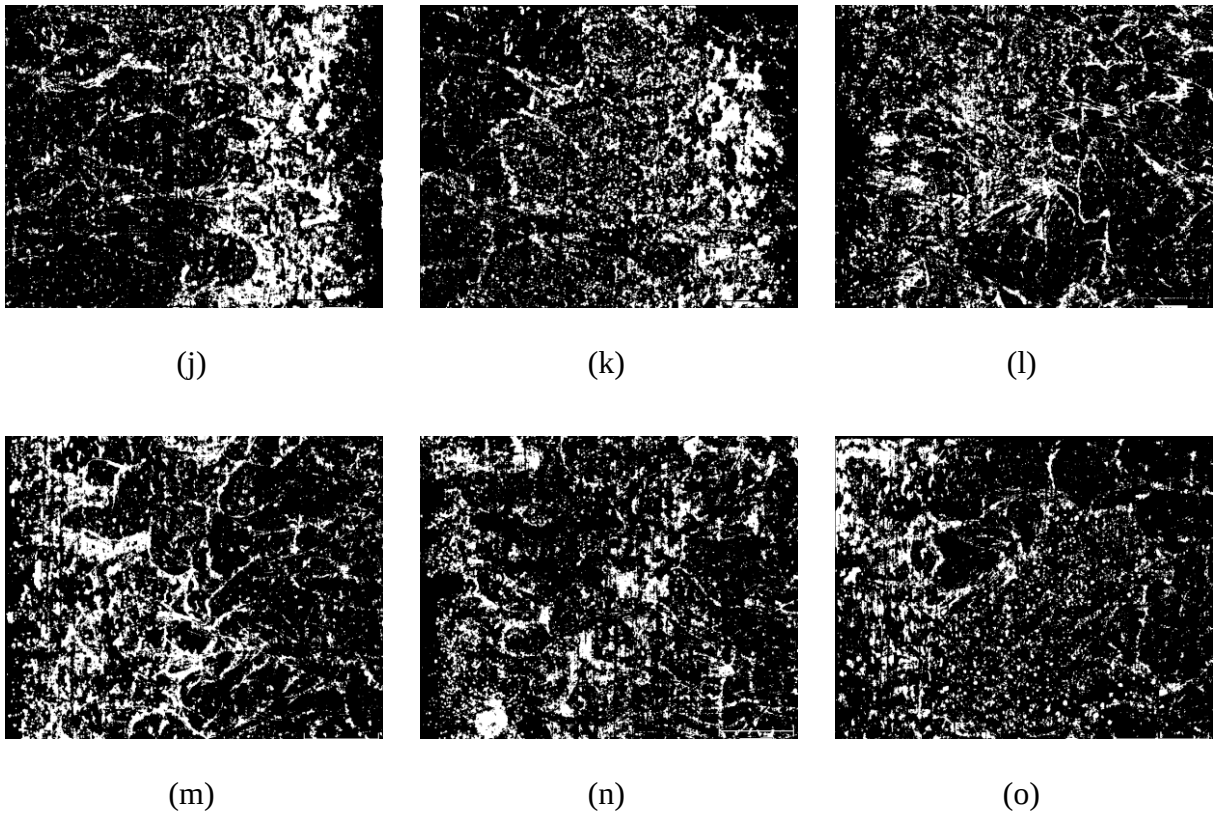

Figure 4.9: Binary image of fracture surface of test coupons with adhesive thickness of 0.03-0.04 mm and various surface treatments, at 5 X magnification (a) PAA+BR127 (RT), (b) UT+BR127 (120^{o}C), (c) Alodine (d) Alodine+EC3901 (RT), (e) Alodine+BR127 (RT), (f) PAA, (g) UT, (h) UT+BR127 (RT), (i) Alodine+EC3901 (90^{o}C), (j) PAA+EC 3901(RT), (k) PAA+EC3901 (90^{o}C), (l) PAA+BR127 (120^{o}C), (m) UT+EC3901 (90^{o}C), (n) UT+EC3901 (RT), (o) Alodine+BR127 (120^{o}C)

Similar to the case of UT, few surface treated specimens were examined using the profilometer to confirm the regions of adhesive failure. Profilometer results for UT+BR127 (120^{o} C), Alodine, PAA, and UT+EC3901 (90^{o} C) are presented in Figures 4.10-4.13, respectively. Part (a) of each Figure represents the scan of the treated surface before bonding. The difference in amplitude corresponding to mean line for UT and conversion coating / primer was taken to be average coating thickness. The thickness of two primer coatings and two conversion coatings are tabulated in Table 4.4. Alodine coating is thicker than PAA and BR127 coating is thicker than EC3901. The ranges of roughness for each of these coatings are superposed onto the surface profile for the fractured surface in part (b) of each figure. Minimum in valleys in some locations the fracture surface coincides with the range for the coating confirming the adhesive crack propagation in these locations of the fracture surface.

Despite choosing the lowest adhesive thickness, complete interfacial fracture could not be achieved in surface treated specimens to enable direct comparison of the IFSS values corresponding to various treatments. However, the increase in % cohesive area in Table 4.3, relative to Untreated, is believed to be an indirect indication of the increase in the true interfacial shear strength, since the adhesive thickness was maintained constant for all treatments. Alternatively, the decrease in % cohesive area in Table 4.3, relative to Untreated, is believed to be an indirect indication of the decrease in true interfacial strength. Hence, the ordering presented in the table based on the apparent IFSS is believed to be reflective of the changes in true IFSS with surface treatments.

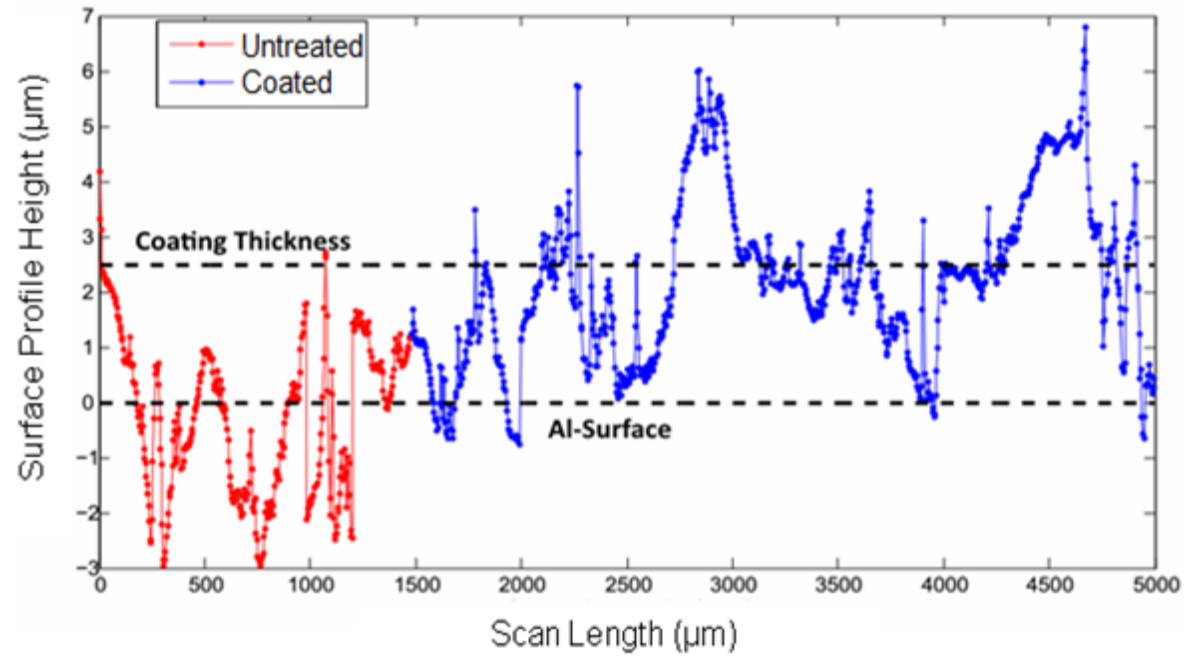

(a)

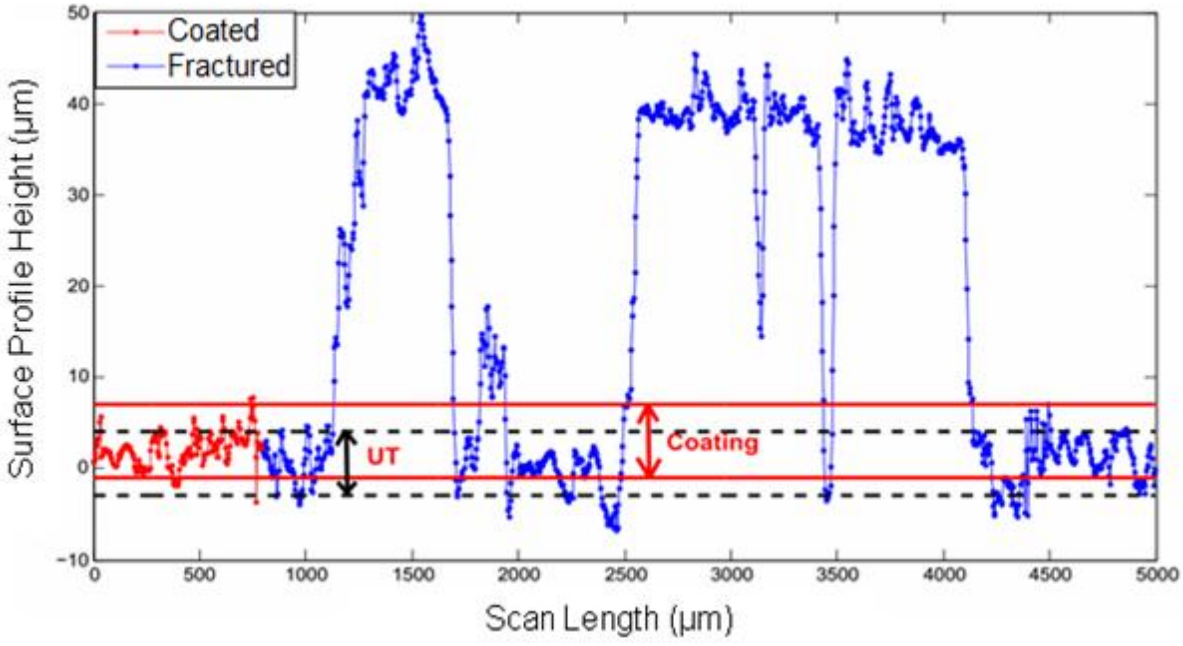

(b)

Figure 4.10: (a) Surface profile of the Alodine coated specimen before bonding, (b) surface profile of fractured Alodine test coupon

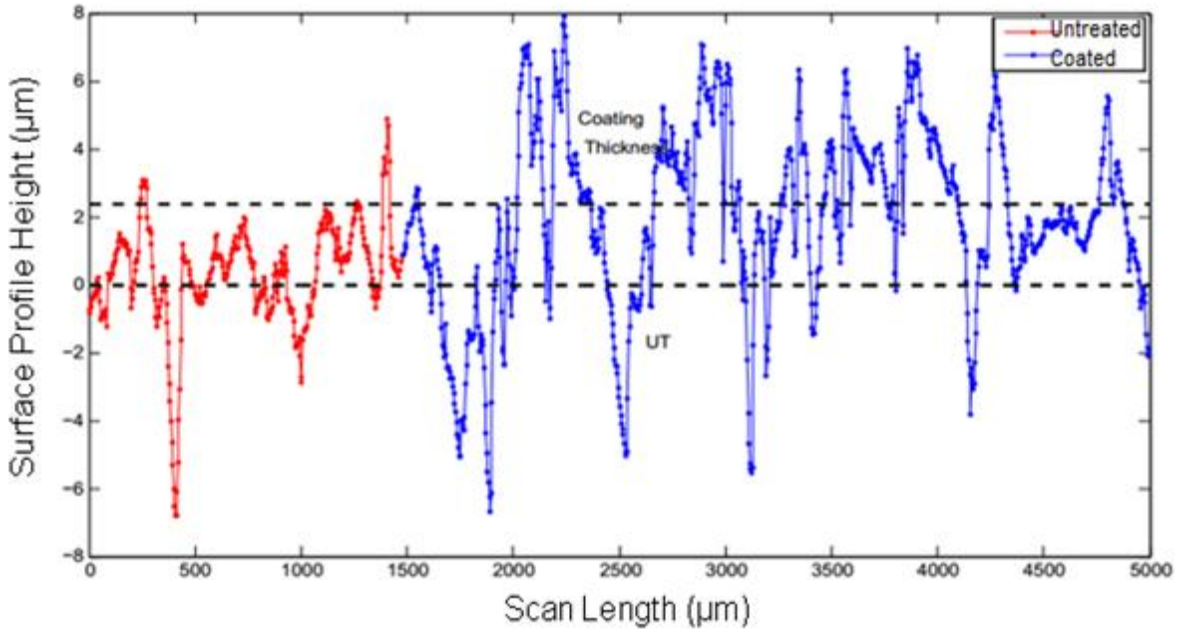

(a)

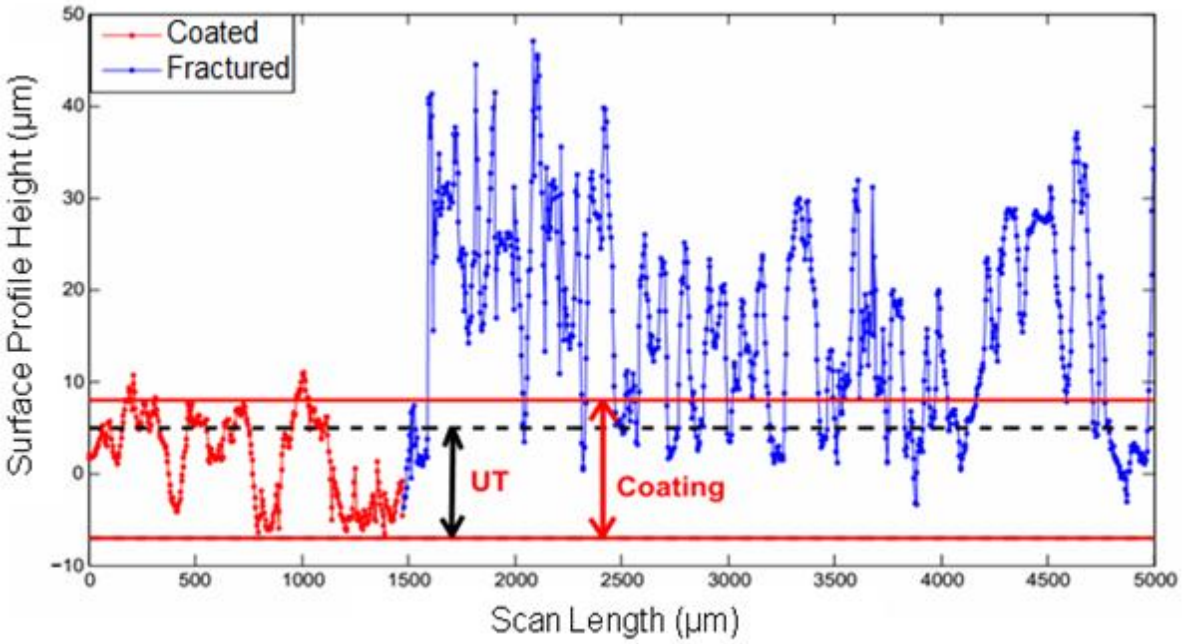

(b)

Figure 4.11: (a) Surface profile of UT+EC3901 (90^{o}C) coated specimen before bonding, (b) surface profile of fractured UT+EC3901 (90^{o}C) test coupon

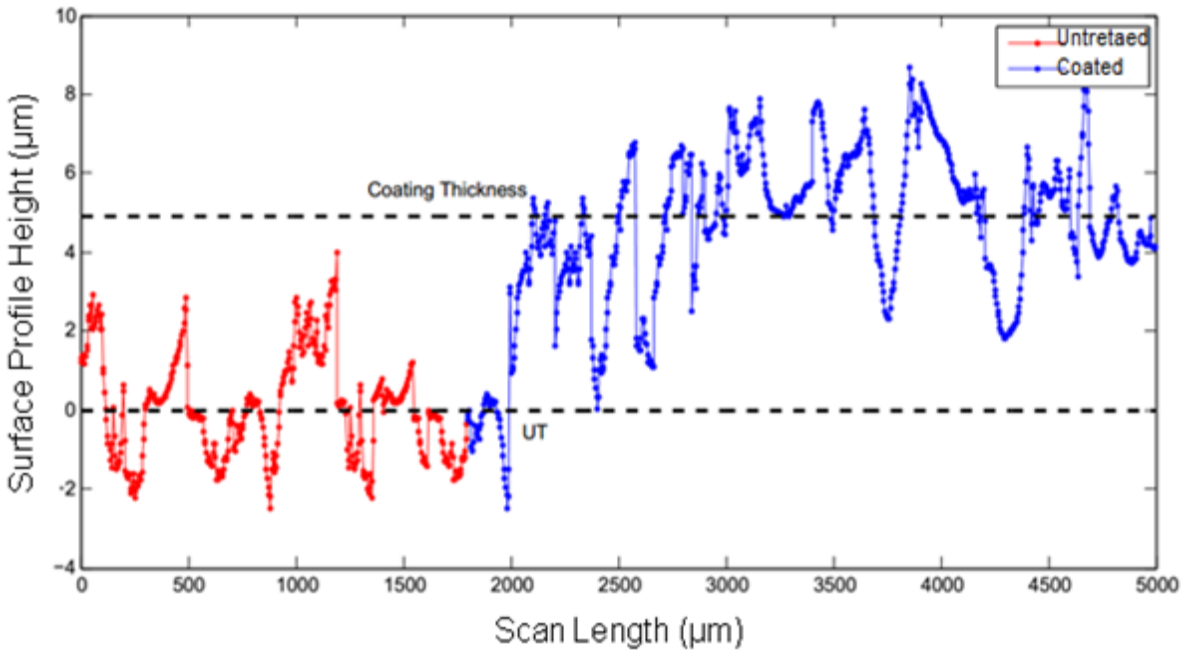

(a)

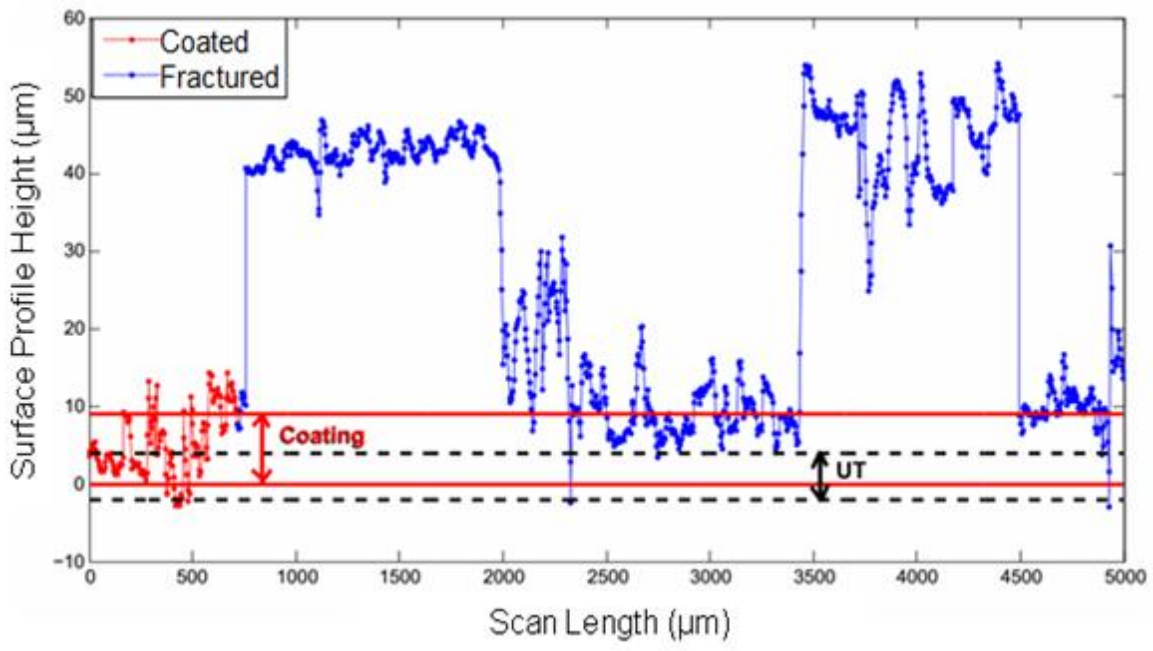

(b)

Figure 4.12: (a) Surface profile of UT+BR127 (120^{o}C) coated specimen before bonding, (b) surface profile of fractured UT+BR127 (120^{o}C) test coupon

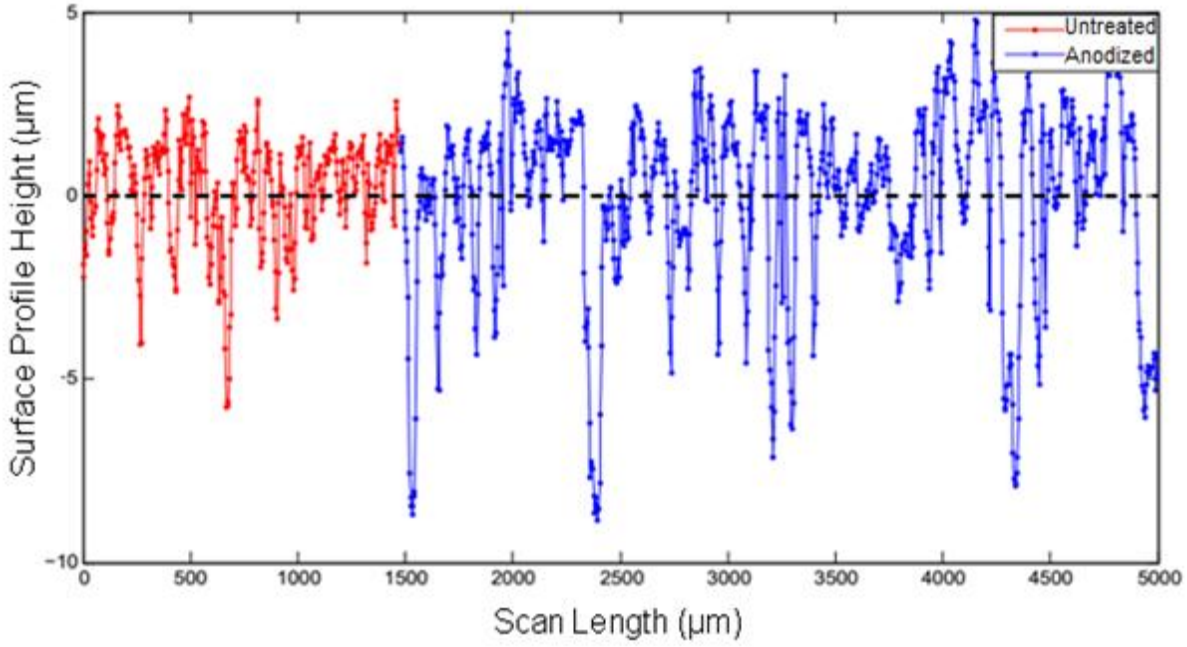

(a)

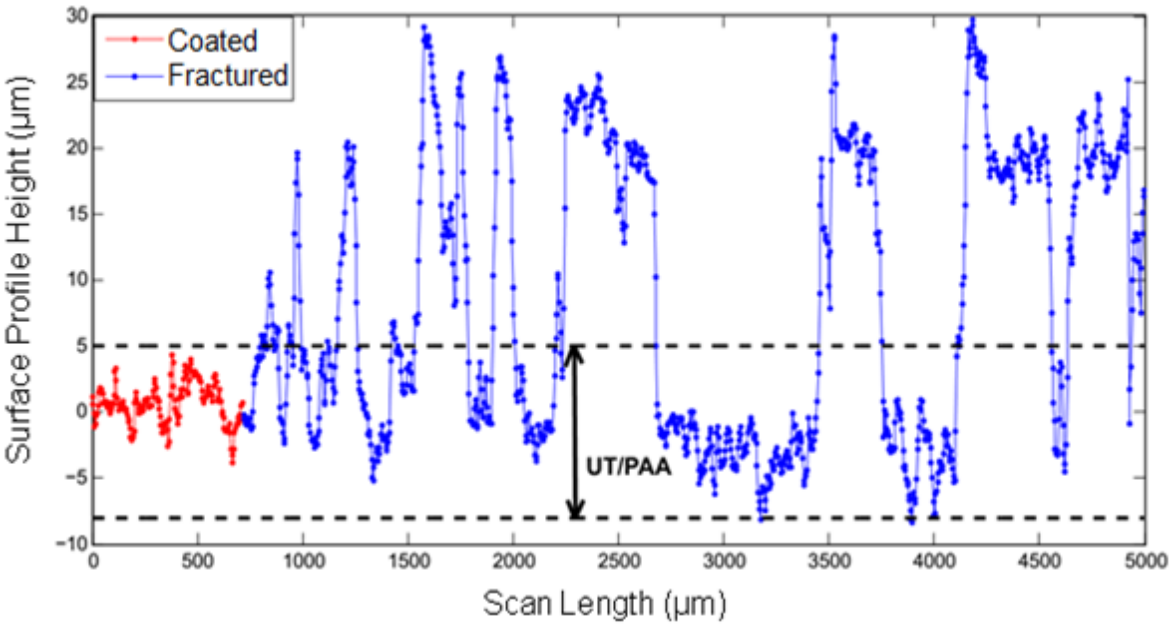

(b)

Figure 4.13: (a) Surface profile of PAA specimen before bonding, (b) surface profile of fractured PAA test coupon

Table 4.4: Coating thickness measured by profilometer.

Coating	**Coating Thickness (µm)**
Alodine	0.81
PAA	0.48
EC 3901	0.68
BR127	1.23

The tensile load versus displacement curves are plotted in Figure 4.14 for various treatments. The ordering of various curves follow the ordering in IFSS in Figure 4.8.The thickness of adhesives was same in all the test coupons used to generate this result. The thickness of conversion coatings and primer coatings does not change the thickness of bond in these test coupons. Hence, bending of the joint during testing due eccentricity of loading cannot be the reason for the difference in steepness of these curves. Hence, the observed difference in steepness is believed to be reflective of the difference in bonding at the Al-composite adhesive interface brought about by the chemical treatments, resulting in the ordering of these curves similar to the ordering in their IFSS. 3M's EC3901 primer appears to more suitable, than Cytec's BR127, for use with the composite adhesive used in this study for room temperature bonding.

4.4 Effect of Surface Treatments on Tensile Strength of Al Substrate -Composite Adhesive Interfacial bond

Since WC test results to be presented in the next section correspond to tensile loading of joint, the tensile strength of the bond between the Al substrate and the composite adhesive is required to interpret these results. Hence, tensile strength of the bond was measured using flatwise tensile test. The thickness of the adhesive was maintained constant at ~ 0.3-0.04 mm. Based on the results presented in the previous section, four treatments that resulted in the maximum IFSS were selected. They were UT+ EC3901 (90^{o} C), PAA+BR127 (120^{o} C), Alodine+BR127 (120^{o} C), and PAA+EC3901 (90^{o} C). These results were compared with UT. In addition, attempts were made to measure the tensile strength of bond for PAA and Alodine. PAA and Alodine treated test coupons debonded with complete interfacial failure while gripping them.

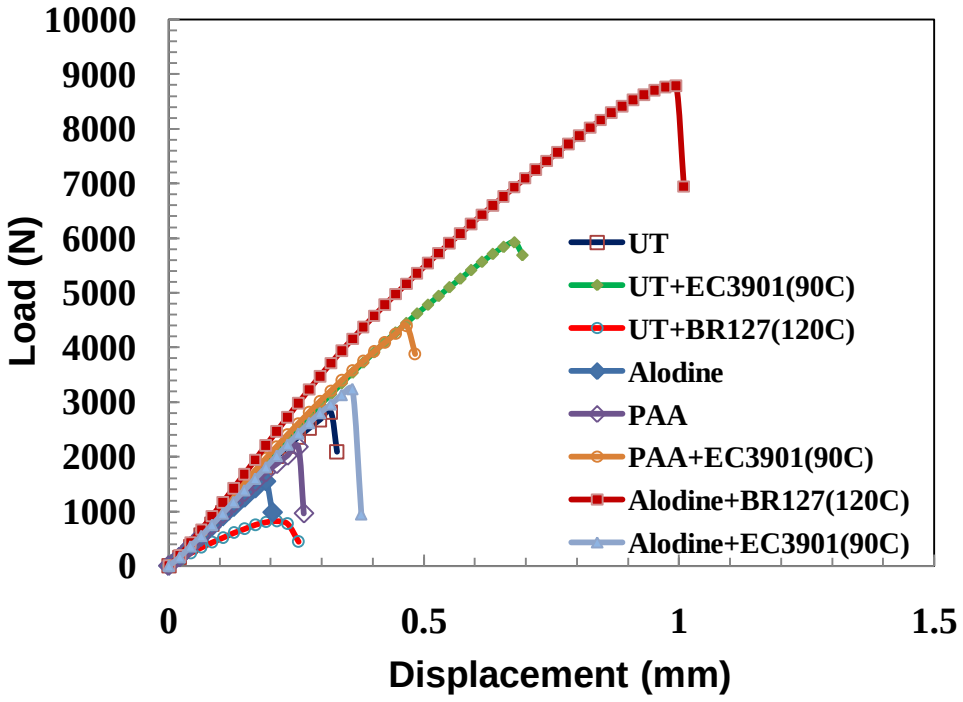

Figure 4.14: Load/displacement plots for various surface treatments

The tensile strength results are presented in Table 4.5 and Figure 4.15. The ordering of surface treatments in terms of increasing tensile strength is similar to that observed for IFSS. The conversion and primer coatings significantly increased the tensile strength of the bond when compared to UT. The EC3901 primer appears to result in marginally higher tensile strength when compared to BR127 in case of PAA while this was reversed for IFSS. UT +EC3901 (90^{o} C) resulted in the highest tensile strength (almost 8 times increase when compared to UT). The % different in tensile strength due to various treatments is relatively higher than the % difference in IFSS due to various surface treatments. So tensile strength of bonds may be a better discriminator than IFSS while evaluating the effect of surface treatments.

The fracture surfaces for the tested coupons are provided in Figure 4.16. The binary image of the fracture surfaces were analyzed using ImageJ software and the % cohesive fracture areas are tabulated in Table 4.5. The fracture mode is mixed mode and hence, the reported values are apparent tensile strength only. The % cohesive area increases with the tensile strength, similar the case of IFSS.

4.5 Environmental Durability of Bond Between Al Substrate and Composite Adhesive

Moisture in the environment can attack the interface between the Al substrate and the adhesive resulting in the degradation of the bond strength (true IFSS and tensile strength).Surface treatments should be able to prevent this environmental degradation of the bond in addition to enhancing the bond strength. Hence, the effect of various surface treatments on the environmental durability of the bond was studied using WC, SLS and FWT tests.

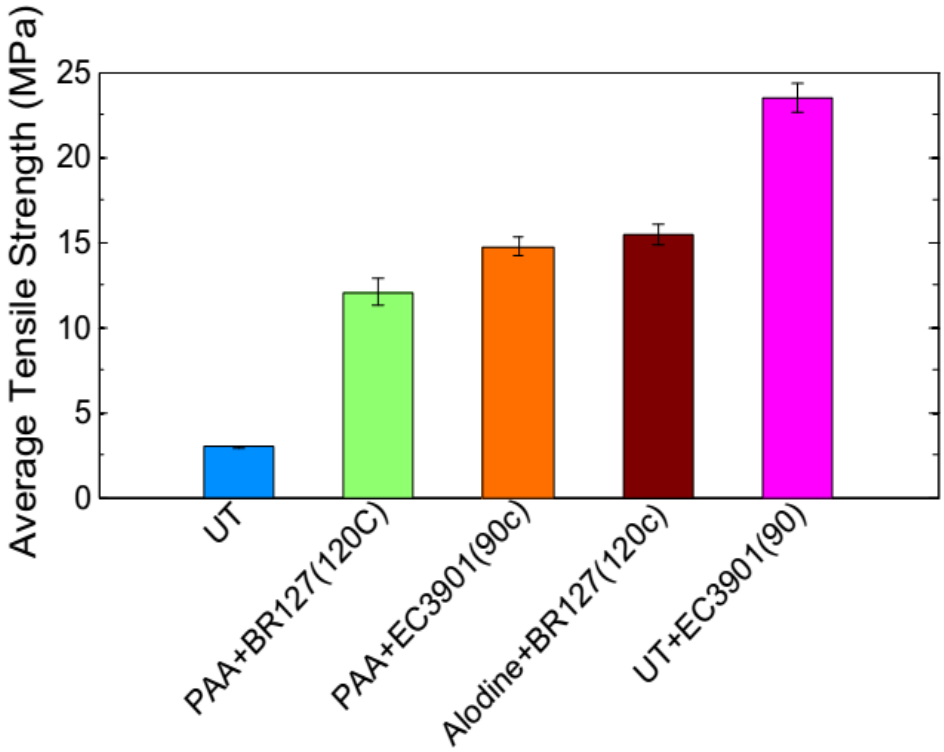

Figure 4.15: Tensile Strength of Bond formed using various surface Treatments

Table 4.5: Tensile strength and % of cohesive fracture

Treatment	**Tensile Strength (MPa)**	**Percentage of Cohesive Fracture (%)**
UT (untreated)	2.95±0.06	60±11
PAA+BR127 (120^{o} C)	12.06±0.75	73±8.8
PAA+EC3901 (90^{o} C)	14.75±0.58	71±13.5
Alodine+BR127 (120^{o} C)	15.45±0.54	75±8
UT+EC3901(90^{o} C)	23.46±0.88	82±4.9

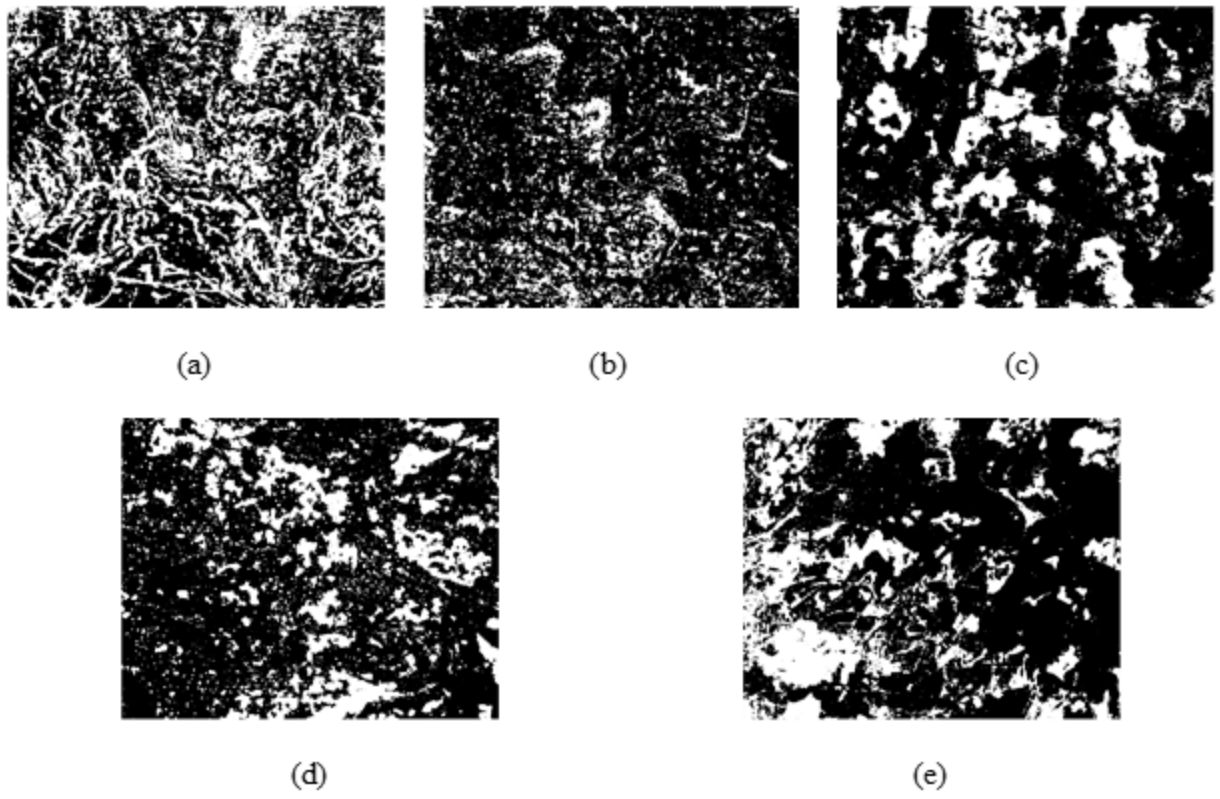

Figure 4.16: Binary image of fracture surface of flatwise tension specimen at 5 X magnification

(a) UT, (b) UT+EC3901 (90^{o} C), (c) PAA+BR127 (90^{o} C), (d) Alodine+BR127 (120^{o} C)

PAA+EC3901 (90^{o} C)

In addition, the absorbed moisture can lower the T_g (glass to rubber transition temperature) and hence, can lower the strength of the thermoset. If the degradation in the strength of the adhesive is more than the degradation in the strength of the bond, then the joint would fail by cohesive failure and vice versa. Due to the brittle nature of the composite adhesive, environmental degradation of its strength could not be ascertained experimentally. However, possibility of such degradation was taken into account while interpreting the results from WC, SLS, and FWT tests.

To start with, the moisture absorption in the composite adhesive was studied to determine the time to reach saturation level of moisture. Based on this, the WC, SLS, and FWT test coupons were conditioned to various duration ranging from 0 (dry) to saturation time (saturation moisture) and tested to understand the effect of moisture on the environmental durability of the bond. Hot-humid environment of 95% RH at 40 ^{o}C was chosen to simulate the worst case scenario. Only those surface treatments that resulted in higher IFSS than UT for dry conditions were used to evaluate the environmental durability. In addition, constant adhesive thickness of 0.03-0.04 mm was used in all test coupons.

4.5.1Moisture Absorption of Composite Adhesive

The percentage of weight gain for cured composite adhesive is plotted as a function of square root of conditioning time in Figure 4.17. The weight gain increased with time and reached a plateau value of 1.425% in ~11 days. Hence, the WC, SLS, and FWT test coupons were conditioned and tested at various time intervals from 0-11 days. In addition, some test coupons were tested beyond 11 days.

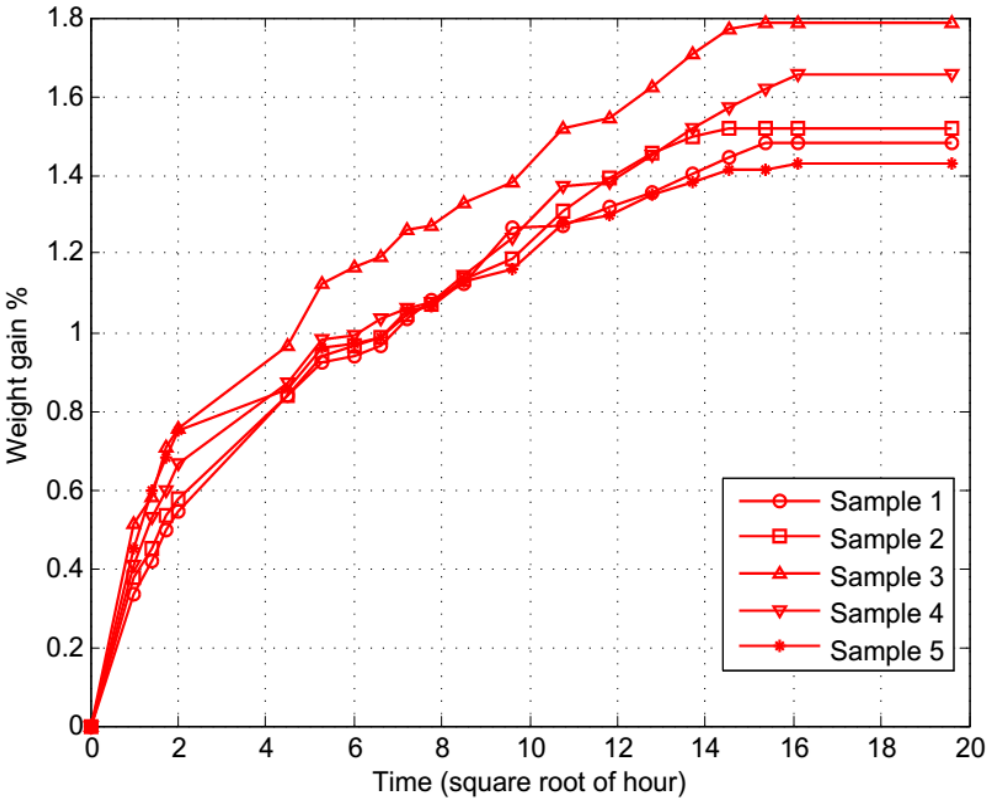

Figure 4.17: Percentage of moisture absorption in composite adhesive as a function of time

4.5.2 WC Test Results: Effect of Temperature and Humidity on Crack Propagation

The crack propagation is plotted as function of conditioning time in Figure 4.18, for different surface treatments. The crack length increased with time and reached a plateau value beyond ~450 hours for all treatments except PAA+EC3901 (RT), which failed after 350 hours.

In Figure 4.19, plateau values (average of results from test coupons) of the crack lengths for various treatments are presented. Each test coupon had different initial crack lengths (see Table 4.6) and these values are subtracted from the total crack length to plot only the length of the crack propagation. If the wedge insertion force were same, then the initial crack would be inversely proportional to the tensile strength of the joint (or bond if the fracture is interfacial) in Figure 4.18. No such relation is found in this Table 4.5. This is believed to due to lack of control over the wedge insertion force, from specimen to specimen, which was applied manually. The tensile force available at the crack tip for extension would decrease with increase in crack length. Hence, the magnitude of force available at the start of conditioning for various treatments may have been different for various treatments due to the difference in the initial crack length and may have influenced the initial rate of crack growth.

Two possible reasons for the cracks reaching the plateau are (a) the crack extension (tensile) force at the crack tip decreasing to zero, and (b) the moisture reaching the saturation level. The plateau crack length as well as the rate of crack growth (beyond 50 hours) increased in following order:

Alodine+EC3901 (90 ^{o}C)<Alodine+BR127 (120 ^{o}C)<PAA+BR127 (120^{o}C)<PAA+EC3901 (90 ^{o}C)<UT<UT+EC3901 (RT)<UT+EC3901 (90 ^{o}C)<PAA+EC3901 (RT).

Table 4.6: Initial crack length for various surface treatments

Treatment	**Initial Crack Length(mm)**
Alodine+EC3901(90 ^{o}C)	40.70±2.17
Alodine+BR127(120 ^{o}C)	51.56±1.47
PAA+EC3901(90 ^{o}C)	42.05±2.34
PAA+BR127(120 ^{o}C)	42.77±1.175
UT	45.79±5.07
UT+EC3901(90 ^{o}C)	55.22±7.25
UT+EC3901(RT)	46.15±2.18
PAA+EC3901(RT)	41.60±1.94

The crack length was least inthe test coupons treated with Alodine+EC3901 (90^{o} C) and the Alodine+BR127(120 ^{o}C) and maximum in test coupons treated with PAA+EC3901 (RT). The PAA+EC3901 (RT) test coupons were completely debonded apart at 350 hour of exposure. While EC3901 cured at 90 ^{o}C and RT on UT resulted in very high IFSS in dry condition, their durability in hot- moisture environment is low. The crack length for UT+ EC3901 is higher than that for UT specimens. However, EC3901 cured at 90 ^{o}C on PAA and Alodine treated coupons resulted in least crack growth suggesting that PAA and Alodine treatments combined with primers result in better environmental durability than UT, a conclusion similar to that reached by past studies on high temperature bonding. Also, curing EC3901 at 90 ^{o}C results in a better environmental durability of PAA and Alodine treated surfaces when compared to EC3901 cured at RT.

The crack growth in PAA and Alodine test coupons coated with BR127 and cured at 120 ^{o}C was comparable (within experimental scatter) to the crack growth in these test coupons coated with EC 3901 and cured at 90 ^{o}C. Alodine coated with either BR127 (120 ^{o}C) or EC 3901 (90 ^{o}C) appears to have a slight edge over PAA coated with either of these primers, in imparting the best environmental durability to the bond formed between the room temperature curing composite adhesive and the Al substrate.

4.5.2.1 Analysis of Fracture Modes in WC Test Coupons

Once the crack growth had stopped (i.e. crack length had reached a plateau value), the test coupons were opened to examine the fracture surface. The fractographs are shown in Figure 4.20. The starter crack length, the increase in crack length due to propagation during

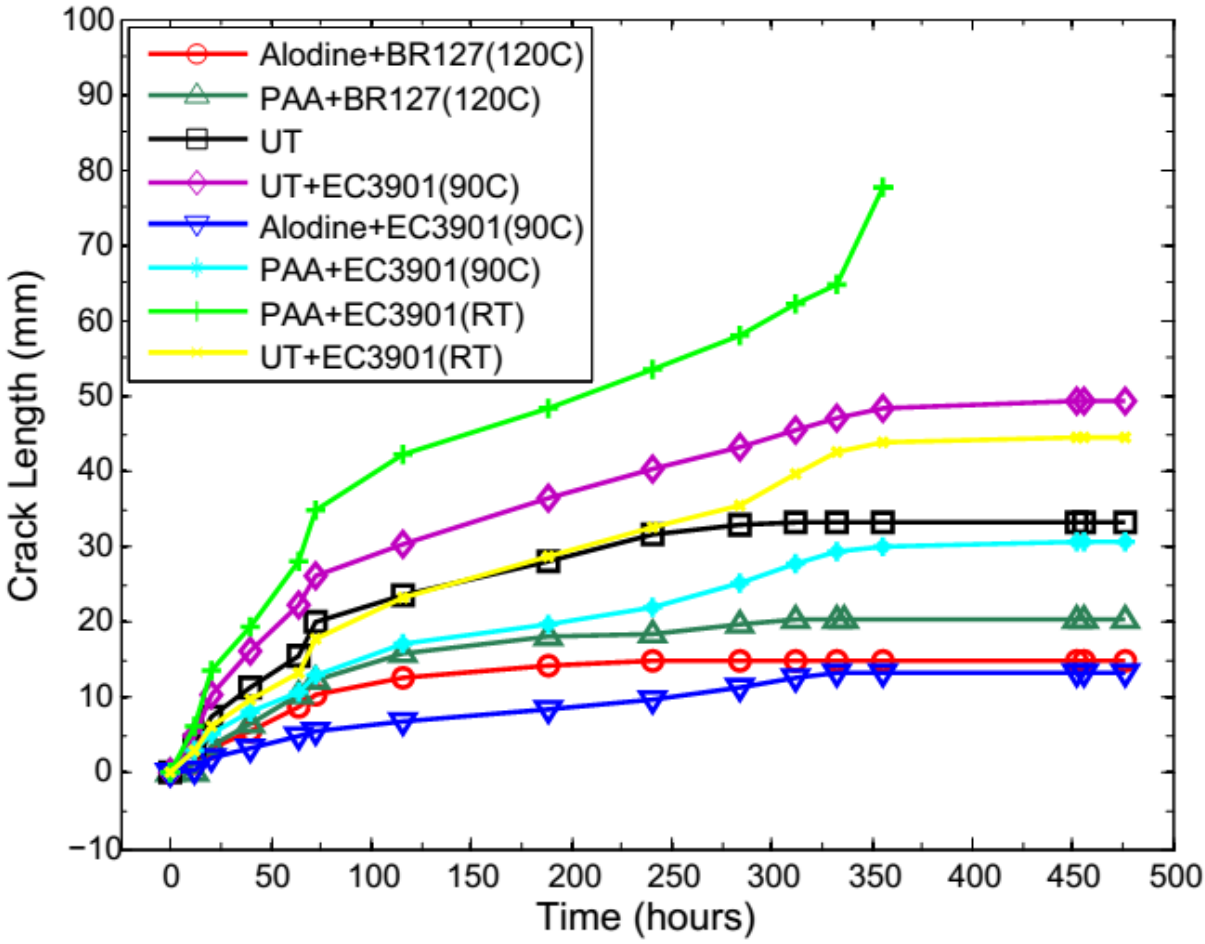

Figure 4.18: Crack propagation in WC test coupons, with various surface treatments, as a function of conditioning time at 95% RH and 40 ^{o}C

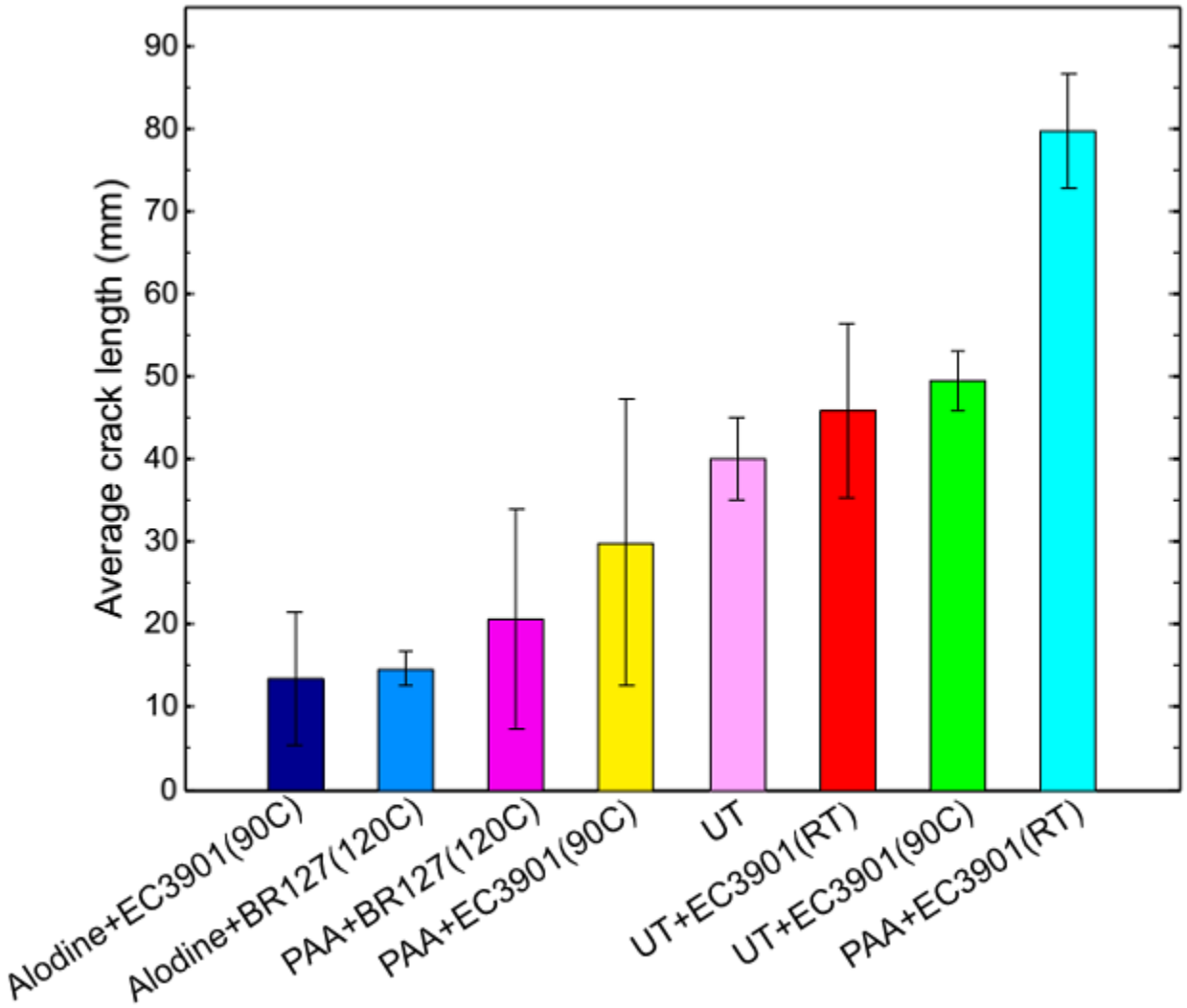

Figure 4.19: Plateau crack lengths in WC test coupons with various surface treatments

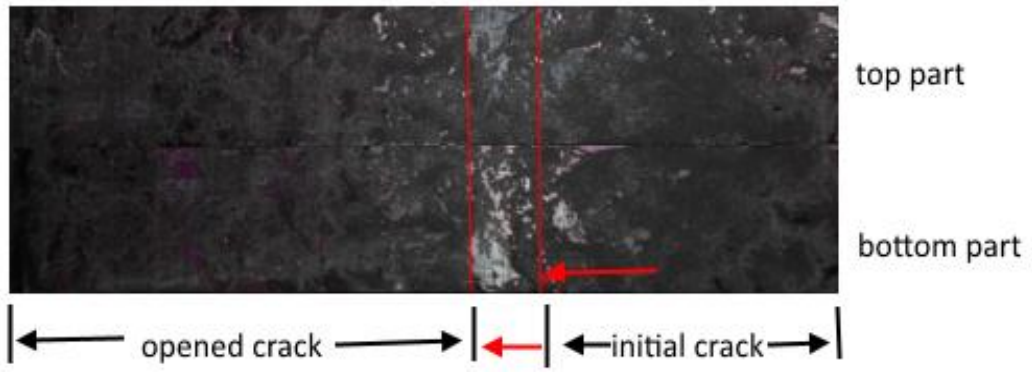

Alodine+EC3901 (90 ºC)

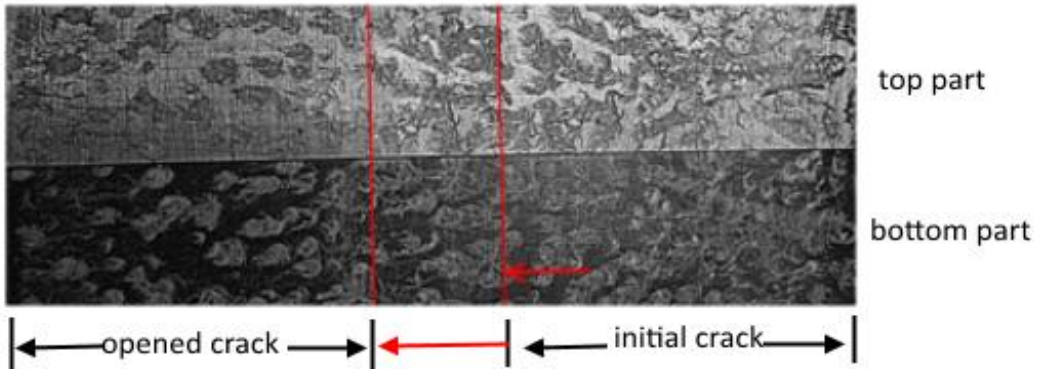

(b) Alodine+BR127 (120 ºC)

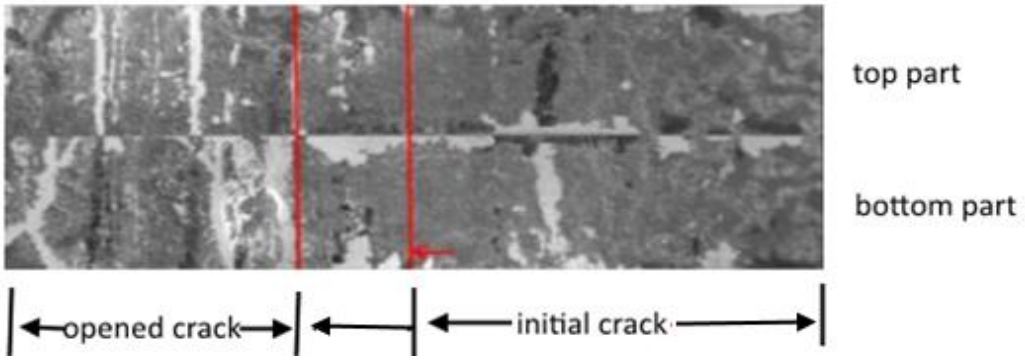

(c) PAA+BR127 (120 ºC)

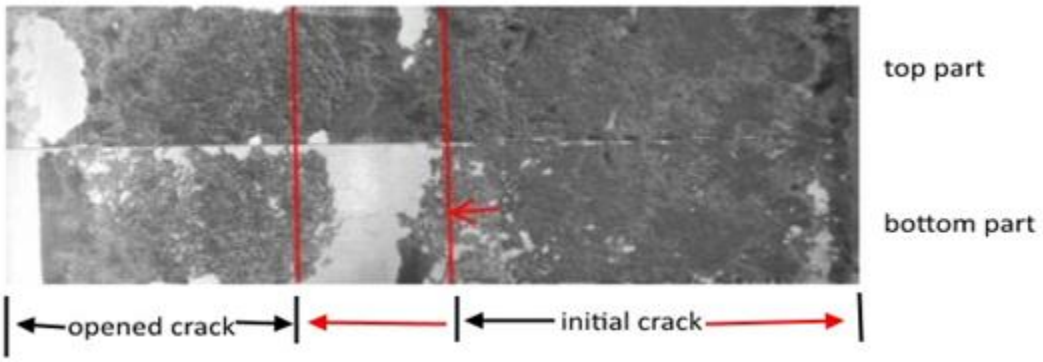

(d) PAA+EC3901(90 ^{o}C)

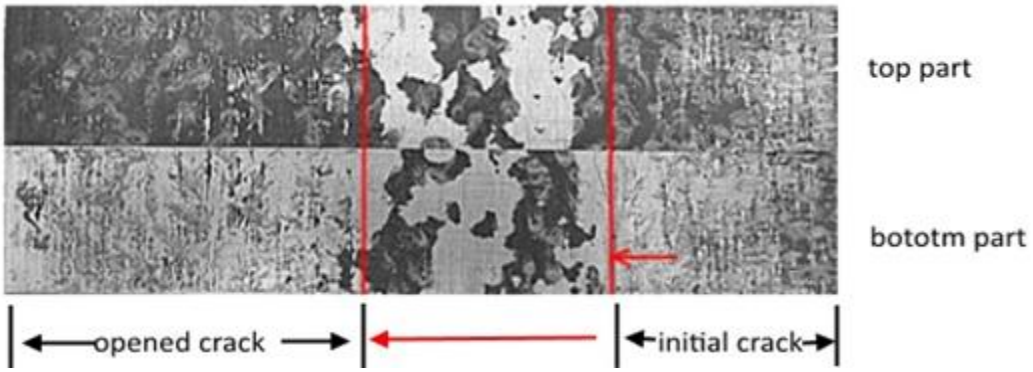

(e) UT

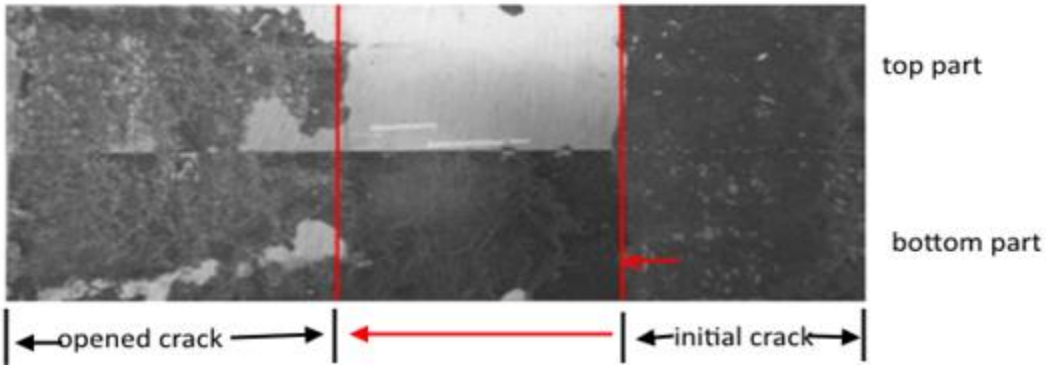

(f) UT+EC 3901 (RT)

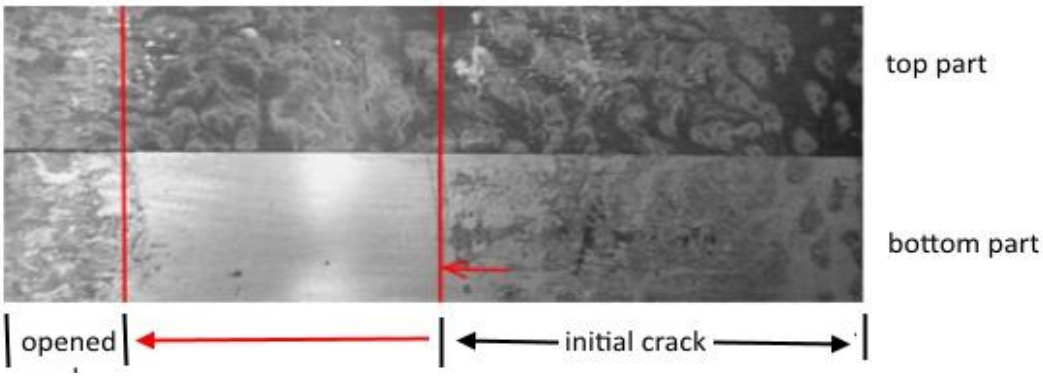

(g) UT+ EC3901 (90 ^{o}C)

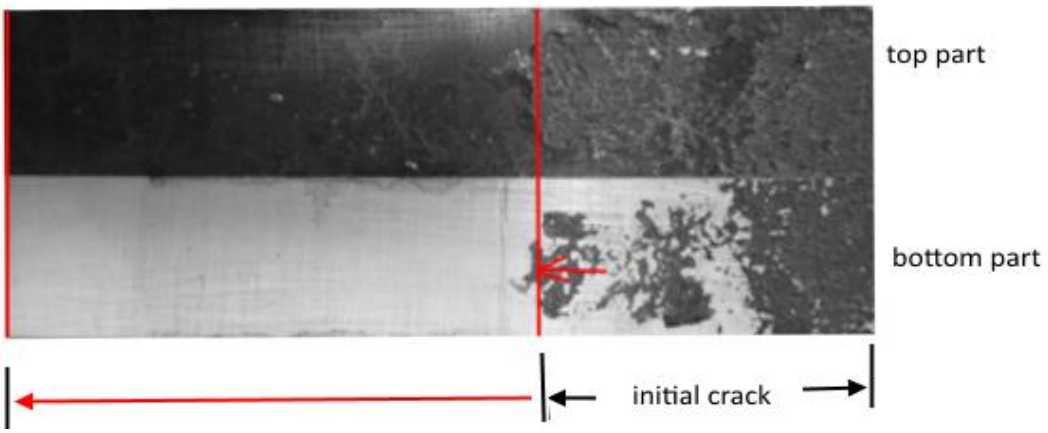

(h) PAA+EC3901 (RT)

Figure 4.20: Fracture surface of WC test coupons.

environmental conditioning (propagated crack length), and length of the bonded region fractured during opening are identified in this figure.

The initial crack's tip was at the interface for UT, UT+EC3901 (90 ^{o}C), UT+EC3901 (RT), and PAA+EC3901 (RT). During conditioning the crack propagated along the interface; while the crack staggered from one interface to another in UT, it propagated along the same interface for other three treatments. This could be one reason why the plateau crack length for UT is lower than the other three.

The initial crack tip, in Alodine+ BR127 (120 ^{o}C), PAA+BR127 (120 ^{o}C), PAA +EC3901 (90 ^{o}C), and Alodine+EC3901 (90 ^{o}C), staggered between adhesive and interface and the subsequent propagation was also mixed mode. It can be estimated from this figure that the % cohesive area increased in the following order: PAA +EC3901 (90 ^{o}C), PAA+BR127 (120 ^{o}C), Alodine+ BR127 (120 ^{o}C), and Alodine + EC3901 (90 ^{o}C). Correspondingly, the plateau crack length decreased in that order, suggesting that environmental durability of the interfacial bond increased in that order. The % cohesive area and binary images of fracture surface of first four WC test coupons are presented in table 4.7 and Figure 4.21. It can be observed from table 4.7 that the % cohesive fracture area has decreased as the crack length increases for these four treatments.

4.5.3 Effect of Hot-Humid Environment on IFSS

The IFSS for test coupons conditioned for 0, 3, 7 and 30 days are tabulated in Table 4.8 and plotted in Figure 4.22, as a function of time, for various surface treatments. Test coupons treated withAlodine+BR127 (120 ^{o}C) and PAA+BR127 (120 ^{o}C) exhibited least degradation in IFSS.

Table 4.7 % cohesive fracture area for first four WC test coupons

Treatments	**Cohesive Fracture Area (%)**
Alodine+EC3901(90 ^{o}C)	75±9
Alodine+BR127(120 ^{o}C)	57±10
PAA+BR127(120 ^{o}C)	63±13
PAA+EC3901(90 ^{o}C)	28±5

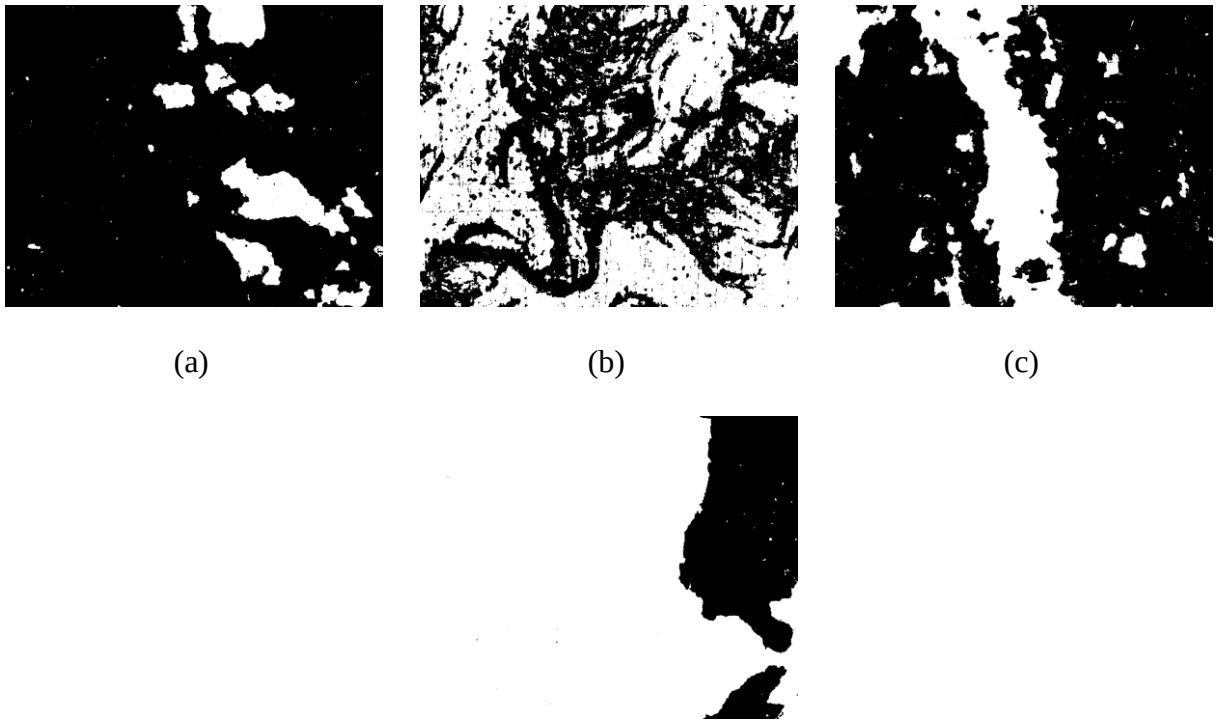

(a) (b) (c)

(d)

Figure 4.21: Binary images of (a) Alodine+EC3901 (90^{o}C) (b) Alodine+BR127(120^{o}C)

PAA+BR127(120 ^{o}C) PAA+EC3901(90 ^{o}C)

Table 4.8: Normalized and absolute IFSS at different conditioning time for different treatments

Treatment	Conditioning Duration (Days)	Normalized Residual IFSS	Absolute IFSS (MPa)
Alodine+BR127 (120 ^{o}C)	0	1	14.32±0.97
	1	1	14.32±0.20
	3	0.93±0.04	13.38±0.33
	7	0.83±0.09	11.94±0.81
	30	0.82±0.12	11.76±0.29
PAA+BR127(120 ^{o}C)	0	1	13.08±0.21
	1	1±0.03	13.08±0.21
	3	1±0.05	13.08±0.21
	7	0.92±0.10	12.03±0.68
	30	0.83±0.06	10.85±0.23
Alodine+EC3901(90 ^{o}C)	0	1	7.65±0.38
	1	0.94±0.09	7.19±0.50
	3	0.91±0.03	6.96±0.38
	7	0.81±0.07	6.19±0.23
	30	0.70±0.11	5.46±0.78
UT	0	1	6.60±0.23
	1	1±0.04	6.60±0.23
	3	1±0.06	6.60±0.78
	7	0.63±0.12	4.15±0.60

Treatment	Conditioning Duration (Days)	Normalized Residual IFSS	Absolute IFSS (MPa)
	30	0.55±0.08	3.63±0.39
UT+EC3901(90 ^{o}C)	0	1	13.18±0.19
	1	0.96±0.02	12.65±0.67
	3	0.74±0.09	9.75±0.49
	7	0.60±0.11	7.9±0.79
	30	0.44±0.02	5.79±0.47
PAA+EC3901(90 ^{o}C)	0	1	12.10±0.44
	1	1±0.09	12.10±0.44
	3	0.82±0.11	9.92±0.88
	7	0.58±0.13	7.02±0.57
	30	0.44±0.08	5.32±0.34
UT+EC3901(RT)	0	1	13.28±0.50
	1	0.0.83±0.08	11.02±0.59
	3	0.75±0.09	9.96±0.77
	7	0.63±0.06	8.36±0.43
	30	0.37±0.10	4.90±0.91
PAA+EC3901(RT)	0	1	11.72±0.67
	1	0.88±0.11	10.30±0.50
	3	0.72±0.08	8.43±0.59
	7	0.52±0.08	6.08±0.44

Treatment	Conditioning Duration (Days)	Normalized Residual IFSS	Absolute IFSS (MPa)
	30	0	0

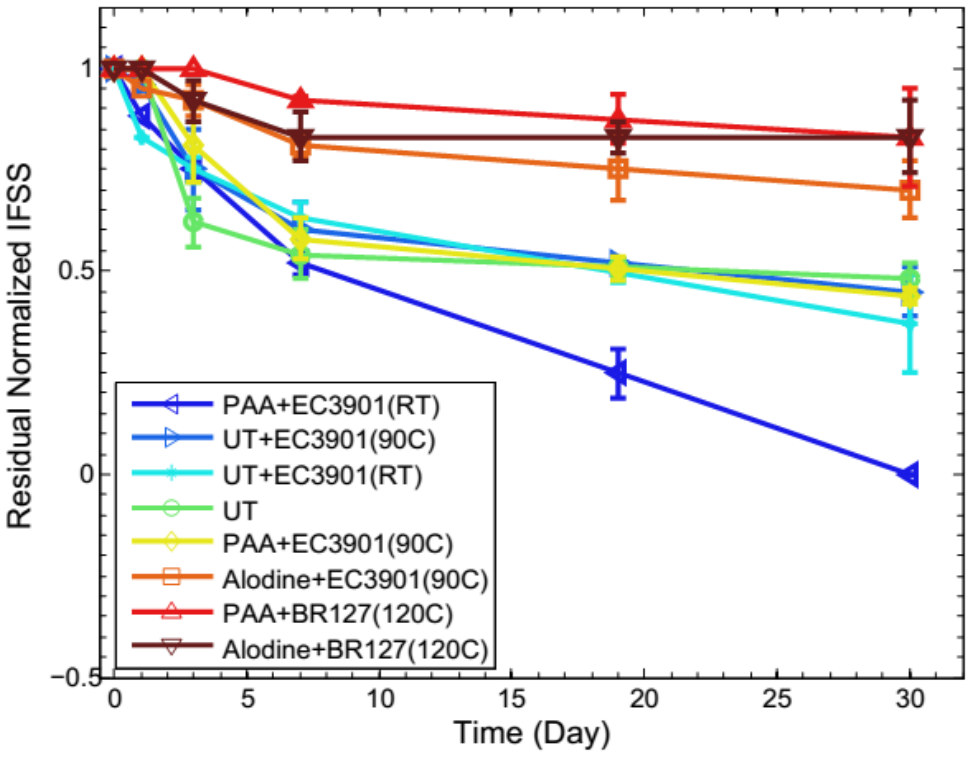

Figure 4.22: Normalized residual IFSS as a function of time

They retained more than 80% of their initial IFSS after 30 days exposure to the hot-humid environment. This was followed by Alodine+EC3901 (90 ^{o}C), that retained 70% of the initial IFSS. On the other hand, test coupons treated with PAA+EC3901 (RT) retained no strength after 30 days of exposure; the test coupons could not be tested since they debonded during removal from the chamber. UT +EC3901 (RT) were slightly better than this. The EC3901 cured at 90 ^{o}C on UT and PAA exhibited residual IFSS slightly less than that for UT. The normalized residual IFSS at 30thday for different treatments increased in following order.

[Alodine+BR127 (120 ^{o}C) = PAA+BR127 (120^{o}C)]> Alodine+EC3901 (90 ^{o}C) > UT > [UT+EC3901 (90^{o}C) = PAA+EC3901 (90 ^{o}C)] PAA+EC3901 (RT) ≥ UT+EC3901 (RT) > PAA+EC3901 (RT)

This ordering similar to the trend observed in WC test results.

4.5.3.1 Analysis of Fracture Surface of SLS Test Coupons Subjected to Hot-Humid Exposure

The fracture surfaces SLS samples exhibited increase in interfacial fracture mode with increase in conditioning time, for each treatment. Representative binary images of the fracture surfaces of PAA+EC3901 (RT) test coupon is presented in Figure 4.23 to show the gradual decrease in cohesive failure mode (increase in interfacial failure) with increase in conditioning time. Binary images of fracture surfaces of other treatments are shown in Figure 4.24 for a conditioning time of 30 days. Image analysis results of fracture surfaces of test coupons conditioned for 30 days are tabulated for all treatments in Table 4.9.

Table 4.9: % Cohesive fracture area and % reduction in cohesive fracture area after exposure for 30 days, for different treatments

Treatment	**% Cohesive Fracture Area**	**% Reduction in Cohesive Fracture Area**
Alodine+BR127 (120 ^{o}C)	62	24
PAA+BR127 (120 ^{o}C)	60	21
UT+EC390 (RT)	46	42
UT+EC390 (90 ^{o}C)	43	47
PAA+EC3901 (90 ^{o}C)	37	53
Alodine+EC3901 (90 ^{o}C)	32	30
UT	23	34
PAA+EC3901 (RT)	16	78

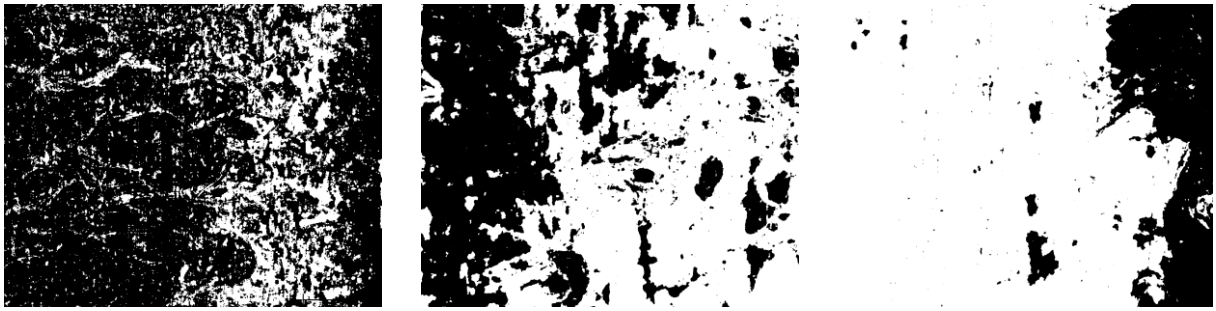

(a) (b) (c)

Figure 4.23: Fracture surfaces (imaged at 5X) of PAA+EC3901 (RT) SLS test coupon tested after exposure to hot-humid environment (a) 0 day with 73% cohesive fracture area, (b) 7 days with 43% cohesive fracture area and (c) 30 days with 16% cohesive fracture area

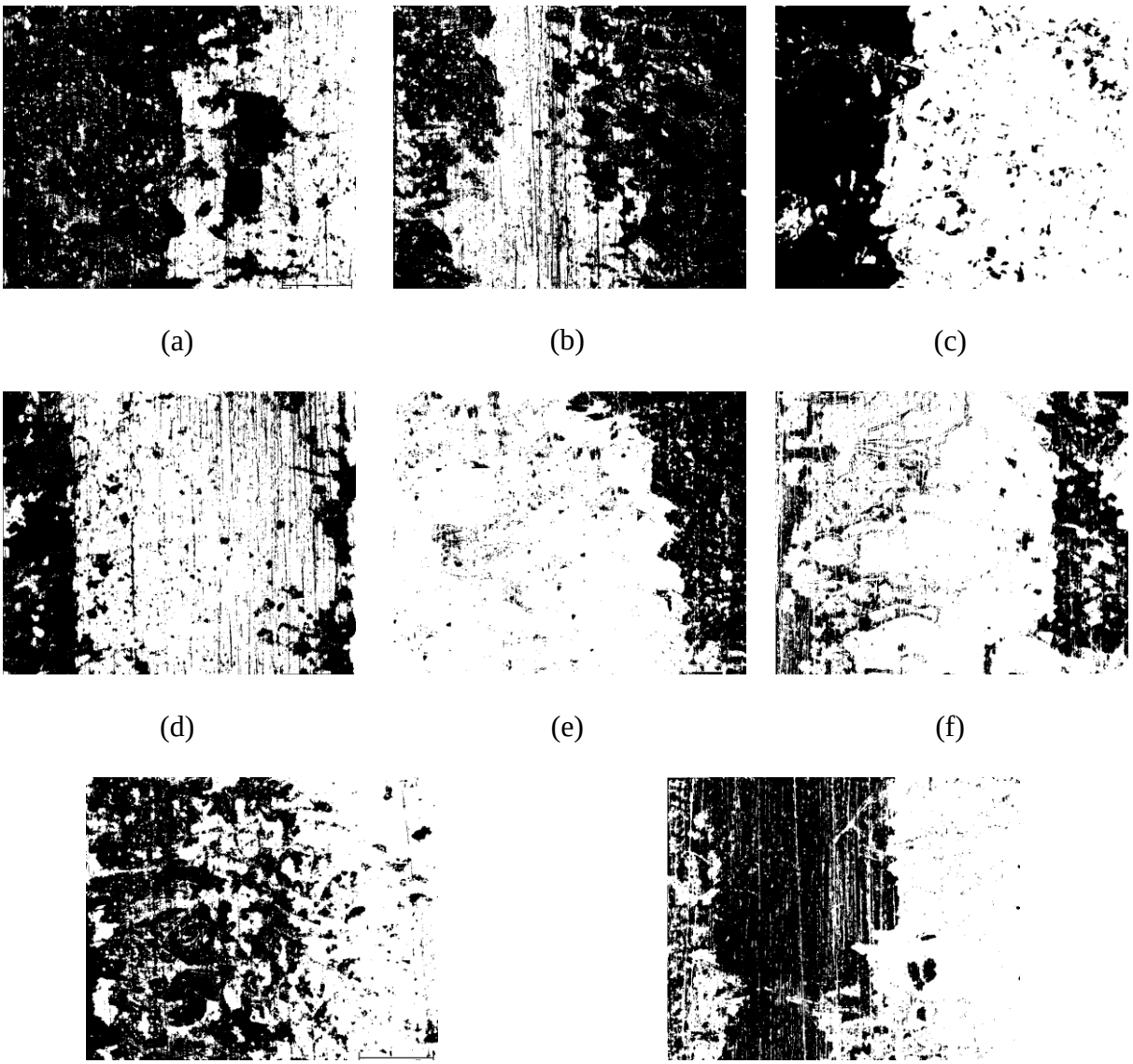

Figure 4.24: Fracture surfaces (imaged at 5X)of SLS test coupons, tested after exposure to hot-humid environment for 30 days (a) Alodine+BR127 (120 ^{o}C), (b) PAA+BR127 (120 ^{o}C), (c) Alodine+EC3901 (90 ^{o}C), (d) PAA+EC3901 (90 ^{o}C), (e) PAA+ EC3901 (RT), (f) Untreated, (g) UT+ EC3901 (90 ^{o}C), (h)UT+EC3901(RT)

The reduction in the cohesive area was minimum for test coupons treated with Alodine and PAA followed by application and curing of BR127 primer at 120 ^{o}C. They also exhibited least reduction in IFSS (i.e. highest residual normalized IFSS) after 30 days of exposure. PAA+EC3901 (RT) exhibited the lowest % of cohesive fracture area (maximum reduction in % of cohesive fracture area). From Table 4.6, it is observed that PAA+EC3901 (RT) retained no strength at all after 30 days of exposure to the hot-humid environment. The EC3901 cured at 90 ^{o}C on Alodine resulted in lower reduction in % cohesive area (and IFSS) than on PAA or UT. In general, the reduction in the IFSS (alternatively the % normalized residual strength) is proportional to the % reduction in cohesive fracture area (i.e. increase in % adhesive fracture area). Hence, the reduction in the IFSS is believed to be due to reduction in the environmental durability of the bond between the Al substrate and the composite adhesive.

4.5.3.2 Relation Between Degradation in IFSS and Crack Propagation in WC Specimen

The normalized residual IFSS is plotted as a function of propagated crack length in Figures 4.25. Since the environmental exposure testing of SLS test coupons were continued beyond the time when the crack propagation in WC test coupons reached a plateau value, the IFSS corresponding to this time 9~19 days) was interpolated from the IFSS values shown in Figure 4.22. The plots for different treatments are presented in two figures using the UT as the reference to improve readability. The crack length does not increase proportionately with increase in % reduction in IFSS (alternatively, decrease in % normalized residual IFSS). For example, Alodine+EC3901 (90 ^{o}C) has resulted in lower crack length when compared to PAA+BR127 (120 ^{o}C) despite resulting in a lower % normalized residual IFSS. Hence, the WC test results may not be directly correlated with the reduction in IFSS.

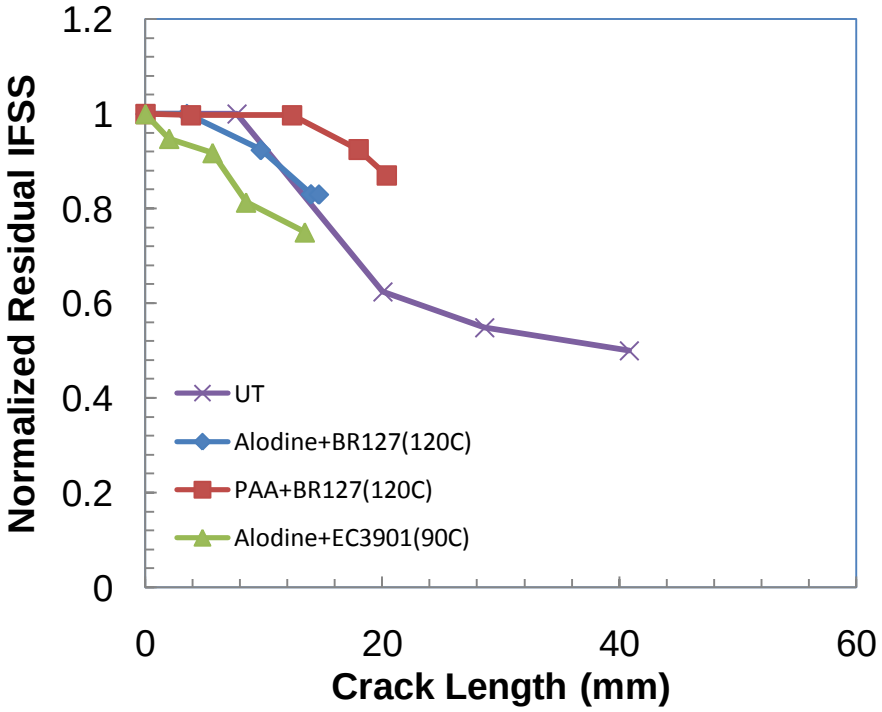
Normalized Residual IFSS
1.2
1
0.8
0.6
0.4
0.2
0
0
20
40
60
Crack Length (mm)
UT
Alodine+BR127(120C)
PAA+BR127(120C)
Alodine+EC3901(90C)

(a)

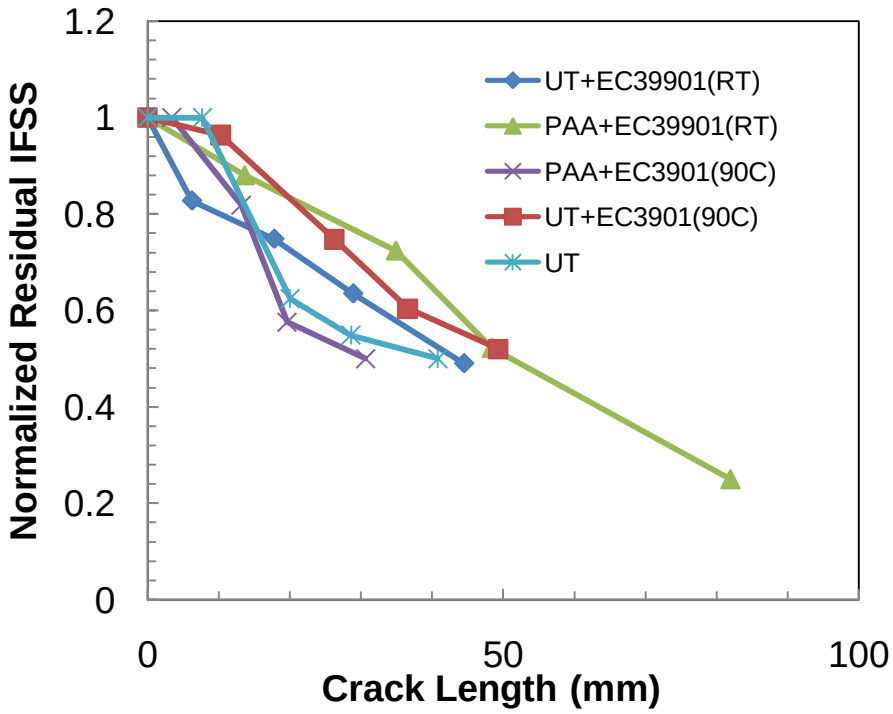

(b)

Figure 4.25: Normalized residual IFSS as a function of propagated crack length for (a) Alodine+BR127 (120 ^{o}C), PAA+BR127 (120 ^{o}C), Alodine+EC3901 (90 ^{o}C), and UT; (b) UT+EC3901(RT), UT+EC3901(90 ^{o}C), PAA+ EC3901(90 ^{o}C), PAA+ EC3901(RT) and UT

4.6 Effect of Hot-Humid Environment on Tensile Strength of Bond Between the Al substrate and the Composite Adhesive

The normalized residual tensile strengths for various surface treatments are tabulated in Table 4.10 and plotted in Figure 4.26 as a function of exposure time. PAA+BR127 (120 ^{o}C) and Aodine+BR127 (120 ^{o}C) exhibited maximum residual strength. UT and PAA+EC3901 (90 ^{o}C) exhibited similar reduction in the tensile strength, although higher than that for PAA+BR127 (120 ^{o}C) and Aodine+BR127 (120 ^{o}C). UT+EC3901 (90 ^{o}C) couldnot be tested since they debonded while removing from the chamber. This trend is similar to the trend in degradation in IFSS and propagated crack length.

4.6.1 Analysis of Fracture Surface of FWT Test Coupons Exposed to Hot-Humid Environment

The binary images of fracture surfaces of PAA+EC3901 (90 ^{o}C) are shown in Figure 4.27 as a function of exposure time. Similar to SLS test coupons, the FWT test coupons also showed a gradual decrease in % cohesive fracture with increase in reduction in tensile strength (i.e. decrease in the % normalized residual tensile strength). Similar trend was observed for other treatments. The binary images of fracture surface of test coupons, subjected to other surface treatments, tested after exposure to hot-humid environment for 30 days are shown in Figure 4.28.The % cohesive area and % reduction in cohesive fracture area are tabulated in Table 4.11. Residual tensile strength for Alodine+BR127(120 ^{o}C) and PAA+BR127(120 ^{o}C)was 60% and they showed minimal reduction in cohesive fracture area. The % reduction in cohesive fracture area for UT+EC3901 (90 ^{o}C) was maximum (87%) and it retained no strength after 30 days of

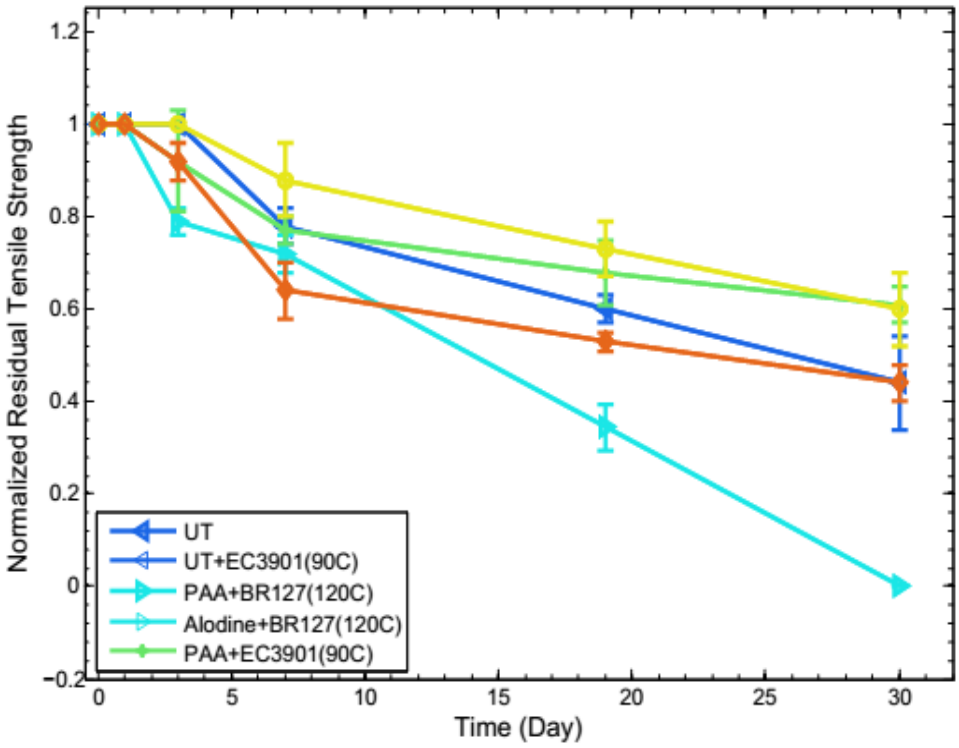

Figure 4.26: Normalized residual tensile strength as a function of exposure time, for various treatments

Table 4.10: Normalized Residual Tensile Strength as a function of exposure time

Treatment	Exposure Duration (Days)	Normalized Residual Tensile Strength	Absolute Tensile Strength
Alodine+BR127(120 ^{o}C)	0	1	15.45±0.54
	1	1	15.48±0.79
	3	1	15.45±0.12
	7	0.88±0.03	13.60±0.43
	30	0.60±0.10	9.27±0.90
PAA+BR127(120 ^{o}C)	0	1	12.06±0.74
	1	1	12.56±0.79
	3	.92±0.04	11.09±0.84
	7	0.77±0.03	9.26±0.98
	30	0.61±0.07	7.36±0.75
UT	0	1	2.96±0.06
	1	1	3.02±0.16
	3	1	2.98±0.06
	7	0.78±0.05	2.30±0.26
	30	0.44±0.05	1.29±0.23
PAA+EC3901(90 ^{o}C)	0	1	14.75±0.59
	1	1	14.89±0.76
	3	.92±0.02	13.70±0.63
	7	0.64±0.11	9.57±0.69

Treatment	Exposure Duration (Days)	Normalized Residual Tensile Strength	Absolute Tensile Strength
	30	0.44±0.03	6.55±0.11
UT+EC3901(90 ^{o}C)	0	1	23.46±0.88
	1	1	23.81±0.34
	3	0.79±0.12	18.53±0.82
	7	0.72±0.09	16.89±0.97
	30	0.0	0

(a)71% cohesive failure at 0 day

(b) 40% cohesive failure after 7 days

(c) 27% cohesive failure after 30 days

Figure 4.27: Binary image of fracture surface (imaged at 5X) of PAA+EC3901 (90 ^{o}C) tested after exposure to hot-humid environment for various duration.

Table 4.11: % Cohesive fracture area after exposure for30th days and corresponding % reduction in cohesive fracture areaforvarious surface treatments

Treatment	**% Cohesive fracture area**	**% Reduction in cohesive fracture area**
UT (untreated)	47±9.45	20
UT+EC3901 (90 ^{o}C)	9.10±3.78	87
PAA+BR127 (120 ^{o}C)	51±10.8	30
Alodine+BR127 (120 ^{o}C)	59±11.23	21
PAA+EC3901 (90 ^{o}C)	27±7.8	62

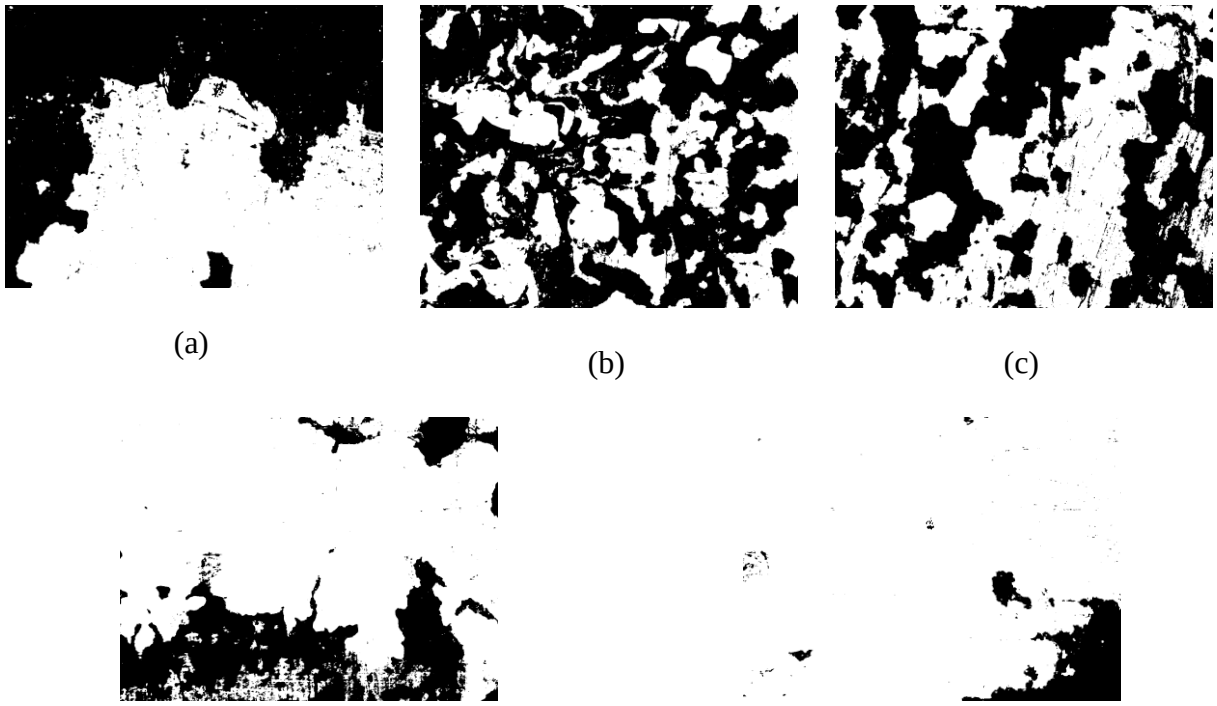

Figure 4.28:Binary images fracture surfaces (imaged at 5X) of FWT tension coupons tested after exposure to hot-humid environment for 30 days(a)UT, (b) Alodine+BR127 (120 ^{o}C) (c) PAA+BR127 (120 ^{o}C), (d) PAA+EC3901 (90 ^{o}C) and (e) UT+EC3901 (90 ^{o}C)

exposure. Although the % cohesive area and the % reduction in cohesive area for UT are more than that for PAA+EC3901 (90^{o}C), both had similar % normalized residual strength.

4.6.2 Relation Between Degradation in Tensile Strength and Crack Propagation in WC Specimen

The normalized residual tensile strength is plotted as a function of propagated crack length in Figure 4.29. Since the environmental exposure testing of FWT test coupons were continued beyond the time when the crack propagation in WC test coupons reached a plateau value, the tensile strength corresponding to this time (~19 days) was interpolated from the tensile strength values shown in Figure 4.26. The crack length increased proportionately with increase in % reduction in tensile strength (alternatively, decrease in % normalized residual tensile strength). This is in contrast to the trend in IFSS. Hence, the WC test results may be directly correlated with the reduction in tensile strength.

In Figure 4.30 the normalized residual IFSS and residual tensile strength corresponding to 19 days of exposure are plotted as a function of plateau propagated crack length. The surface treatment corresponding to each data point is also identified. It is obvious that the propagated crack length increased with decrease in normalized residual strength.

PAA+BR127 (120^{o}C) andAlodine+BR127 (120^{o}C) offers the best environmental durability in a hot-humid environment for the room temperature bonding of composite adhesive to the Al substrate. This is also the conclusion reached by previous researchers for high temperature bonding. In addition, the EC3901 primer on PAA and Alodine coated substrates also gave

comparable environmental durability provided the primer was cured at 90 ^{o}C. Curing at room temperature resulted in least environmental durability. Although UT combined with EC3901 resulted in very high IFSS and tensile strength in dry condition, it does not have good environmental durability.

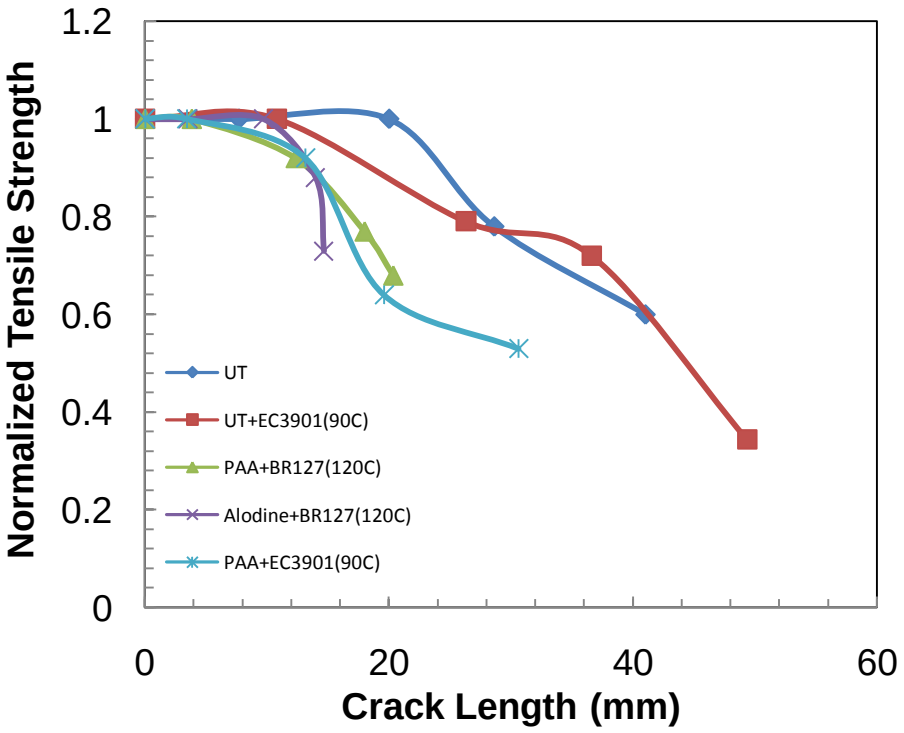

Figure 4.29: Normalized Residual Tensile strength as a function of crack length

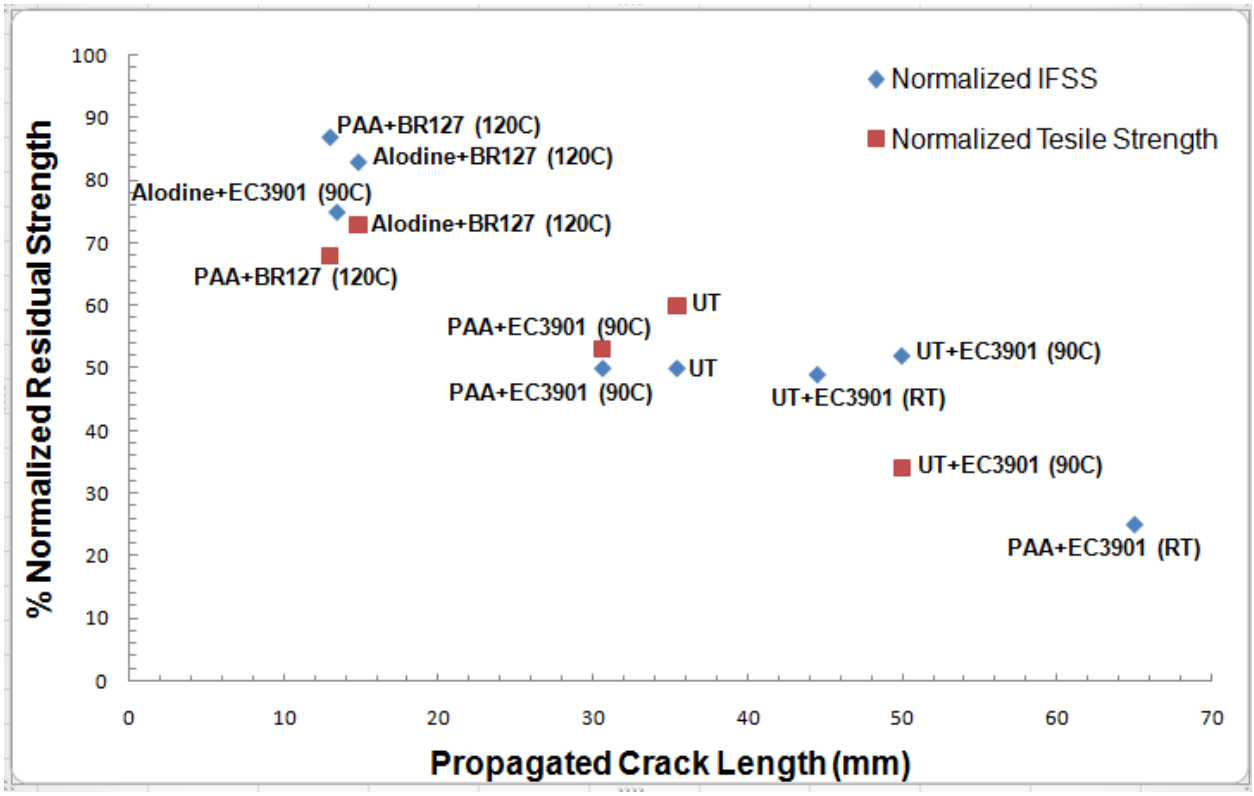

Figure 4.30: Total degradation in normalized IFSS and tensile strength as a function of total crack length of WC samples.

Chapter 5

Conclusion

The goal of this thesis was to determine the optimal surface treatment that would maximize the room temperature bonding between an Al substrate and a composite adhesive as well as maximize the environmental durability of this bond. The five objectives, identified to realize this goal, were successfully accomplished through following tasks.

- An optimal test geometry thickness, overlap length, and fillet width that maximized the % interfacial fracture area was determined and was subsequently used in manufacturing test coupons with various surface treatments to study the effect of surface treatments on strength and durability.

- Three basic surface treatments untreated (UT), phosphoric acid anodizing (PAA), and Alodine were used with and without application of two high temperature curing primer, Cytec' BR127 and 3M's EC3901.These primers were cured at manufacturer's recommended temperature (120 ^{o}C and 90 ^{o}C respectively) and room temperature (RT) to evaluate their suitability at room temperature bonding process.

- SLS (Single Lap Shear) tests, FWT (Flatwise Tensile) tests, and WC (Wedge Crack) tests were used to determine the interfacial shear and tensile strengths (in dry and hot-humid condition of 95% RH at 40 ^{o}C) and crack growth (in hot- humid condition). The fracture

surfaces were examined using image analysis and surface profilometer to quantify the amount of cohesive and adhesive fracture areas.

Results from the above tasks can be summarized as follows:

- The optimal thickness, overlap length, filler width for SLS test coupons were determined to be 0.03-0.04 mm, 20 mm, and 0 mm respectively. The same thickness was used for FWT and WC test coupons. The IFSS and % cohesive fracture area, of dry SLS test coupons, increased in the following order:

  PAA+BR127(RT)<UT+BR127(120^{o}C)<Alodine<Alodine+EC3901(RT)<Alodine+BR127(RT)<PAA<UT<UT+BR127(RT)<Alodine+EC3901(90^{o}C)<PAA+EC3901(RT)<PAA+EC3901(90^{o}C)<PAA+BR127(120^{o}C)<UT+EC3901(90^{o}C)<UT+EC3901(RT)<Alodine+BR127(120^{o}C).

  The increase in % cohesive area relative to UT, is believed to be an indirect indication of the increase in the true interfacial shear strength, since the adhesive thickness was maintained constant for all treatments. Alternatively, the decrease in % cohesive area relative to Untreated, is believed to be an indirect indication of the decrease in true interfacial strength. Hence, the ordering presented above based on the apparent IFSS is believed to be reflective of the changes in true IFSS with surface treatments.

- Both BR127 and EC3901 resulted in high IFSS when cured at high temperatures. However, curing of EC3901 at room temperature resulted in high IFSS only on UT Similar trend was observed for tensile strength of the bond.

- The plateau crack length and % interfacial area, in WC test coupons exposed to hot-humid environment, increased as following order: Alodine+EC3901(90^{o}C)<Alodine+BR127(120^{o}C)<PAA+BR127(120^{o}C)<PAA+EC3901(90^{o}C)<UT< UT+EC3901(RT)<UT+EC3901(90^{o}C)<PAA+EC(RT).

- The normalized residual shear and tensile strength also decreased in the above order suggesting that the above trend is due to environmental durability of the interfacial bond between the composite adhesive and the Al substrate

Based on these results, it can be concluded that PAA and Alodine when combined with BR127 and EC3901 primers cured at high temperatures result in high strength and best environmental (hot-humid) durability for the bond formed at room temperature between the composite adhesive and the Al substrate.

Recommendations for Future Work: Evaluate the IFSS for varying level of thicknesses (0.04 mm-0.32 mm) for the studied surface treatments in this thesis. If the IFSS vs. thickness (along with measurement of % fracture modes) were to follow the same trend observed in this study, the merit of the approach used in present study will be confirmed.

References

[1] Sara Black, "Structural adhesives, Part I: Industrial," *Composite World*, pp. 30-36, June 2016.

[2] Francesco Franco and Nicola Montefusco Fabrizio Ricci, "Bonded composite patch repairs on," *Advances in Composites Materials - Ecodesign and Analysis*, no. 20, pp. 445-464, March 2011.

[3] F.M.L., Carbas R.J.C., Critchlow, G.W., M.A.V. Figueiredo a, K. Brown Silva, "Effect of material, geometry, surface Treatment and Environment on the shear Strength of Single lap Joints," *International Journal of Adhesion & Adhesive*, vol. 29, pp. 621- 632, 2009.

[4] Won Jong Choi, Heung Soap Choi, Hyuk Kwon, and Sang Hwan Kim Sang Yoon Park, "Recent Trends in Surface Treatment Technologiesfor Airframe Adhesive Bonding Processing: A Review," *The Journal of Adhesion*, vol. 86, pp. 192-221, 2010.

[5] E.M. Petrrie, "Adhesive bonding of aluminum alloys," *http://www.metalfinishing.com*, 2007.

[6] Po-Nien Chen, "The effect of chromate on adhesion between epoxy coating and Al substrate," Lehigh University, Theses and Dissertations.

[7] M D Banea1 and L F M da Silva, "Adhesively bonded joints in composite materials: an overview," *Proceeding IMechE : J. Materials: Design and Applications* , vol. 233.

[8] L.F.M. da Silvab and R.D.S.G. Campilho M.D. Baneaa, "Effect of temperature on the shear strength of aluminium single lap bonded joints for high temperature applications," *Journal of Adhesion Science and Technology*, vol. 28, pp. 1367-1381, 2014.

[9] ASTM Satndard, "Standard Test Method for Thick-Adherend Metal Lap-Shear Joints for Determination of the Stress-Strain Behavior of Adhesives in Shear by Tension Loading".

[10] b,*, F. Lapiquea, B. Johnsenb, K. Nisancioglu O. Lundera, "Effect of pre-treatment on the durability of epoxy-bonded AA6060 aluminum joints," *International Journal of Adhesion & Adhesives*, vol. 24, pp. 107-117, 2004.

[11] R.J.C. Carbas, G.W. Critchlow, M.A.V. Figueiredo, K. Brown Lucas. F.M. da Silva, "Effect of material, geometry, surface treatment and environment on the shear strength of single lap joints," *International Journal of Adhesion & Adhesives* , vol. 29, pp. 621–632, 2009.

[12] P.K. Mallick T.P. Lang, "Effect of spew geometry on stresses in single lap adhesive joints," *International Journal of Adhesion & Adhesives* , vol. 18, p. 167—177, 1998.

[13] "http://www.adhesivestoolkit.com/Docs/test/MECHANICAL%20TEST%20METHOD%201%20-%20Shear%20Tests.xtp".

[14] K.A. Yendall, D. Bahrani, A. Quinn, F. Andrews G.W. Critchlow, "Strategies for the replacement of chromic acid anodising for the structural bonding of aluminium alloys," *International Journal of Adhesion and Adhesives*, vol. 26, pp. 419-453, 2006.

[15] Charles Griffen and D. Robert Askins, "NON-CHROMATE SURFACE PREPARATION for aluminum," *Interim Technical Report Covering Period August 1985 - May 1988*.

[16] Kathleen A. Chabot & Joseph A. Brescia, "Evaluation of primers for adhesively-bonded aircraft repair," *Journal of Adhesion Science and Technology*, vol. 7, pp. 1183-1194, 1993.

[17] "S. Fredel, "Damage tolerant repair techniques for pressureised aircraft fuselages," Wright-Patterson Lab, Ohio, 1994.".

[18] C. W. JENNINGS, "Surface Roughness and Bond Strength of Adhesives," *Journal of Adhesion*, vol. 4, pp. 25-38, 1972.

[19] R.D. Allington, R.P. Digby, N. Porritt, S.J. Shaw, J.F. Watts M.L. Abel, "Understanding the relationship between silane application conditions, bond durability and locus of failure," *International Journal of Adhesion and Adhesives*, vol. 26, pp. 2-15, 2006.

[20] M.G.S Ferreira, D.B Haddow, A Goruppa, R Short, D.G Dixon J.C.S Fernandes, "Plasma-polymerised coatings used as pre treatment for aluminium alloys," *Surface and Coatings Technology*, vol. 154, pp. 8-13, 2002.

[21] J. S., Zhao, X. H., Zuo, Y., & Xiong, J. P Zhang, "The bonding strength and corrosion resistance of aluminum alloy by anodizing treatment in a phosphoric acid modified boric acid/sulfuric acid bath," *Surface and Coatings Technology*, vol. 202, pp. 3149-3156, 2008.

[22] D. L. Bellevou, R. T. Manson, A. A. Martinelli, S. Ridpath, J. R. Arnold and G. B. Gaskin, J. J. Stayrook, ""Performance of Solvent and Water Based Primers in Epoxy Adhesive Systems," *"International SAMPE Symposium and Exhibition (Proceedings)*, vol. 44, p. 5.

[23] Won Jong Choi1, Heung Soap Choi2, Hyuk Kwon, and Sang Hwan Kim Sang Yoon Park1, "Recent Trends in Surface Treatment Technologies for airframe adhesive bonding processing:arevie (1995-2008)," *The Journal of Adhesion*, vol. 86, pp. 192-221, 2010.

[24] J. Dean Minford, "JOINT DURABILITY STUDIES WITH ABRADED, ETCHED, COATED AND anodized aluminum adherend".

[25] T. N. S. S. Rodrigues M. A. V. Figueiredo M. F. S. F. de Moura J. A. G. Chousal Lucas F. M. da Silva, "Effect of Adhesive Type and Thickness on the Lap Shear Strength," *The Journal of Adhesion*, vol. 82, pp. 1091–1115, 2006.

[26] R. D. and Davies, R. Adams, "Strength of lap shear joint," *The Mechanics of Adhesion D. A. Dillard and A. V. Pociu(Eds.)* , vol. (Elsevier, Amsterdam, 2002), pp. 111-144, 2002.

[27] M. J. L. VAN TOOREN and A. BEUKERS D. M. GLEICH ¤, "Analysis and evaluation of bondline thickness effects on failure load in adhesively bonded structures," *Journal of Adhesion Science and Technology* , vol. 15, pp. 1091–1101, 2001.

[28] R. D. and Peppiatt, N. A Adams, *J. Strain Anal. 9, 185–196*, pp. 185-196, 1974.

[29] R. D. S. G. Campilho, "Strength Improvement of adhesively bonded joints using a revese bent geometry," *JOURNAL OF ADHESION SCIENCE AND TECHNOLOGY* , January 2011.

[30] M. Y. Tsai J. Morton, "The effect of a spew fillet on adhesive stress distributions in laminated composite single-lap joints," *Composite Structures* , vol. 32, pp. 123-131, 1995.

[31] P., Sohierb, L., Cognardc, J.Y., Bourmaudd, A., Choqueusea, D., Rinnerte, E., Créac'hcadec, R. Daviesa, "Influence of adhesive bond line thickness on joint strength," *International Journal of Adhesion and Adhesives*, vol. 26, no. 7, pp. 724-736, October 2009.

[32] A. Ozel1, S. Akpinar, and M. D. Aydin M. Doru, "Effect of the Spew Fillet on Adhesively Bonded Single-Lap Joint Subjected to Tensile Loading: Experimental and 3-D Non-Linear Stress Analysis," *The Journal of Adhesion, 90:195–209, 2014*, vol. 90, pp. 195–209, 2014.

[33] E. M. Petrie, "dhesives for the AssembLy of Aircraft Structures and Components," *http://www.metalfinishing.com*, 2008.

[34] J.P. Sargent, "Durability studies for aerospace applications using peel and wedge test," *International Journal of Adhesion & Adhesives*, vol. 25, pp. 247–256, 2005.

[35] K. L. DeVries, C. Child D. O. Adams, "DURABILITY OF ADHESIVELY BONDED JOINTS for ircraft structures".

[36] Collins TJ, "ImageJ for microscopy," *BioTechniques 43*, vol. 43, pp. 25–30, 2007.

[37] A. Higgins, "Adhesive bonding of aircraft structures," *International Journal of Adhesion and Adhesives*, pp. 367-376, 2000.

[38] H. Wang, C. Hicks, X. Yang, B. E. Carlson, Q. Zhou F. Zhang, "Experimental study of initial strengths and hygrothermal degradation of adhesive joints between thin aluminum and steel substrates," *International Journal of Adhesion & Adhesives*, vol. 43, pp. 14–25, 2013.

[39] K. F. Horcajo, G. Del Rosario, A.Urena S. G. Prolongo, "Strength and Durability of Epoxy-Aluminum Joints," *The Journal of Adhesion*, vol. 86, pp. 409-429, 2010.

[40] X. Yang, Hui. Wang, X. Zhang, Y. Xia, Q. Zhou Fan., *International Journal of Adhesion & Adhesives* , vol. 44, pp. 130–137, 2013.